Microstructural and crystallographic evolution of palaeognath (Aves) eggshells

Seung Choi[1,2*], Mark E Hauber[3], Lucas J Legendre[4], Noe-Heon Kim[5], Yuong-Nam Lee[5], David J Varricchio[1*]

[1]Department of Earth Sciences, Montana State University, Bozeman, Montana, United States; [2]Key Laboratory of Evolutionary Systematics of Vertebrates, Institute of Vertebrate Paleontology and Paleoanthropology, Chinese Academy of Sciences, Beijing, China; [3]Department of Evolution, Ecology, and Behavior, School of Integrative Biology, University of Illinois Urbana-Champaign, Urbana-Champaign, Illinois, United States; [4]Department of Geological Sciences, University of Texas at Austin, Austin, Texas, United States; [5]School of Earth and Environmental Sciences, Seoul National University, Seoul, South Korea

Keywords: Dinosauria, EBSD, Eggshell, Homology, Homoplasy, Palaeognathae

For correspondence: seung0521@gmail.com (SC); djv@montana.edu (DJV)

Abstract

The avian palaeognath phylogeny has been recently revised significantly due to the advancement of genome-wide comparative analyses and provides the opportunity to trace the evolution of the microstructure and crystallography of modern dinosaur eggshells. Here, eggshells of all major clades of Palaeognathae (including extinct taxa) and selected eggshells of Neognathae and non-avian dinosaurs are analysed with electron backscatter diffraction. Our results show the detailed microstructures and crystallographies of (previously) loosely categorized ostrich-, rhea-, and tinamou-style morphotypes of palaeognath eggshells. All rhea-style eggshell appears homologous, while respective ostrich-style and tinamou-style morphotypes are best interpreted as homoplastic morphologies (independently acquired).

Ancestral state reconstruction and parsimony analysis additionally show that rhea-style eggshell represents the ancestral state of palaeognath eggshells both in microstructure and crystallography. The ornithological and palaeontological implications of the current study are not only helpful for the understanding of evolution of modern and extinct dinosaur eggshells, but also aid other disciplines where palaeognath eggshells provide useful archive for comparative contrasts (e.g. palaeoenvironmental reconstructions, geochronology, and zooarchaeology).

Introduction

Non-avian dinosaurs became extinct at the end of Mesozoic (During et al., 2022), but avian dinosaurs are still extant and flourishing today as the most speciose land-vertebrate lineage (Jarvis et al., 2014; Lee et al., 2014; Brusatte et al., 2015; Prum et al., 2015). For example, their eggshell sizes, shapes, and patterns show phenomenal diversity (Mikhailov, 1997a; Hauber, 2014; Stoddard et al., 2017). In the palaeontological record, even more diverse forms of dinosaur eggs and eggshells have been recovered (Mikhailov, 1997b; Grellet-Tinner et al., 2006; Norell et al., 2020; Oser et al., 2021), with many divergent designs disappearing with the extinction of non-avian dinosaurs. Eggshell is mainly a biomineral ($CaCO_3$) (with an inner proteinous shell membrane and outer cuticle cover; Kulshreshtha et al., 2022) that can be well-preserved in the fossil record (Mikhailov and Zelenkov, 2020; Varricchio et al., under review), thereby, dinosaur eggs are a valuable subject for evolutionary biology for the tracking of phenotypic changes over geological timescales from the Early Jurassic onward (Stein et al., 2019; Choi and Lee, 2019). However, how eggs and eggshells evolve in a single dinosaur clade is not well understood and homoplastic similarities can obscure understanding. Documenting the evolution of eggs among modern avian dinosaurs provides

helpful insights into the evolution among extinct taxa.

Palaeognathae is one of the two major clades of modern birds (or modern dinosaurs) (Jarvis et al., 2014). Extant Palaeognathae are usually larger than their sister-clade Neognathae and are flightless except for the poorly-flighted tinamous (Yonezawa et al., 2017; Altimiras et al., 2017). However, the Palaeogene palaeognaths Lithornithidae might have been a fully volant clade (Torres et al., 2020; Widrig and Field, 2022). Proportional to their body size, absolute sizes of eggs and eggshells of Palaeognathae are usually large and thick, respectively (Grellet-Tinner, 2006; Birchard and Deeming, 2009; Legendre and Clarke, 2021). Furthermore, eggshells of Palaeognathae show distinctive microstructures compared to those of Neognathae (Mikhailov, 1997a; Zelenitsky and Modesto, 2003; Grellet-Tinner, 2006). Species diversity of Palaeognathae is much lower than that of Neognathae (Prum et al., 2015) but it is critical for avian egg research; due to their lower diversity, it is feasible to investigate the egg features of all major clades of Palaeognathae. More importantly, considering that most Palaeognathae are flightless and that flight influences egg mass in Dinosauria (Legendre and Clarke, 2021), which influences eggshell thickness (Ar et al., 1979; Legendre and Clarke, 2021), the eggs and eggshells of Palaeognathae might be more appropriate modern analogues for those of flightless non-avian dinosaurs than those of volant Neognathae.

Previous studies of palaeognath eggs and eggshells (Zelenitsky and Modesto, 2003; Grellet-Tinner, 2006) interpreted the features in the light of morphology-based phylogenies of Palaeognathae. However, the phylogeny of Palaeognathae has drastically changed since late 2000s, mainly due to the advancements of molecular approaches (Harshman et al., 2008; Phillips et al., 2010; Mitchell et al., 2014; Grealy et al., 2017; Yonezawa et al., 2017; Sackton et al., 2019; Cloutier et al., 2019). For example, morphological phylogenies interpreted tinamous as the sister clade of all other Palaeognathae (Livezey and Zusi, 2007), but a more

recent molecular view regards tinamou and moa as sister clades (Phillips et al., 2010), which are a less inclusive clade within Palaeognathae (Sackton et al., 2019). Thus, revisiting eggs and eggshells of Palaeognathae with a revised phylogeny of Palaeognathae is a timely issue for a comprehensive and updated understanding of avian egg evolution.

Tracing the evolution of palaeognath eggs and eggshells is important for both ornithology and palaeontology. For ornithology, it provides a representative case on how the macro-, microstructure and crystallography of eggs have evolved in the avian clade where speciation timelines are now available owing to molecular clocks (Yonezawa et al., 2017). Based on a recent evolutionary scenario, stating that diverse palaeognath clades lost flight and acquired gigantism independently (Harshman et al., 2008; Phillips et al., 2010; Mitchell et al., 2014; Grealy et al., 2017; Yonezawa et al., 2017; Sackton et al., 2019; *contra* Cracraft, 1974), palaeognath eggshells provide chances to appraise potential homologies (similarities inherited from the most recent common ancestor [MRCA]) and homoplasies (similarities caused by similar selective regime [or neutral factors] rather than common ancestry; see Patterson, 1988; de Pinna, 1991; Losos, 2011 for further information) in the evolution of avian eggshells.

For palaeontology, firstly, palaeognath eggs offer the chance to track appearance/disappearance and character change rates of phenotypes in modern dinosaur eggs. The molecular-clock-based approach is impossible for non-avian dinosaur eggs because DNA is not preserved in Mesozoic fossils (Saitta et al., 2019) or at least non sequenceable (Bailleul and Li, 2021). Consequently, in palaeontology, inferring the evolutionary pathways of eggshell must rely on a phylogeny of egg-layers that is solely based on morphological traits, but morphology-based trees can conflict with molecular data (e.g. Bunce et al., 2009; Darlim et al., 2022; see also Wiens, 2004; Quental and Marshall, 2010; Lee and Palci, 2015).

Moreover, morphological phylogenetic trees generated in palaeontology are usually based on insufficient chronologies due to the shortage of absolute radiometric age data. In this sense, palaeognath eggs and eggshells can be helpful modern exemplars for palaeontology that show how, and at what rate, evolution has worked in flightless dinosaur eggs.

Secondly, in the Cenozoic deposits, palaeognath eggshells have been frequently reported in diverse regions of the world (Sauer, 1972; Harrison and Msuya, 2005; Bibi et al., 2006; Worthy et al., 2007; Patnaik et al., 2009; Donaire and López-Martínez, 2009; Wang et al., 2011; Pickford, 2014; Blinkhorn et al., 2015; Mikhailov and Zelenkov, 2020). However, most of previous investigations focused on the thickness and pore canal structures on the outer surface of eggshells. They are useful information, but a few published images show peculiar microstructure (e.g. Patnaik et al., 2009; Wang et al., 2011), which are not observed in modern palaeognath eggshells (see below). It means that there may be diverse eggshell microstructures in the fossil record and to understand the difference correctly, a more comprehensive, baseline understanding of the microstructure and crystallography of modern palaeognath eggshells is necessary.

Here we: (i) document the microstructure and crystallography of all major clades of palaeognath eggshells (and several selected neognath and non-avian dinosaur eggshells for comparison) using three different mapping techniques acquired by electron backscatter diffraction (EBSD), a state-of-the-art tool for eggshell microstructural and crystallographic study; (ii) reinterpret the evolution of palaeognath eggshells based on the radically revised phylogeny of Palaeognathae; (iii) discuss the implications of evolution of palaeognath eggshells for the aforementioned research areas; and (iv) suggest future research topics for which this study can be a basis.

Results

Description for EBSD maps

Ostrich (*Struthio camelus*)

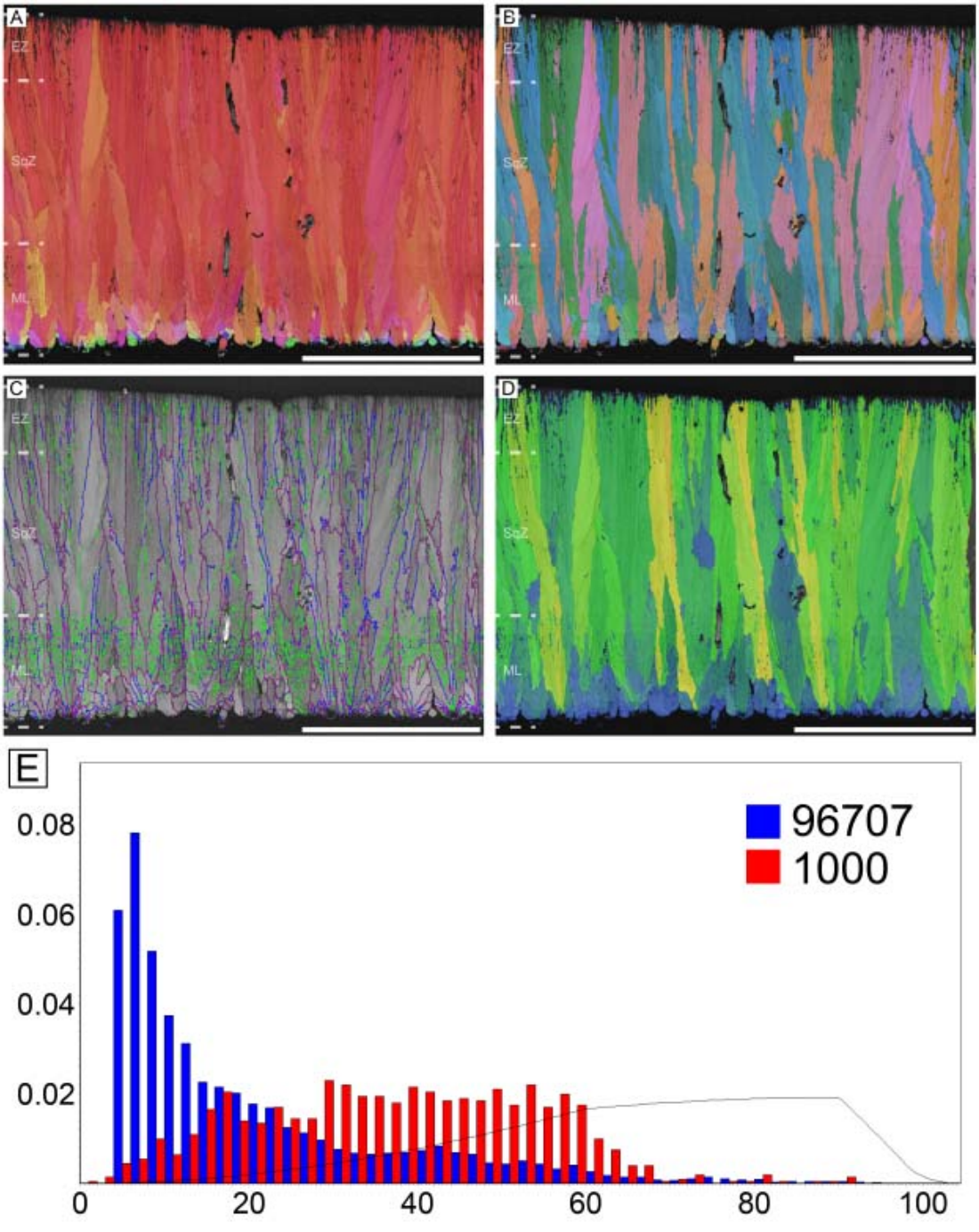

124 **Figure 1.** Ostrich eggshell. (**A**) IPF, (**B**) Euler, (**C**) GB, and (**D**) AR mappings (see Figures
125 13–15 for legends). The dashed lines in the maps mark the boundary between the ML and
126 SqZ; SqZ and EZ. Scale bars equal 1000 μm. (**E**) A misorientation histogram. The numbers
127 in x- and y-axis represent degree between the two selected grains (either adjacent [blue;
128 neighbour-pair method] or random [red; random-pair method]; see also Figure 16) and
129 frequency, respectively. The numbers at the upper right corner mean the number of selected
130 grains in each selection method. The explanation herein is applicable to the Figures 2–12 and
131 Appendix 1—figures 4–12.

132

133 The overall microstructure and crystallography are peculiar compared to other palaeognath
134 eggshells (Figure 1; Zelenitsky and Modesto, 2003; Grellet-Tinner, 2006). The entire
135 thickness of the eggshell is composed of prismatic calcite grains (Zelenitsky and Modesto,
136 2003; Choi et al., 2019). The mammillary layer (ML) is composed of wedge-like calcite
137 grains and these grains are usually extend to the outer edge of the eggshell. Low-angle (< 10˚;
138 green lines in Figure 1C) grain boundaries (GB) are widespread in the eggshell, but they are
139 concentrated at the outer part of ML (the existence and portion of ML is clearer in polarized
140 light microscopic and scanning electron microscopic images; Dauphin et al., 2006). This
141 feature has not been reported in any other avian and non-avian maniraptoran eggshell. Unlike
142 most other avian eggshells that have rugged GB in squamatic zone (SqZ) and linear GB in
143 external zone (EZ) (Grellet-Tinner et al., 2012, 2016, 2017; Choi et al., 2019), the GB in the
144 SqZ of ostrich eggshell are seemingly linear. This makes it hard to identify the boundaries
145 between the ML and SqZ, and between the SqZ and EZ in inverse pole figure (IPF) Y and
146 Euler maps (Zelenitsky and Modesto, 2003; Mikhailov, 2014). However, EBSD provides
147 highly-magnified images such that weakly developed rugged GB in the SqZ and slightly

148 more linear GB in the EZ are observed (Appendix 1—figure 1). Thus, we support the view
149 that there is a SqZ/EZ boundary near the outer surface of eggshell (Mikhailov, 2014). The
150 peculiar prismatic microstructure of ostrich eggshell might have been derived from weakened
151 development of squamatic ultrastructure and 'splaying' calcite growth.

152

153 Rhea (*Rhea* sp.)

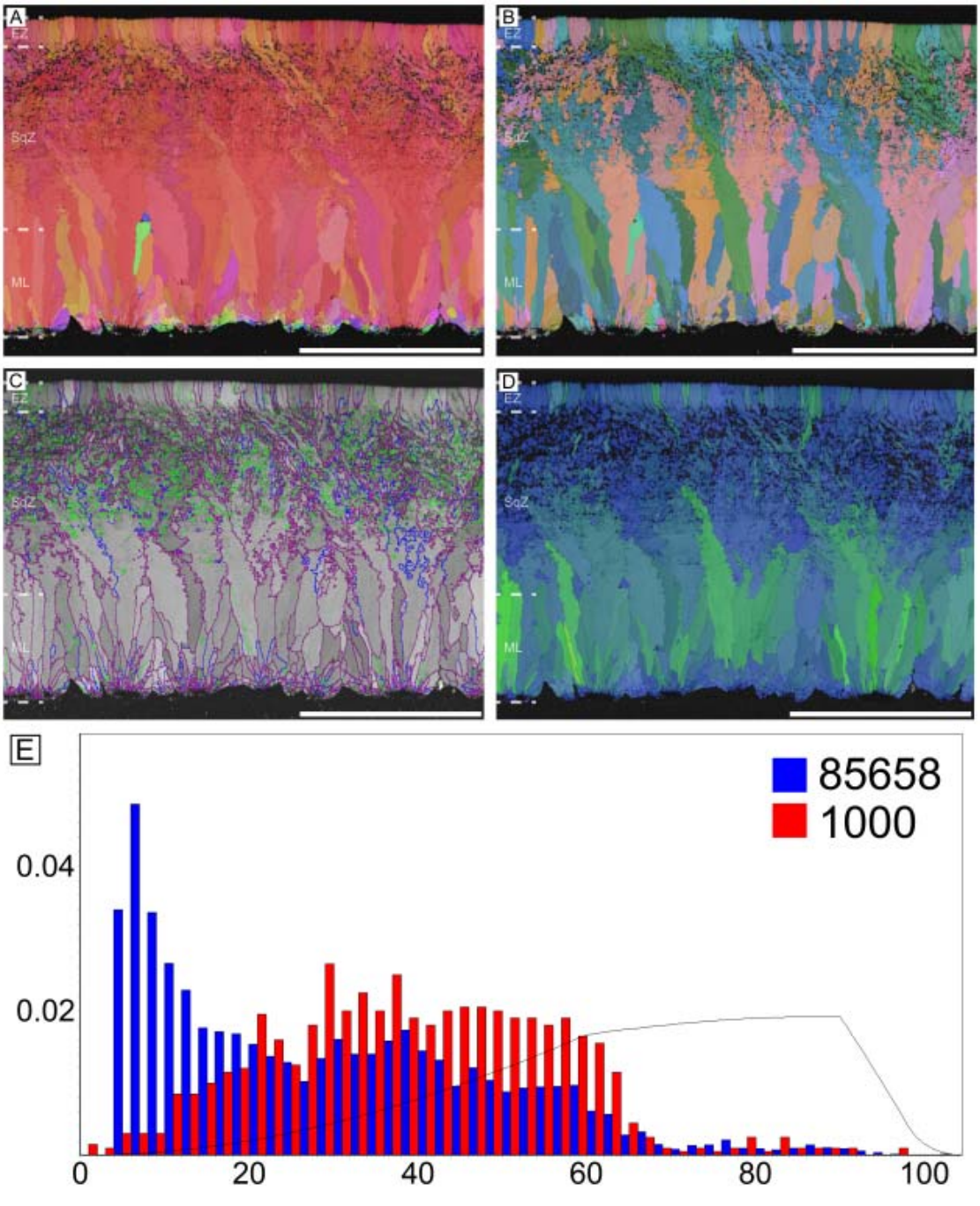

Figure 2. Rhea eggshell. Scale bars equal 500 μm.

Rhea possesses microstructure and crystallography common to most palaeognath eggshells (Figure 2). The ML is comparatively thick and composed of wedge-like calcite. The

159 boundary between the ML and SqZ is clear and can be identified by the contrasting
160 microstructures. The SqZ is characterized by 'splaying' of the grain shape. There is
161 crystallographic continuity between the SqZ and EZ, but calcite crystals in the EZ are usually
162 prismatic in shape. Note that the overall microstructure is nearly the same as that of *Sankofa*
163 *pyrenaica* and *Pseudogeckoolithus*, which are Late Cretaceous ootaxa (fossil egg-types) from
164 Europe (López-Martínez and Vicens, 2012; Choi et al., 2020). Low-angle GB are mostly
165 concentrated in the SqZ. In ML and EZ, GB are linear, while in SqZ, GB are highly rugged.
166 This trait can be observed even in simple secondary electron SEM images of rhea eggshells
167 (Choi et al., 2019).

168

169 Emu (*Dromaius novaehollandiae*) and cassowary (*Casuarius casuarius*)

170

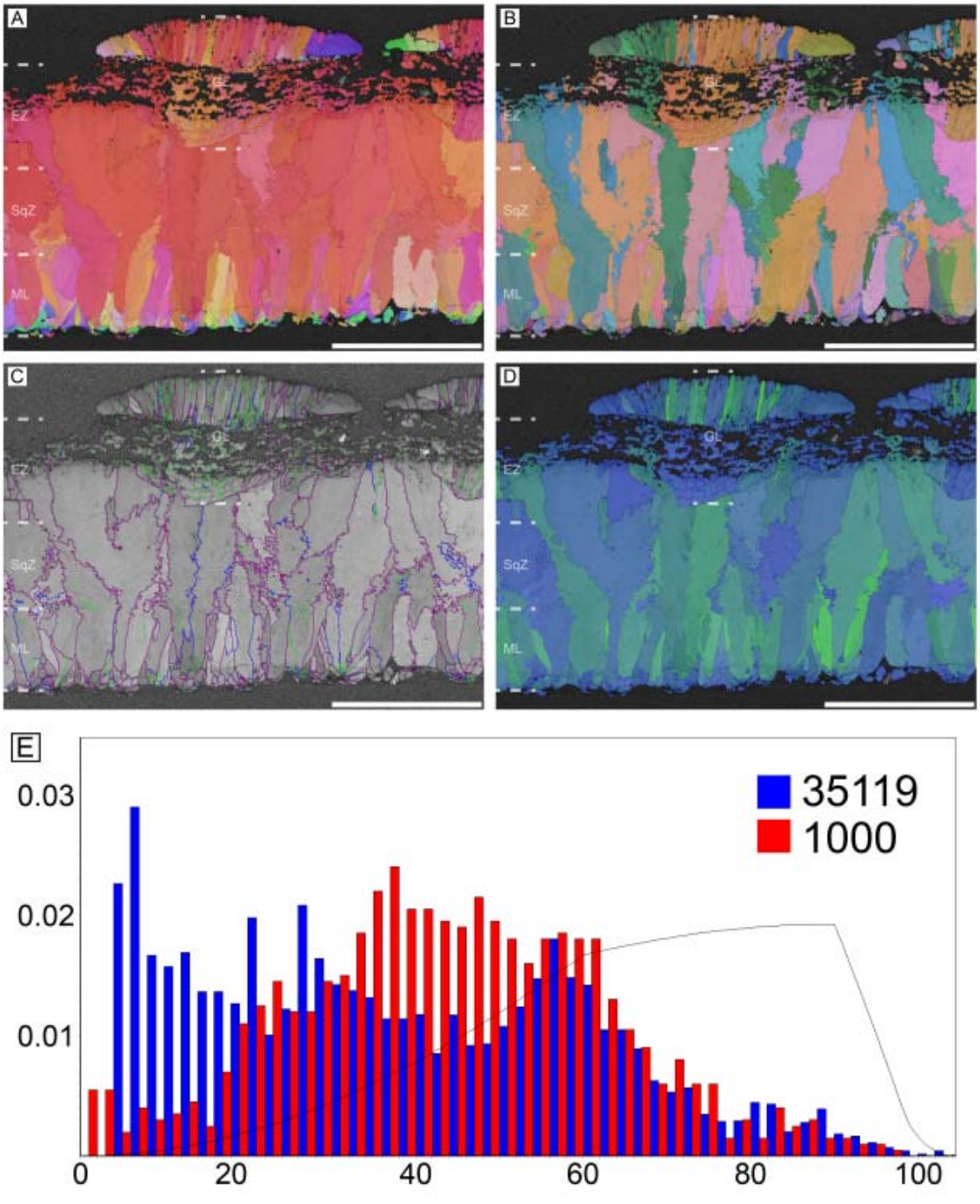

Figure 3. Emu eggshell. Note that deposition of granular layer (GL) begins in the EZ. Scale bars equal 500 µm.

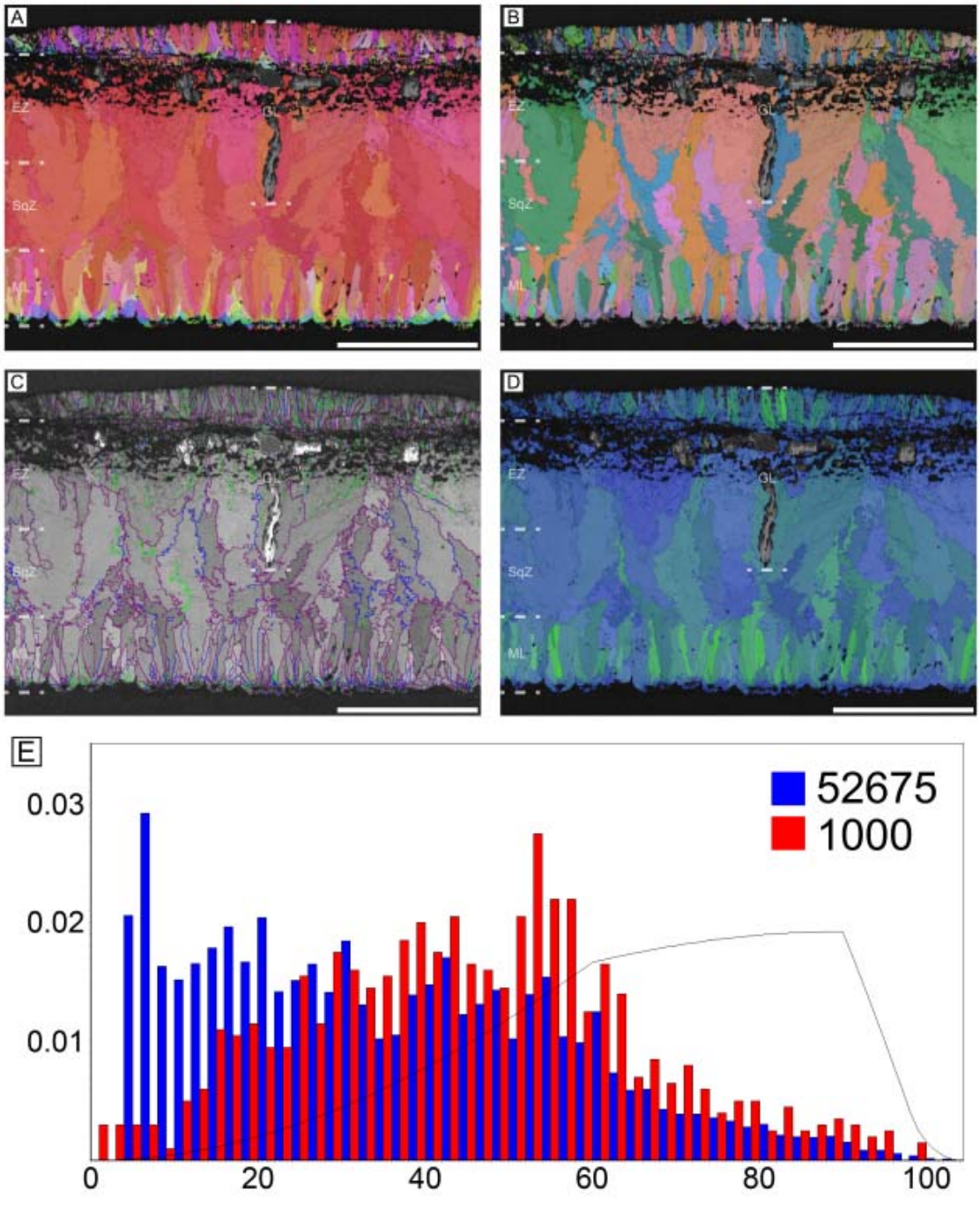

Figure 4. Cassowary eggshell. Note that deposition of granular layer (GL) begins in the middle of SqZ. Scale bars equal 500 µm.

Microstructure and crystallography of both genera are nearly the same, thus, they are

described together (Figures 3 and 4). The major differences are that cassowary eggshell has a higher density of calcite grains in their ML and SqZ and presence of EZ is less clear. The ML of both genera has wedge-like calcite. The boundary between the ML and SqZ is clear. SqZ is characterized by 'splaying' of the grain shape. The SqZ is changed into EZ in outer region of compact part of the eggshell, which is characterized by different GB conditions. The 'resistant zone' (*sensu* Zelenitsky and Modesto, 2003; see Appendix 1—figure 2B) of the eggshell shows crystallographic continuity with EZ. Therefore, we suggest that the 'resistant zone' be interpreted as a modified EZ that acquired porosity (Appendix 1—figure 2D). This view is different from that of Zelenitksy and Modesto (2003) who regarded 'resistant zone' as a modified SqZ. Additionally, Grellet-Tinner (2006) interpreted this 'resistant zone' as a 'third layer' (= EZ in our terminology), which is partly in agreement with our view. In contrast, we suggest that the outer part of the 'second layer' (= SqZ in our term) in Grellet-Tinner (2006) is, in fact, part of EZ. Another unique feature of cassowary and emu eggshells is their 'granular layer' (*sensu* Mikhailov, 1997a; Appendix 1—figure 2A). Although this layer was consistently reported in earlier studies (Mikhailov, 1997a; Zelenitsky and Modesto, 2003; Grellet-Tinner, 2006), it was usually treated as a layer simply overlying the porous EZ. However, this layer has a deep triangular 'root' to the middle of eggshell (Lawver and Boyd, 2018; Choi et al., 2020; note that the granular layer begins in SqZ in cassowary eggshell but in EZ in emu eggshell in our Figures 3 and 4, but it was not clade-specific and variable in both eggshells). Note that except for 'resistant zone' and granular layer, the overall microstructure of both emu and cassowary eggshells is very similar to those of *Pseudogeckoolithus* and *Sankofa* (López-Martínez and Vicens, 2012; Choi et al., 2020). Dissimilar to the rhea eggshell, the low-angle GB are not concentrated in SqZ, but usually present in granular layer (both outer granular part and its 'root'). In ML, GB are linear. The GB becomes highly rugged in the SqZ. The GB becomes linear again before they reach

205 'resistant zone', but this pattern is more prominent in emu eggshells. In the outer granular
206 layer, GB are usually linear and lie parallel to each other.

207

208 Kiwi (*Apteryx mantelli*)

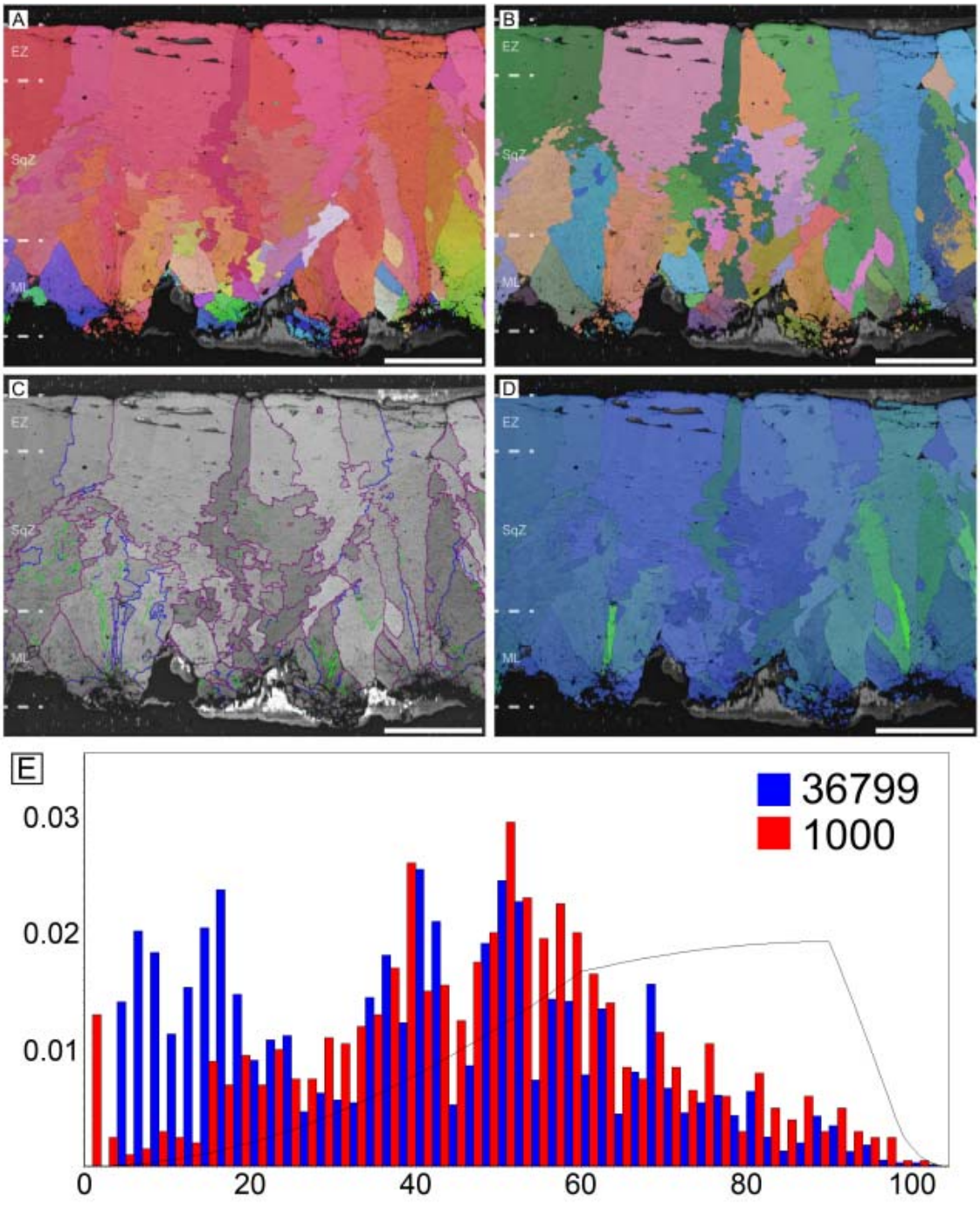

Figure 5. Kiwi eggshell. Scale bars equal 100 µm.

In ML, grains are mostly wedge-like but in some parts, the width of the grains are very

narrow so that needle-like (acicular) in shape (Figure 5; Zelenitsky and Modesto, 2003; but see Grellet-Tinner, 2006). The contour of ML is usually round. The boundary between the ML and SqZ is clear due to the contrasting grain shapes but the boundary can be extended into the middle of eggshell. The EZ crystals are massive and comparatively thick. Low-angle GB are mostly situated at the ML but low-angle GB are not abundant unlike other palaeognath eggshells. In ML and EZ, GB are linear. In SqZ, the GB are highly rugged.

Elephant bird (Aepyornithidae)

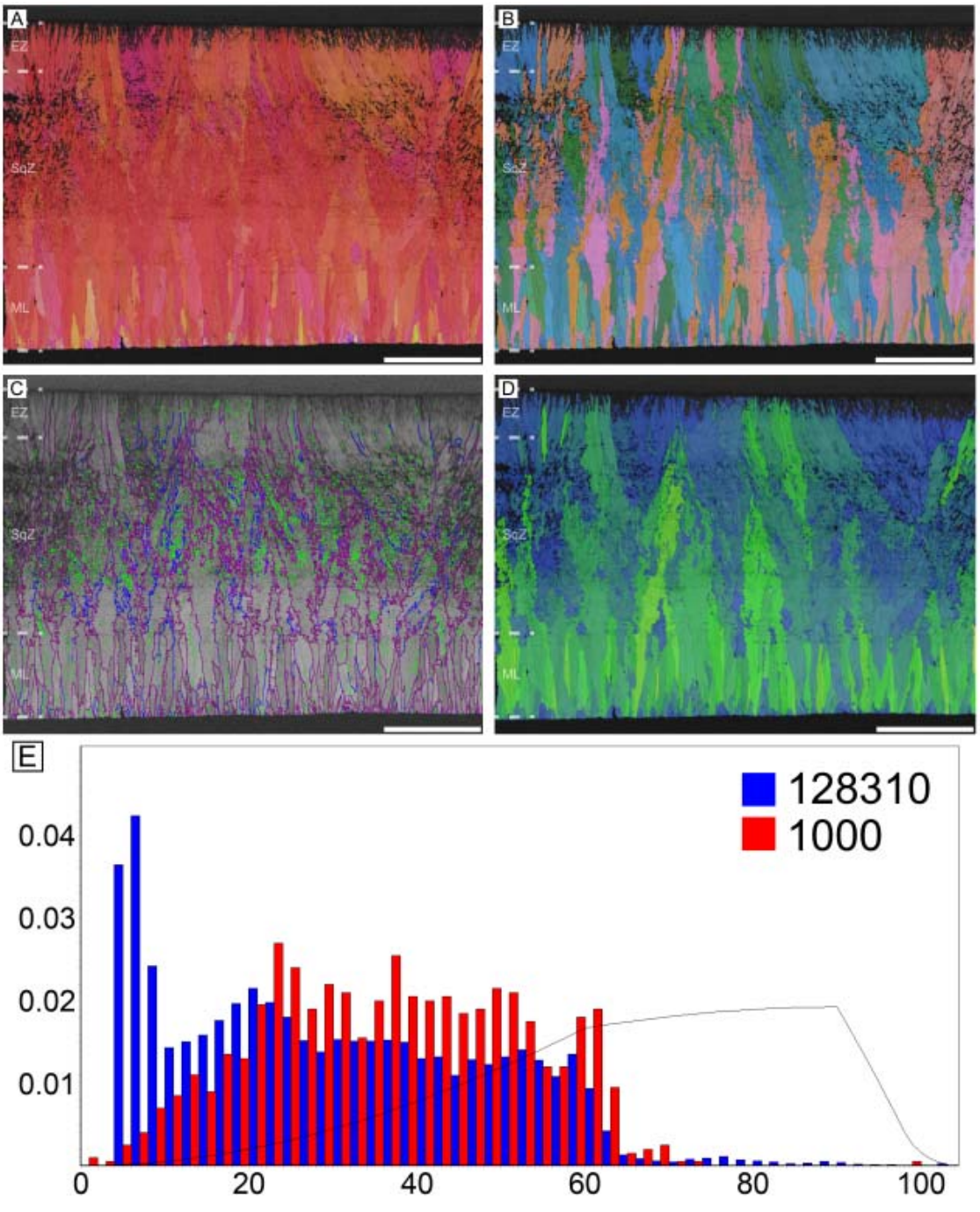

221

222 **Figure 6.** Elephant bird eggshell. Scale bars equal 1000 µm.

223

224 As the largest known avian egg, it has the thickest eggshell (3.8 mm in average) (Figure 6;

225 Schönwetter, 1960–1978, Ar et al., 1979; Juang et al., 2017). Its microstructure and
226 crystallography are closely similar to those of rhea eggshell despite the difference in
227 thickness (Figure 2). The ML is composed of wedge-like calcite. The boundary between the
228 ML and SqZ is easily identifiable due to the microstructural difference. However, extent of
229 'splaying' in SqZ is far less than that of rhea eggshell and more similar to a 'cryptoprismatic'
230 SqZ reported from non-avian maniraptoran eggshell *Macroelongatoolithus* (Jin et al., 2007).
231 The grains in the EZ becomes weakly prismatic. Low-angle GB are mostly situated at SqZ as
232 in rhea eggshell. In ML and EZ, GB are linear. In the SqZ, GB are rugged.

233

234 Tinamous (*Eudromia elegans* and *Nothoprocta perdicaria*)

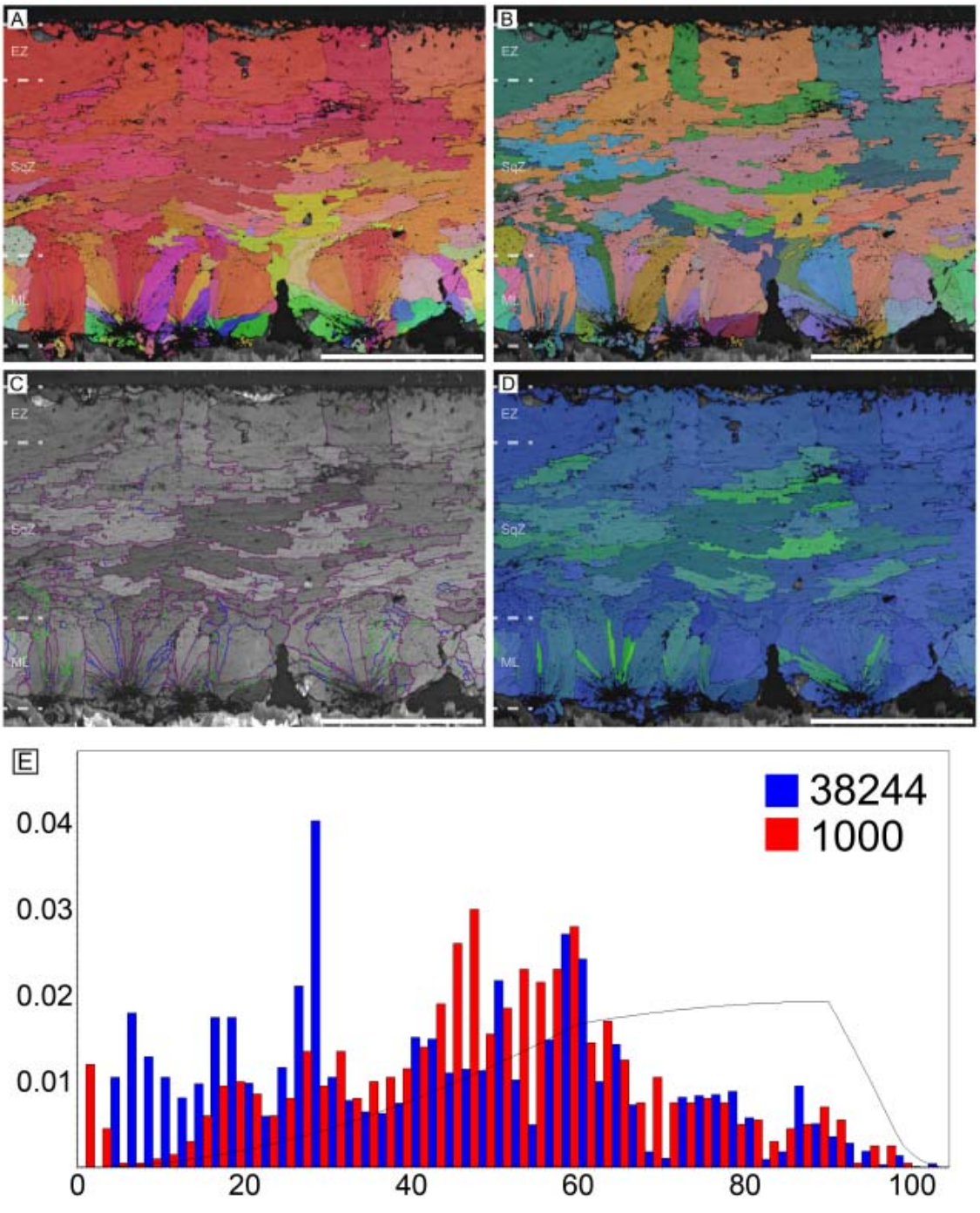

Figure 7. Elegant crested tinamou eggshell. Scale bars equal 100 µm.

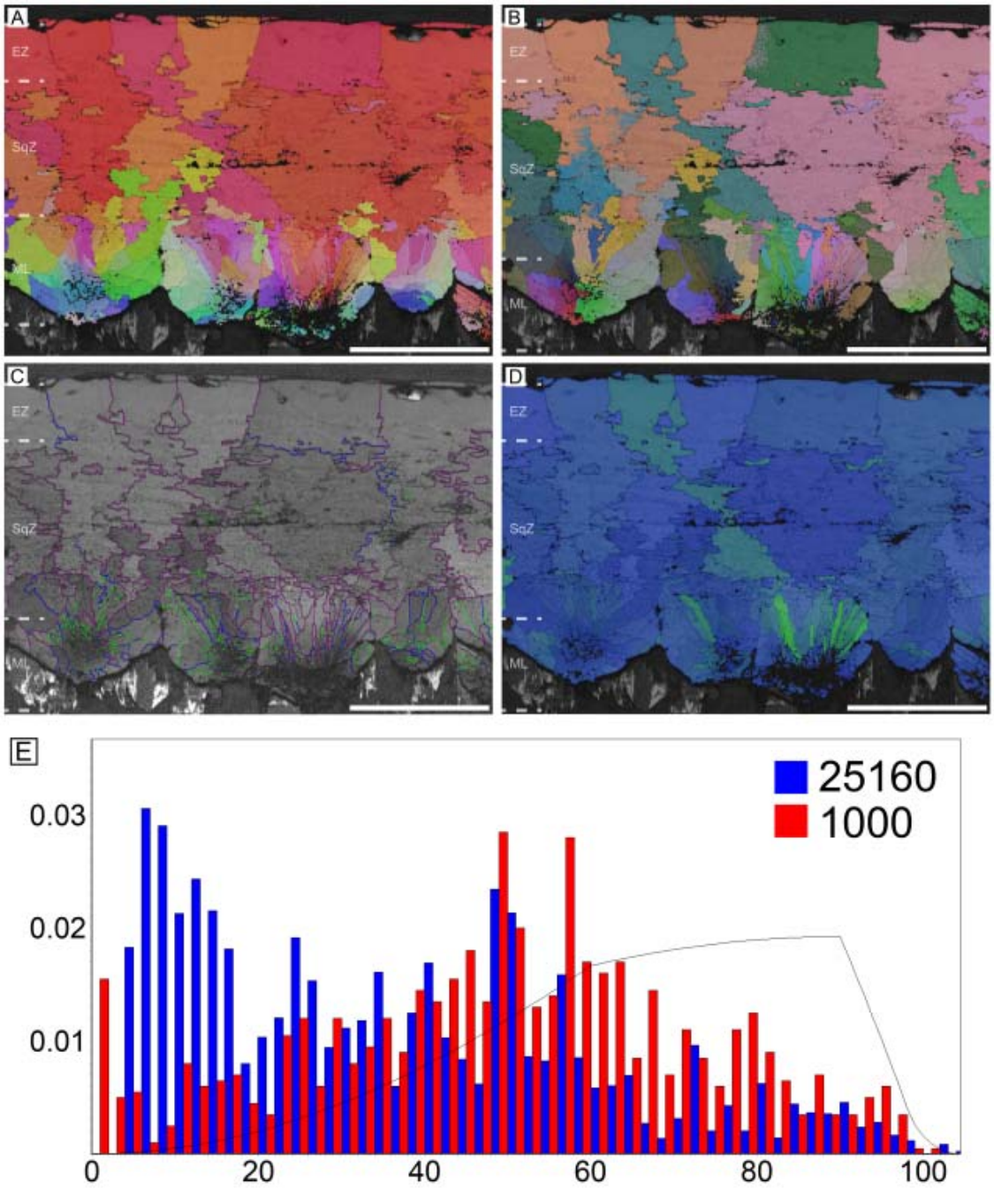

Figure 8. Chilean tinamou eggshell. Scale bars equal 100 µm.

243 The eggshells of elegant crested tinamou (*Eudromia elegans*) and Chilean tinamou
244 (*Nothoprocta perdicaria*) are described together due to their similarity (Figures 7 and 8). The
245 ML is characterized by clear needle-like calcite grains (Zelenitsky and Modesto, 2003;
246 Grellet-Tinner and Dyke, 2005; Grellet-Tinner, 2006), which is reminiscent of that of non-
247 avian maniraptoran eggshells (especially *Elongatoolithus* and *Reticuloolithus*) (Appendix 1—
248 figure 3). The overall contour of ML is usually round (Grellet-Tinner, 2006). The boundary
249 between the ML and SqZ is clear. In SqZ, the grain shape is highly irregular in elegant
250 crested tinamou eggshell, but Chilean tinamou eggshell has 'splaying' structure. In EZ, the
251 grains are massive. Low-angle GB mostly exist in ML. In ML and EZ, GB are linear but in
252 the SqZ, GB are highly rugged.

253

254 Thin (possibly *Pachyornis geranoides*) and middle (possibly *Euryapteryx curtus*) thickness
255 moa eggshells (Dinornithiformes)

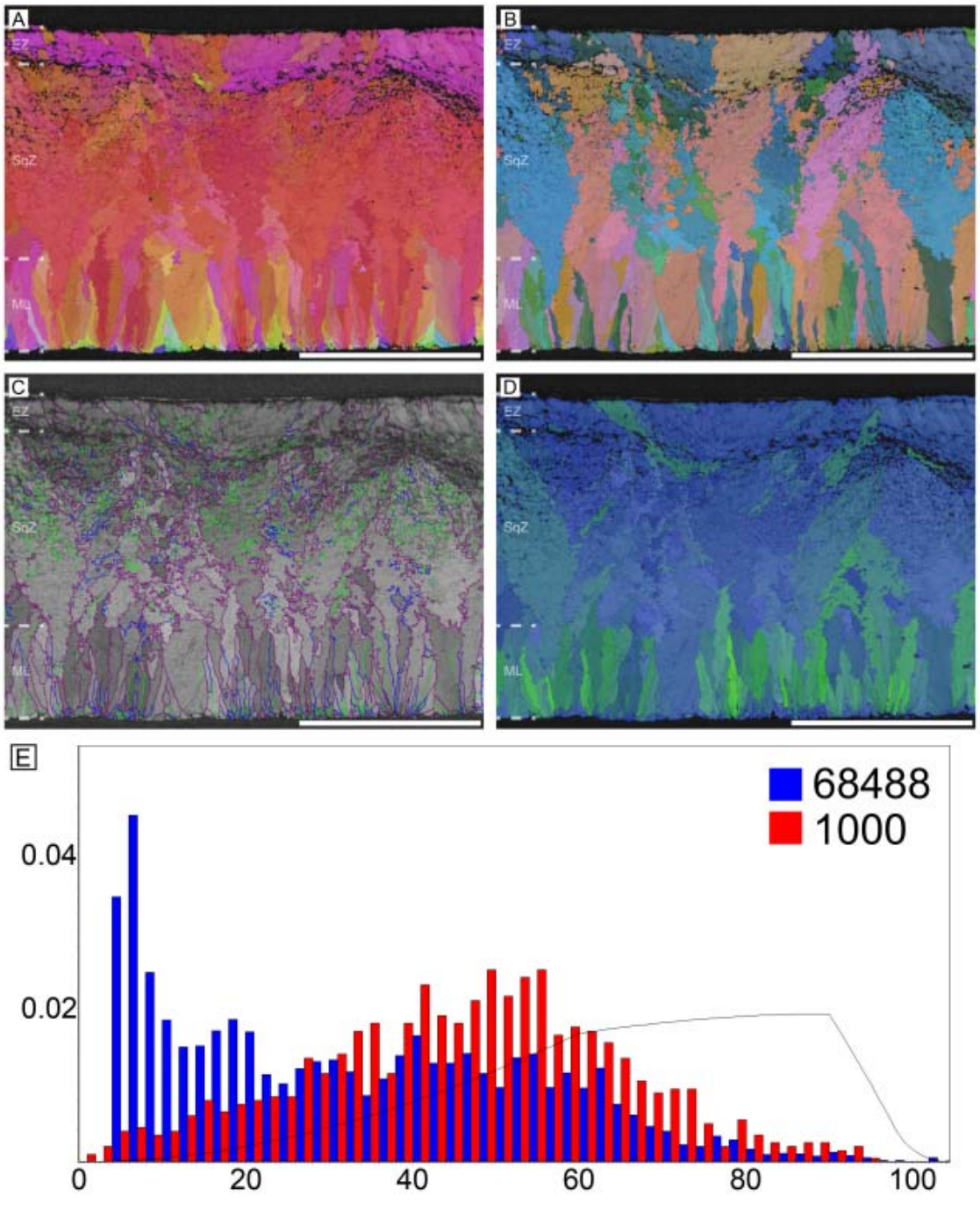

256

257 **Figure 9.** Thin moa eggshell (potential egg of *Pachyornis*). Scale bars equal 500 µm.

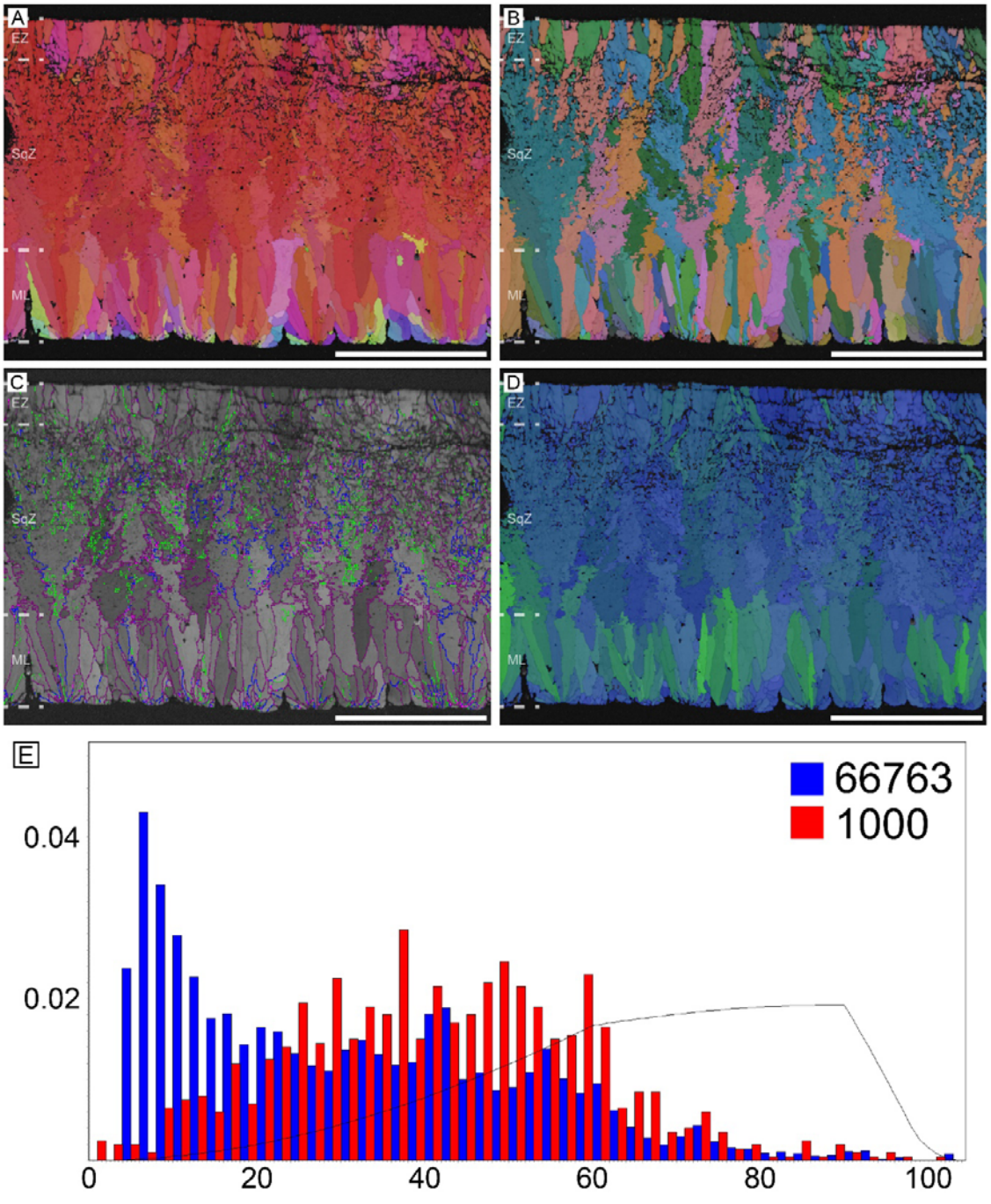

258

259 **Figure 10**. Middle thickness moa eggshell (potential egg of *Euryapteryx*). Scale bars equal

260 500 µm.

261

262 These samples are most likely eggshells of *Pachyornis geranoides* and *Euryapteryx curtus*,

263 respectively, although they may belong to a single species (see Appendix 1; Gill, 2021). The
264 overall microstructure and crystallography of both eggshells are similar to those of rhea
265 eggshell (Figures 9 and 10). The ML is composed of wedge-like calcite grains. The boundary
266 between the ML and SqZ is clear. The SqZ is characterized by the 'splaying' of the grain
267 shape. However, the EZ is not as prominent as that of rhea eggshell although grain boundary
268 is comparatively linear in the middle thickness moa eggshell (Figure 10). The grains in the
269 EZ are irregular in shape, and this may be the reason why EZ of moa eggshell was not
270 reported until the early 2000s notwithstanding the fact that moa eggshells had been described
271 since the late 1800s (Zelenitsky et al., 2002). The GB features for thin and middle thickness
272 moa eggshells are similar to that of rhea eggshell. The only difference is that the GB linearity
273 at the EZ of thin and middle thickness moa eggshells is much weaker than that of rhea
274 eggshell.

275

276 Thick moa (*Dinornis novaezealandiae*) eggshells (Dinornithiformes)

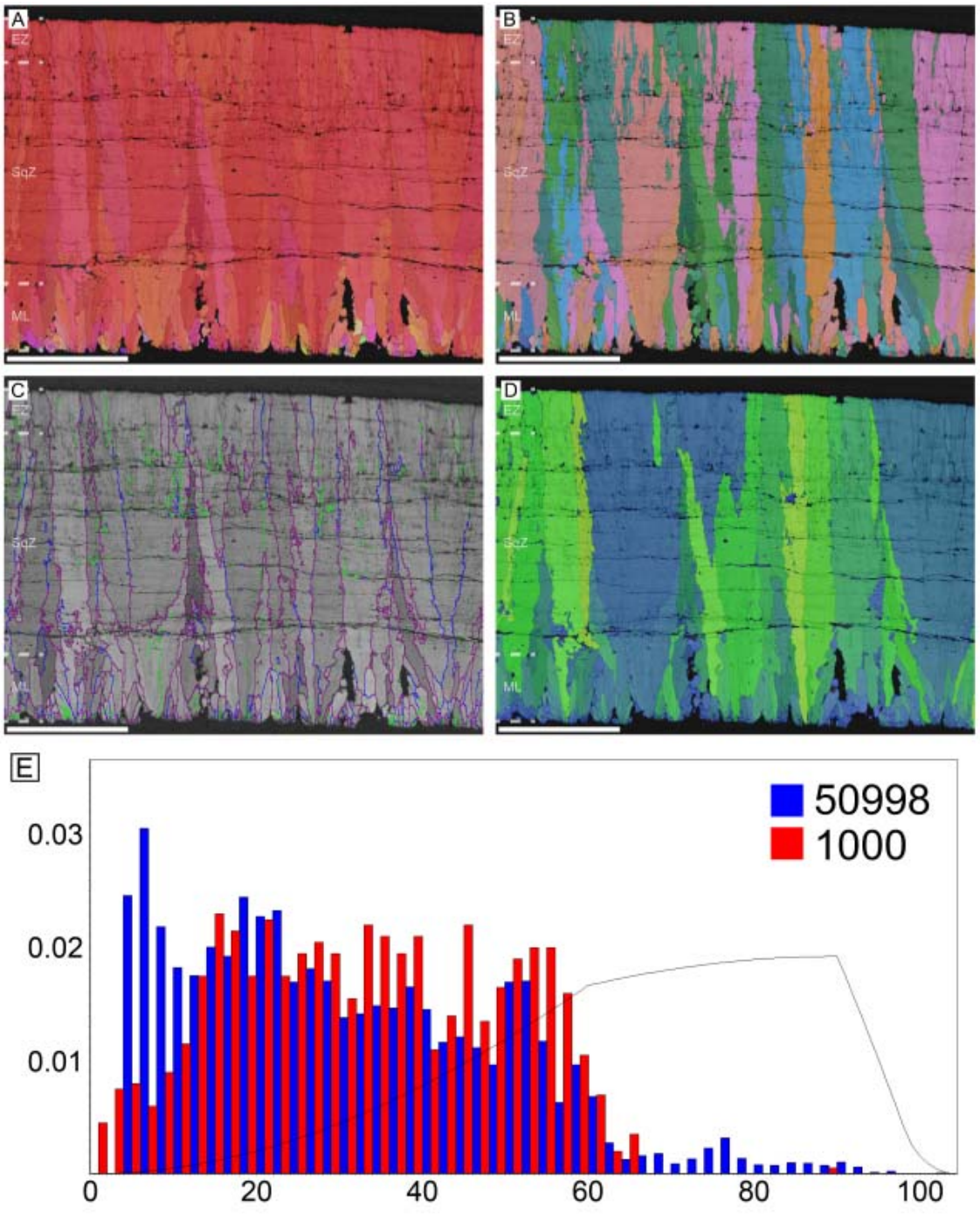

Figure 11. Thick moa eggshell (potential egg of *Dinornis*). Scale bars equal 500 µm.

This specimen is an unequivocal eggshell of *Dinornis novaezealandiae* (see Appendix 1; Gill,

2021). The microstructure is similar to that of ostrich eggshell in that long prismatic shell units occupy the whole thickness of the eggshell although the shell units are not as narrow as those of ostrich eggshell (Figure 11). The ML is wedge-like. It is worth mentioning that the outline of ML is round (Appendix 1—figure 3E). The boundary between the ML and SqZ, SqZ and EZ are not clear because the 'splaying' of the SqZ is very weak as in ostrich eggshell. However, as in the case of ostrich eggshell, the GB condition provides an alternative way for identification of SqZ and EZ (Appendix 1—figure 1D). Low-angle GB are not confined to a certain layer, but widespread in the eggshell. Similar to ostrich eggshell, GB are mostly linear and lack 'splaying' microstructure and highly rugged GB in SqZ. However, in magnified view, one can observe slight ruggedness in SqZ (Appendix 1—figure 1D).

Lithornis

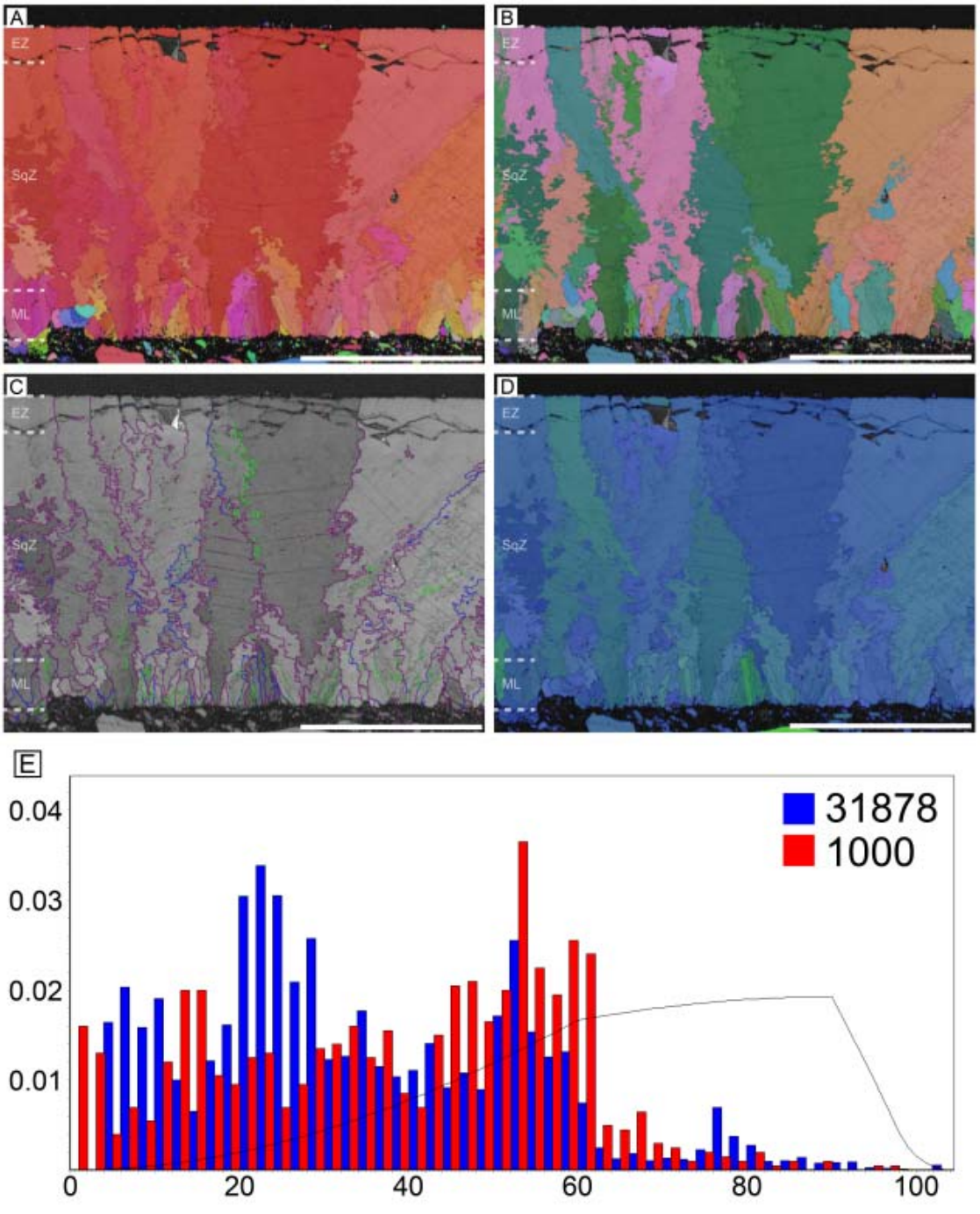

Figure 12. *Lithornis* eggshell (see also Houde, 1988; Grellet-Tinner and Dyke, 2005). Scale bars equal 250 µm.

298 Paleocene *Lithornis* eggshell has many features in common with tinamou eggshells (Figure
299 12; Houde, 1988; Grellet-Tinner and Dyke, 2005). The ML of *Lithornis celetius* eggshell is
300 composed of needle-like calcite and overall shape of ML is weakly round in some parts of the
301 eggshell. The SqZ shows clear 'splaying' structure and the crystals of EZ is massive.
302 *Lithornis* eggshell is more similar to the Chilean tinamou eggshell compared to the elegant
303 crested tinamou eggshell. Low-angle GB is mostly present in ML. ML and EZ are composed
304 of linear GB, while SqZ is composed of rugged GB. The prominent slash patterns inside the
305 SqZ are calcite twinning, which are diagenetically deformed calcite structure only found in
306 fossil eggshells (i.e. abiogenic in origin; Choi et al., 2021, under review). See also Grellet-
307 Tinner and Dyke (2005) for SEM micrographs of *Lithornis vulturinus* eggshell that has
308 wedge-like ML.

309 See also Appendix 1 and Appendix 1—figures 4–12 for selected neognath and non-avian
310 maniraptoran dinosaur eggshells for comparison.

311

312 Overview for inverse pole figure mapping

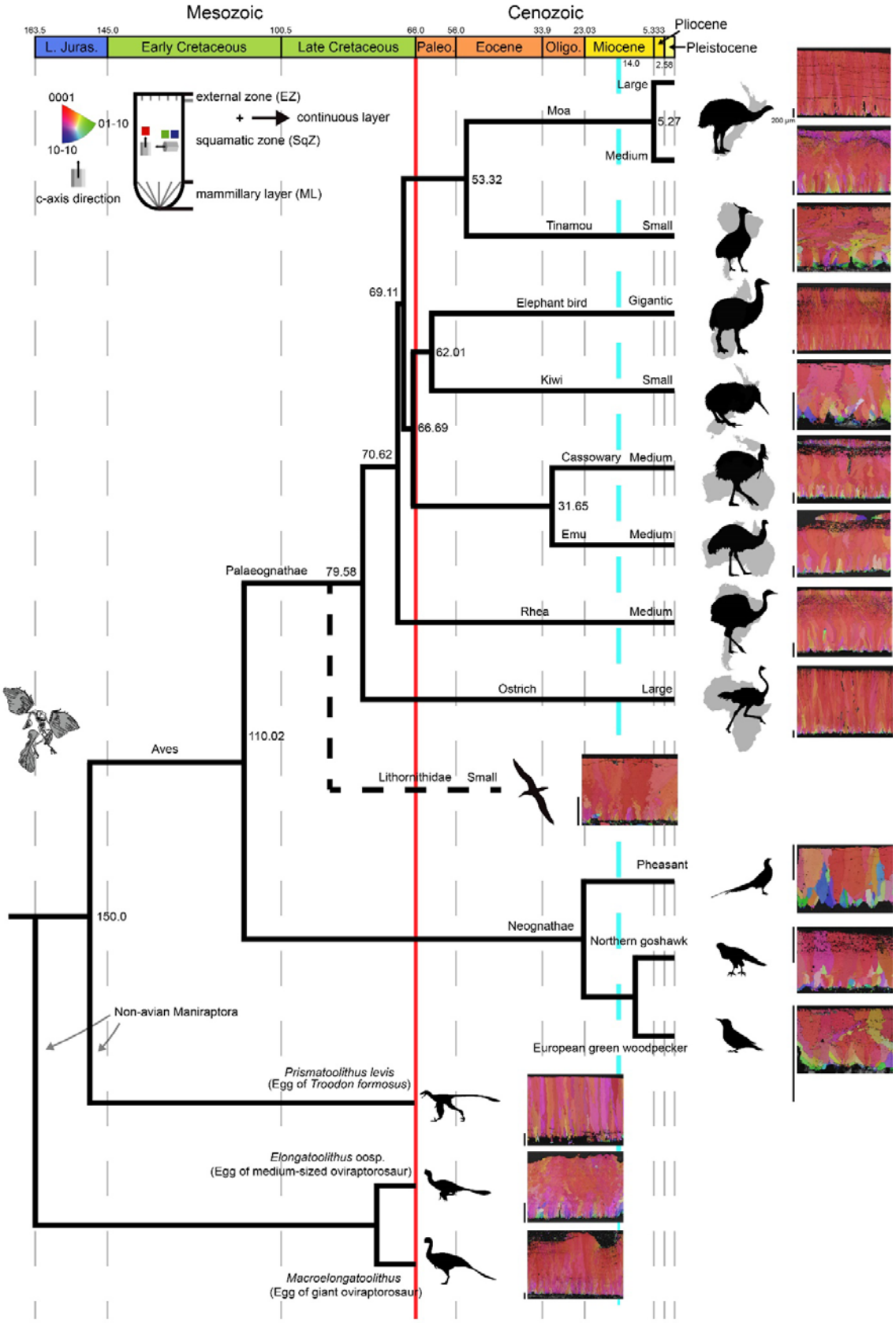

313

Figure 13. IPF mappings of palaeognath, neognath, and non-avian maniraptoran eggshells. The phylogeny and speciation timelines of palaeognath are based on Yonezawa et al. (2017) and Bunce et al. (2009); branching in neognath and non-avian Maniraptora are arbitrary, not reflecting specific time. The speciation time of Lithornithidae (marked with a dashed line) is unknown. Silhouettes represent taxa and their habitats. All scale bars left to the IPF mappings is 200 μm. A red solid line marks K/Pg boundary; a dashed skyblue line denotes the initiation of cooling events in Miocene that might have caused gigantism of Palaeognathae (Crouch and Clarke, 2019). Silhouettes are attributable to (http://www.phylopic.org): Emily Willoughby (*Citipati*); Scott Hartman (Paraves), and Matt Martyniuk (*Gigantoraptor*). Other artworks are drawn by SC and NHK.

Morphologically, palaeognath eggshells had been loosely categorized into three morphotypes (Zelenitsky and Modesto, 2003; Grellet-Tinner and Dyke, 2005; Grellet-Tinner, 2006). Ostrich-style (i.e. ostrich and thick moa eggshell) consists of wedge-like ML and prismatic shell units with near-absence of 'splaying' SqZ. Rhea-style (i.e. rhea, emu, cassowary, elephant bird, and thin & middle thickness moa eggshells) has been characterized by wedge-like ML and splaying SqZ. Finally, the tinamou-style (i.e. tinamou, kiwi, and *Lithornis* eggshells) is represented by needle-like ML, splaying SqZ, and massive EZ (but see below). Noticeable qualitative features (Figure 13) of palaeognath eggshells are: (i) calcite grains have strong vertical *c*-axis alignment (hence, mostly reddish in IPF Y mappings), which may be homologous to that of Mesozoic maniraptoran eggshells (Moreno-Azanza et al., 2013; Choi et al., 2019, 2020, 2022); (ii) ML is mostly composed of wedge-like calcite but needle-like calcite is present or dominant in tinamou-style eggshells (Zelenitsky and Modesto, 2003; Grellet-Tinner and Dyke, 2005; Grellet-Tinner, 2006; Appendix 1—figure 3); (iii) tinamou-

style eggshells have round (or barrel-shaped) ML (Grellet-Tinner, 2006); thick moa eggshell appears to have round ML (Appendix 1—figure 3); (iv) ML and SqZ are easily differentiated due to grain shape differences except for in ostrich-style eggshells where the boundary between the two layers is unclear; (v) calcite in SqZ are mostly 'splaying' (*sensu* Panhéleux et al., 1999). However, calcite in SqZ of ostrich-style eggshells are nearly prismatic; (vi) EZ exists in all palaeognath eggshells; (vii) cassowary and emu eggshells have peculiar ornamentation on the outer surface (= 'granular layer' *sensu* Mikhailov, 1997a) and very porous outer EZ (see Appendix 1—figure 2).

Compared to palaeognath eggshells, neognath eggshells are characterized by: (i) comparatively weak vertical *c*-axis alignment (see Appendix 1—figures 4–8 for selected neognath eggshells; Grellet-Tinner et al., 2017; Choi et al., 2019; López et al., 2021; see also Oser et al., 2021 for a similar case of Mesozoic egg); (ii) boundary between ML and SqZ is not easily identified because of prismatic shell units (Mikhailov, 1997b). However, SqZ of common murre (*Uria aalge*) (Charadriiformes) eggshell is similar to that of rhea-style palaeognath eggshell in that 'splaying' is clear (Appendix 1—figure 7) and the overall structure of European green woodpecker (*Picus viridis*) eggshell (Appendix 1—figure 8) is remarkably similar to that of tinamou-style palaeognath eggshell. Mikhailov (1997a, 2019) pointed out that some eggshells of four neognath clades (Galliformes, Anseriformes, Coraciiformes, and Piciformes) have palaeognath-eggshell-like microstructure and Charadriiformes might be added to this list (Appendix 1—figure 7).

Non-avian maniraptoran eggshells (see Appendix 1—figures 9–12 for selected examples) have strong vertical *c*-axis alignment as in palaeognath eggshells (Moreno-Azanza et al., 2013; Choi and Lee, 2019; Choi et al., 2019, 2020, 2022). Shell unit structure of oviraptorosaur eggshells is similar to that of rhea-style palaeognath eggshells except for

362 needle-like ML, whereas shell unit structure of troodontid eggshell is strikingly similar to
363 ostrich-style palaeognath eggshell. See Choi et al. (2019) for further information.

364

365 Grain boundary mapping and actual size & thickness of egg

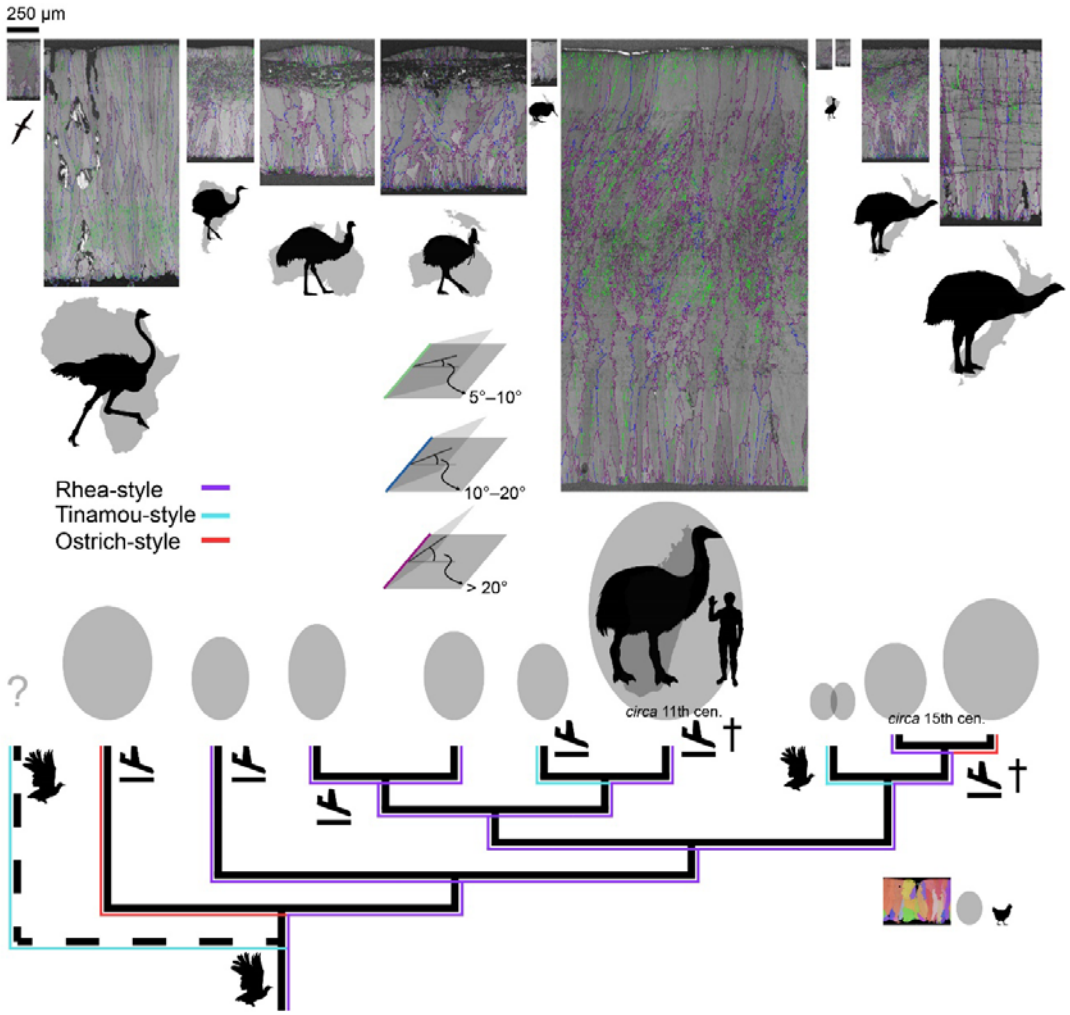

366

367 **Figure 14.** GB mappings, eggshell thickness, and egg size of Palaeognathae. The green, blue,
368 and purple lines in GB mapping denote the angle range between the calcite grains. All
369 eggshell maps (including IPF mapping of chicken eggshell for comparison) are drawn to
370 scale; note a scale bar at the upper left corner. The silhouettes of palaeognath are drawn to

371 scale (note a human next to elephant bird and a chicken at the lower right corner). Egg shape
372 and size are drawn to scale (Hauber, 2014; Stoddard et al., 2017). Two recently extinct
373 lineages are marked by daggers and the extinct Lithorinithidae by a dashed branch. Landing
374 symbols denote potential independent losses of flight (Mitchell et al., 2014; see also Sackton
375 et al., 2019) and flying bird silhouettes denote volant taxa. Sky blue lines show
376 microstructural and crystallographic similarities among tinamou-style eggshells that is
377 attributable to homoplasy. Red lines mean the homoplastic similarities between ostrich-style
378 eggshells. Purple lines represent potential homologies of rhea-style eggshells.

379

380 The main features of palaeognath eggshells are: (i) ostrich-style and rhea-style eggshells have
381 extensive low-angle GB (lower than 20 degrees; green and blue lines in Figure 14) although
382 the positions of high densities of low-angle GB vary in each clade. In ostrich eggshell, low-
383 angle GB are concentrated at the outer part of ML. In rhea, elephant bird, and thin moa
384 eggshells, low-angle GB are mostly concentrated at the SqZ. In emu and cassowary
385 eggshells, low-angle GB are not widespread in SqZ, but abundant in the granular layer. In the
386 thick moa eggshell, low-angle GB is not confined to certain positions; (ii) High-angle GB are
387 dominant in tinamou-style eggshells and low-angle GB are mostly present in ML as in
388 neognath eggshells; (iii) Ruggedness of GB changes abruptly at the boundary between SqZ
389 and EZ in rhea, emu, kiwi, elephant bird, tinamou, and *Lithornis* eggshells although
390 cassowary and thin moa eggshells show less prominent change. The ruggedness of GB is
391 very slightly changed in ostrich-style eggshells, which have prismatic shell units.

392 In general, large eggs have thick eggshells and small eggs have thin eggshells (Figure 14;
393 Ar et al., 1979; Juang et al., 2017). A notable outlier to this trend is kiwi eggs. Although kiwi
394 eggs are large (especially compared to their body size; Abourachid et al., 2019), their

395 eggshell is thin (Vieco-Galvez et al., 2021), comparable to that of smaller tinamou eggshell.
396 Besides, the ellipticity and asymmetry of diverse avian eggs were investigated by Stoddard et
397 al. (2017). We reused their data to present the egg shape indices of palaeognath eggs
398 (Appendix 1—figure 13). The result shows that, compared to neognath eggs, palaeognath
399 eggs are characterized by low asymmetry but ellipticity distribution is not very different from
400 that of neognath eggs, consistent with the result of Deeming (2018).

401

402 Calcite grain aspect ratio

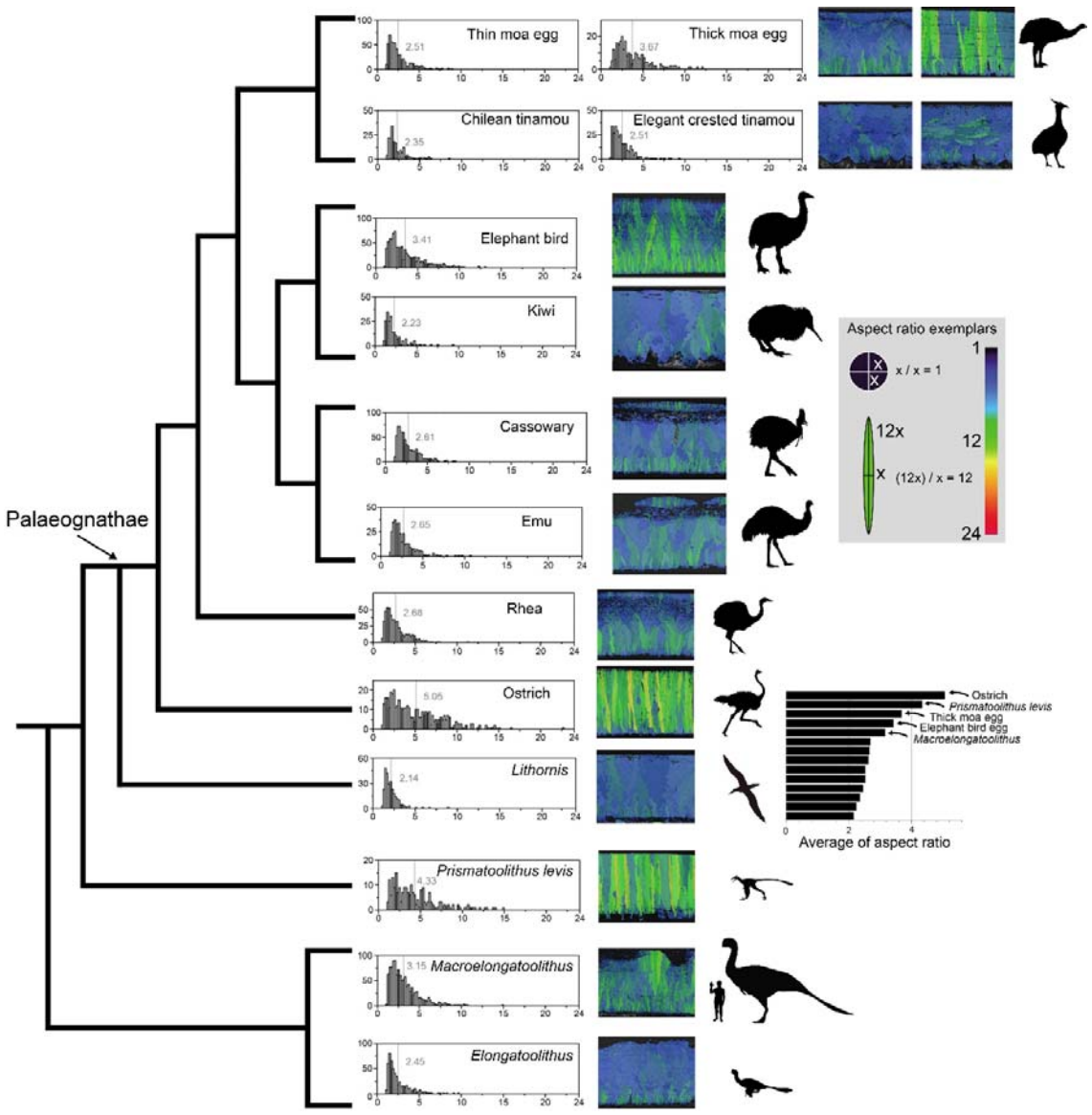

403

404 **Figure 15.** AR mappings and histograms of palaeognath and non-avian maniraptoran
405 eggshells. Note that ostrich, (Late Cretaceous) *Prismatoolithus levis*, giant moa (possibly
406 *Dinornis*), elephant bird, and (Late Cretaceous) *Macroelongatoolithus* eggshells are
407 characterized by higher AR. The vertical bars and numbers in the histograms mean the
408 average point of AR distribution and its value, respectively. Silhouettes of non-avian dinosaur
409 are drawn to scale.

410

411 The main characteristics of palaeognath eggshells are (Figure 15): (i) rhea, emu, cassowary,
412 kiwi, tinamou, thin moa, and *Lithornis* eggshells have relatively low aspect ratio (AR); (ii)
413 ostrich, elephant bird, and thick moa eggshells show high AR. Compared to other
414 palaeognath eggshells, these three eggshells have highly positively skewed AR distribution as
415 well. Notably, these three eggshells are also the thickest among the palaeognath eggshells
416 (Figure 14).

417 Neognath eggshells analysed in this study do not show high AR (Appendix 1—figures 4–
418 8). *Prismatoolithus levis* and *Triprismatoolithus* show high AR, while *Elongatoolithus* has
419 low AR (Appendix 1—figures 9–12). Intriguingly, *Macroelongatoolithus*, which was
420 suggested to have 'cryptoprismatic' shell unit structure (Jin et al., 2007) shows intermediate
421 AR between the two extremes (Figure 15).

422 Appendix 1 and Appendix 1—figure 3 discuss how AR could be used to diagnose 'needle-
423 like' calcite grains in ML.

424

425 Misorientation distribution

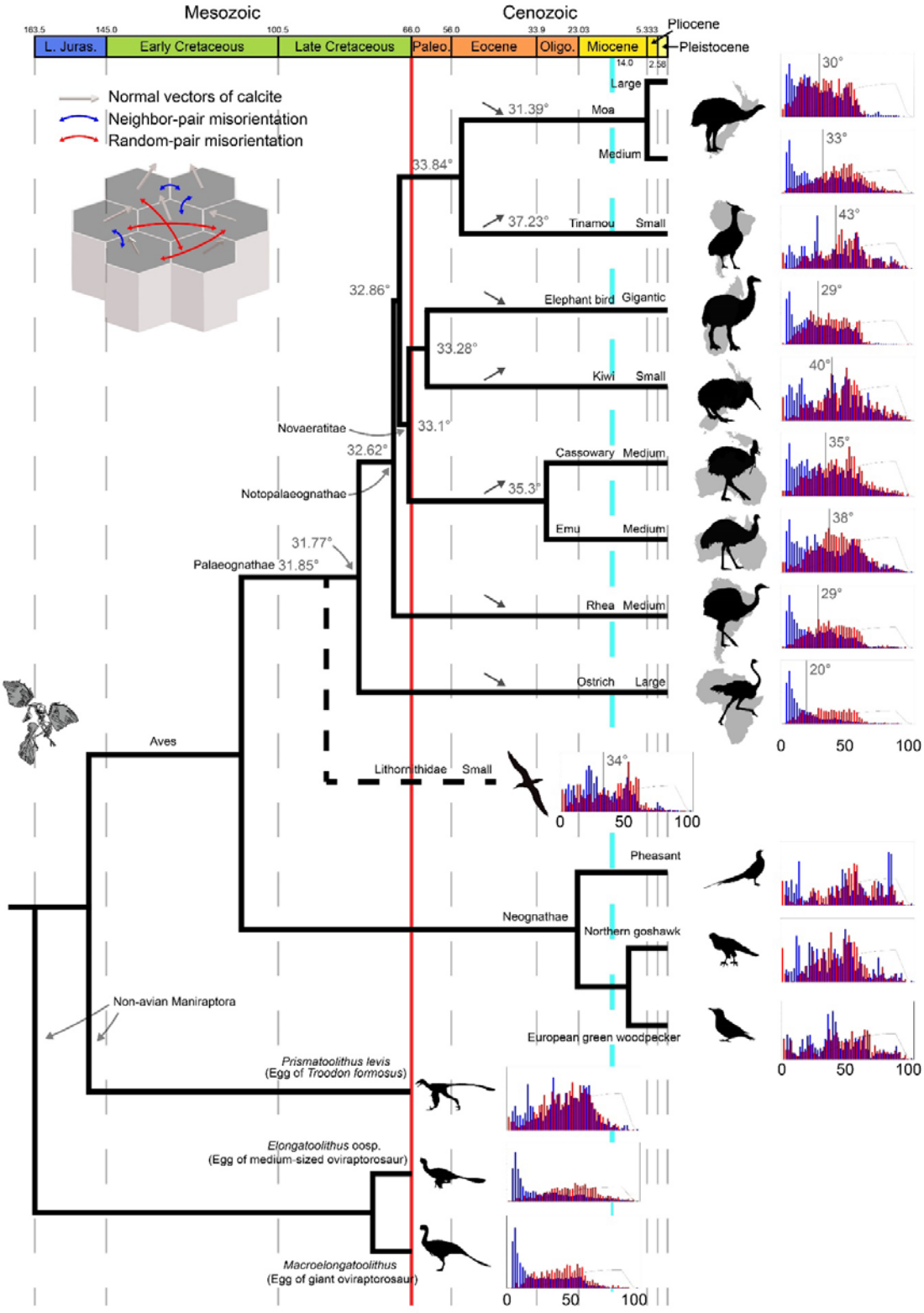

Figure 16. Misorientation distributions of palaeognath, neognath, and non-avian

maniraptoran eggshells (adapted from Figure 13). The vertical bars and numbers in the histograms mean the average point of neighbour-pair misorientation (blue) and its value, respectively. The numbers at the nodes represent the ancestral states for mean of neighbour-pair MD (note that only one MD of tinamou eggshell was shown for brevity). Up and down arrows mark the changing ancestral state trends of each node compared to the nearest ancestral states.

Choi et al. (2019) showed that low-angle (< 20 degrees) are dominant in the misorientation distribution (MD) of ostrich and rhea eggshells whereas high-angle (> 20 degrees) are dominant in MD of neognath eggshells analysed in that study. In this study, MD information of palaeognath eggshell is extended to all clades of Palaeognathae. Ostrich and rhea eggshells show low-angle dominant MD under neighbour-pair method (hereafter Type 1 distribution *sensu* Choi et al., 2019; Figure 16). This pattern is also present in elephant bird, thin, and middle thickness moa eggshell. Emu, cassowary, and thick moa eggshells show slightly different MD: low-angle is less well-dominant compared to the eggshells of the ostrich, rhea, elephant bird, and thin & middle thickness moa eggshells. In contrast, eggshells of kiwi, tinamou, and *Lithornis* have more high-angle dominant MD. The MD patterns of palaeognath eggshells are more diverse than previously postulated by Choi et al. (2019).

Neognath eggshells used in this study showed high-angle (> 20 degrees) dominant MD, consistent with the result of Choi et al. (2019) (hereafter, Type 2 distribution *sensu* Choi et al., 2019; Figure 16). As far as we know, there is no neognath eggshell that has Type 1 distribution. Even though microstructure of common murre eggshell is similar to that of rhea-style palaeognath eggshell, it does not have Type 1 distribution (Appendix 1—figure 7).

As discussed in Choi et al. (2019), Type 1 and 2 distributions already existed in Cretaceous

452 non-avian maniraptoran eggshells (Figure 16; see also Moreno-Azanza et al., 2013; Choi and
453 Lee, 2019; Choi et al., 2020, 2022).

454

455 Ancestral state reconstructions

456 Ancestral states for mean of neighbour-pair MD are very similar for both phylogenetic trees
457 (Yonezawa et al., 2017; Kimball et al., 2019), with a relatively constant ancestral value
458 (~32°) for several major palaeognath clades (Palaeognathae, Notopalaeognathae,
459 Novaeratitae – clade names *sensu* Sangster et al., 2022; Figure 16). A conspicuous increase is
460 observed for both Casuariiformes (34.7° [Kimball] or 35.3° [Yonezawa]) and Tinamiformes
461 (35.5° [Kimball] or 37.2° [Yonezawa]), while Dinornithiformes show a slight decrease (31.2°
462 [Kimball] or 31.4° [Yonezawa]). The Apterygiformes-Aepyornithiformes clade shows only a
463 minor increase (33.3° for both trees), reflecting the divergence between its two sampled
464 members (high value [40.4°] for *Apteryx*, low value [29.5°] for *Aepyornis*). Within
465 Notopalaeognathae, the lowest values are observed in elephant bird and moa, potentially
466 reflecting a low-angle trend associated with gigantism within that clade. The fact that high
467 values are found for both small (tinamous, kiwi) and large (emu, cassowary) taxa suggests
468 that the reverse is not true, although a larger sample size would be necessary to test that
469 hypothesis. The ostrich shows a very low value (20.1°) compared to other Palaeognathae,
470 suggesting a distinctive crystalline structure within its eggshell. This low value in the ostrich,
471 however, does not affect the ancestral state at the Palaeognathae node in either tree – likely
472 due to the inclusion of *Lithornis*, the earliest-diverging taxon in our sample, which shows a
473 misorientation value of 34.0° closer to that of the recovered ancestral state for Palaeognathae
474 (~32°).

475 Ancestral states for AR on the tree from Yonezawa et al. (2017) do not exhibit any

476 conspicuous pattern for major clades, with all internal nodes showing very similar values
477 (~2.6). This is likely due to the small range in values for terminal taxa (2.14–5.05, with all
478 but three species within a 2.14–3 range; Figure 15), which might also explain the very low
479 phylogenetic signal for that trait. The distribution of AR among Palaeognathae seems to be
480 correlated with that of body mass: the highest values (> 3.4) are observed in large species (>
481 100 kg – *Struthio*, Aepyornithidae, and *Dinornis*); small species (< 10 kg – *Apteryx*,
482 *Eudromia*, *Nothoprocta* and *Lithornis*) show lower values (< 2.5); and medium-sized species
483 (*Rhea*, *Dromaius*, and *Casuarius*) present an intermediate AR. The only exceptions are the
484 two smaller moa species, which show a much smaller AR (*Pachyornis*: 2.51; *Euryapteryx*:
485 2.34) than expected for their body mass, comparable to that of tinamous. The two clades
486 (*Eudromia*, *Nothoprocta*) and (*Pachyornis*, *Euryapteryx*) are the only subclades recovered
487 with an ancestral AR under 2.6. This could potentially reflect a synapomorphy of calcite grain
488 structure in Dinocrypturi (moa + tinamou), albeit not recovered for this small sample due to
489 the high value in *Dinornis*. The ostrich is recovered as a clear outlier with the highest value in
490 the sample (5.05), again supporting a highly autapomorphic crystalline structure in its
491 eggshell.

492

493 **Discussion**

494 Evolution of the palaeognath eggshells through time

495 The phylogeny of Palaeognathae has experienced a set of revolutionary changes since 2008
496 (compare Livezey and Zusi, 2007 and Yonezawa et al., 2017) and it provides an unexplored
497 chance to trace the evolution of microstructure and crystallography of modern dinosaur
498 eggshells. We interpret our results following the phylogeny of Yonezawa et al. (2017), which
499 provides estimated speciation timelines. But it should be noted that Cloutier et al. (2019) and

Sackton et al. (2019) report an alternate phylogeny, which are characterized by a switching of the positions of rhea and (tinamou + moa). See Appendix 1 and Appendix 1—figures 14–16 for interpretation based on the phylogeny of Cloutier et al. (2019) and Sackton et al. (2019).

(i) Rhea-style microstructure would be synapomorphic to all Palaeognathae or more inclusive monophyletic group of birds (Figure 14) considering the presence of rhea-style eggshells in the Neognathae (see above; see also Mayr and Zelenkov, 2021 for skeletal similarities between the Neognathae and a potential stem group Struthioniformes) and the presence of supposedly rhea-style eggshells in the Upper Cretaceous deposits (see below). Alternatively, Palaeogene *Lithornis* eggshell may represent the synapomorphic microstructure of Palaeognathae. Volant tinamou and *Lithornis* (Altimiras et al., 2017; Torres et al., 2020) share considerable similarity not only in their skeletal characters (Houde, 1988; Nesbitt and Clarke, 2016), but also in their eggshell microstructure (Houde, 1988; Grellet-Tinner and Dyke, 2005) and crystallography (this study). However, if we assume that similar microstructure of tinamou and *Lithornis* eggshells are indeed homology, then its corollary is that very similar rhea-style microstructure evolved from tinamou-style microstructure independently at least four times (Appendix 1—figure 17). Considering the remarkable microstructural similarities among rhea, casuariid, elephant bird, and moa eggshells, a more reasonable interpretation is that rhea-style eggshells are homologous and the similarity between tinamou and *Lithornis* eggshells is homoplastic (Figure 14). Indeed, the similarity between *Lithornis* and tinamou eggshells is not as complete as that of rhea-style eggshells, and the former similarity may be better described as ‘incomplete convergence’ (*sensu* Herrel et al., 2004; see also Losos, 2011).

(ii) The three tinamou-style eggshells (tinamous, kiwi, and *Lithornis*) would be homoplastic because the tinamou-style of kiwi would be autapomorphic as well. In fact,

524 although Zelenitsky and Modesto (2003) observed acicular ML in kiwi and tinamou
525 eggshells, the EBSD image of kiwi eggshell shows that wedge-like calcite is more dominant
526 in ML (Figure 5) and this view is in agreement with the view of Grellet-Tinner (2006). Thus,
527 the morphological cohesiveness of 'tinamou-style' is not as solid as that of rhea-style
528 eggshell, so we would suggest that the loosely categorized 'tinamou-style' (e.g. Grellet-
529 Tinner and Dyke, 2005) should not be understood as homologous entity.

530 The homoplasy interpretation of tinamou and *Lithornis* eggshells brings about an
531 unresolved question. Among the mostly flightless Palaeognathae, tinamou and *Lithornis* are
532 capable of flight (Figure 14). Legendre and Clarke (2021) showed that flight affects eggshell
533 thickness, but the authors suggested that whether flight affects microstructures of avian
534 eggshells should be further investigated. Mitchell et al. (2014) proposed that there were at
535 least six loss of flight events (Figure 14) in palaeognath lineages (see also Sackton et al.,
536 2019). If so, most of the loss of flight events did not cause a transition in eggshell
537 microstructure (i.e. rhea, Casuariidae, elephant bird and small to medium sized moa). Ostrich,
538 kiwi, and thick moa eggshells are exceptions to this trend although there is possibility that
539 ancestral flightless ostrich, kiwi, and large moa eggshells might have rhea-style
540 microstructure in the first place. This hypothesis can be only testable through (unexplored)
541 fossil record.

542 In this scenario, volant tinamou and *Lithornis* acquired roughly similar microstructure
543 although they maintained flight (Figure 14), meaning that maintaining or abandoning of flight
544 had little influences on microstructures. Instead, the exotic microstructure of tinamou might
545 be related to their cladogenesis (Almeida et al., 2022) because thin and middle thickness moa
546 (a sister clade of tinamou; Phillips et al., 2010) eggshells maintain rhea-style microstructure.
547 Similarly, the microstructure of kiwi eggshell (see also Vieco-Galvez et al., 2021) would be

548 autapomorphic considering the rhea-style microstructure of its sister clade elephant bird
549 (Mitchell et al., 2014). Considering that ancestral kiwi might have been a volant clade
550 (Worthy et al., 2013), the disproportionally large size of egg and peculiar microstructure of
551 kiwi might have appeared when the cladogenesis of (flightless and extremely precocial)
552 Apterygidae took place (Worthy et al., 2013).

553 If cladogenesis is indeed related to the evolution of autapomorphic microstructures (see
554 also ostrich-style and casuariid eggshells below), it may have implication for Lithornithidae
555 monophyly (Widrig and Field, 2022). The monophyly of Lithornithidae is supported by
556 recent views (Nesbitt and Clarke, 2016; Yonezawa et al., 2017) but there are also different
557 results that support lithornithid paraphyly (Houde, 1988; Worthy et al., 2017). Compared to
558 other clades of Palaeognathae, tinamou and kiwi are speciose (Weir et al., 2016; Almeida et
559 al., 2022). If all members of respective group share similar microstructure, it may mean that
560 autapomorphic microstructure may be a feature of monophyletic group. Then, the
561 autapomorphic microstructure of *Lithornis* eggshell may indirectly support lithornithid
562 monophyly rather than paraphyly.

563 (iii) Homoplasy-based explanation can be also applicable to the similarity between the two
564 ostrich-style eggshells. Ostrich have developed their peculiar eggshell microstructure after
565 the split from all other Palaeognathae in Late Cretaceous (Figure 13). In case of moa, the
566 cladogenesis of *Dinornis* (ostrich-style eggshell) and other moa (rhea-style eggshells) might
567 have happened in 5.27 Ma (Bunce et al., 2009). Thus, considering the phylogenetic topology
568 of Palaeognathae, the similarity between ostrich and thick moa eggshells was not derived
569 from the common ancestry, therefore, it is homoplasy (Figure 14).

570 (iv) Casuariid (emu and cassowary) eggshells are nearly identical. We interpret that their
571 MRCA that lived in Palaeogene Australia (a flightless bird most likely adapted to vegetated

572 and very humid habitat as modern cassowary does; Moore, 2007; Worthy et al., 2014;
573 Mitchell et al., 2014) had already acquired this unique microstructure. Cassowary still lives in
574 humid environments of New Guinea and northeastern Australia, but emu is widely distributed
575 in Australia, including arid environments (Langley, 2018). The role of peculiar microstructure
576 in casuariid eggshells in drastically different environments should be further investigated
577 unless emu have maintained their microstructure simply due to 'phylogenetic inertia' effect
578 (Edwards and Naeem, 1993; but see also Shanahan, 2011). The similarity between emu and
579 cassowary eggshells would be homology.

580 (v) The rate of evolutionary change in microstructures of eggshell varies among clades.
581 Casuariid eggshells show long stasis; eggshells of both emu and cassowary changed little
582 since their speciation (31.65 Ma; Figure 13). In contrast, moa eggshells imply a very different
583 story. Bunce et al. (2009) stated that large and medium sized moa diverged in the Pliocene
584 (5.27 Ma; Figure 13). This is not necessarily a long time-interval in evolutionary biology and
585 palaeontology, but moa eggshells show very different microstructures and crystallography
586 (Figures 9–11). The contrasting stubborn conservatism (Casuariidae) and swift change (moa)
587 in eggshell microstructure may mean that phenotypic evolution of microstructure of eggshell
588 might not be gradual (e.g. Gould and Eldredge, 1993; see also Pennell et al., 2014a).

589 (vi) Rhea- and 'ostrich-style' eggshells have Type 1 distribution of MD (or weakened Type
590 1) while 'tinamou-style' eggshells have Type 2 distributions of MD, therefore, MD pattern of
591 palaeognath eggshells are more complicated than the one postulated by Choi et al. (2019).
592 Choi et al. (2019) posed two scenarios to infer the ancestral MD of Neornithes: the first
593 hypothesis assumed that Type 1 distribution of Palaeognathae is directly inherited from non-
594 paravian dinosaurs; the second hypothesis assumed that Paraves acquired Type 2 distribution
595 while Palaeognathae re-evolved Type 1 distribution. However, both hypotheses assumed that

596 the ancestral state of MD of Palaeognathae is Type 1 although Choi et al. (2019) analysed just
597 ostrich and rhea eggshells. According to the ancestral state reconstruction presented in this
598 study, it is highly likely that early-diverging Palaeognathae had the weak Type 1 MD
599 notwithstanding the fact that volant *Lithornis* eggshell is characterized by Type 2 MD (Figure
600 16). Unless this view is negated by future findings, currently, our results show that the two
601 hypotheses posed by Choi et al. (2019) are based on valid postulation (Type 1 MD for
602 ancestral state), which raises additional scientific questions (see below).

603 We note that our interpretation is mainly based on the phylogeny of Yonezawa et al. (2017),
604 but that might not be the final consensus on this issue (e.g. Sackton et al. 2019). Hence, the
605 interpretation of palaeognath eggshell evolution should depend on the ongoing advancements
606 of palaeognath phylogeny and should be updated accordingly (e.g. agreement on the topology
607 of tree, revised timelines of evolution, inclusion of new fossil taxa data).

608

609 Implications to palaeontology

610 Palaeognath eggshells provide useful insights into palaeontology (Figures 13, 15, 16) as a
611 modern analogue.

612 (i) Similar-looking eggshells can be laid by closely-related taxa (e.g. Casuariidae).
613 However, closely-related taxa can lay very different eggshells (e.g., differing eggshell among
614 moa taxa). In palaeontology, an embryo of non-avian dinosaur *Troodon formosus* was found
615 in an egg named *Prismatoolithus levis* (Varricchio et al., 2002). This taxon-ootaxon
616 relationship has been widely (or over-widely) accepted that many prismatoolithid eggs were
617 recognized as troodontid eggshell but it should be used with caution (see Mikhailov, 2019).
618 There is possibility that at least some troodontid dinosaurs might have laid eggshells

619 dissimilar to *P. levis* as in the case among moa species. On the other hand, distantly-related
620 non-avian dinosaur taxa might have laid similar-looking eggshells independently as in the
621 case of ostrich and thick moa eggshells. These palaeognath eggshells are also
622 morphologically very similar to eggshell of *Troodon formosus* (Zelenitsky and Hills, 1996;
623 Zelenitsky et al., 2002; Varricchio and Jackson, 2004), another clear case of homoplasy
624 (Figure 15).

625 (ii) Differentiating homology from homoplasy in similar-looking phenotypes should have
626 paramount importance in morphology-based fossil egg palaeontology (e.g., Choi et al., 2020).
627 It is highly likely that prismatic microstructures of *P. levis*, ostrich, and thick moa eggshells
628 are the outcome of homoplastic evolution. In palaeontology, many different types of
629 eggshells are assigned to the oofamily Prismatoolithidae because they have prismatic shell
630 unit structure, but it might be composed of eggshells from polyphyletic egg-layers. For
631 example, if modern ostrich eggshell and thick moa eggshells are parataxonomically classified
632 solely based on morphological criteria, they may be classified as 'Prismatoolithidae' although
633 (moa + ostrich) is not a monophyletic group. Unless homoplastic characters are appropriately
634 separated, the endeavors of parataxonomic systematics would have little evolutionary
635 biological values but merely limited to morphological classification (Mikhailov, 2014, 2019;
636 see also Varrichio and Jackson, 2004), which is sometimes vulnerable to homoplasy (Livezey
637 and Zusi, 2007; Yonezawa et al., 2017). In addition, for a better understanding of taxon-
638 ootaxon relationship, homoplastic and homologous similarities should be clearly separated
639 (e.g. see case of Tuştea Puzzle; Grigorescu, 2017; Botfalvai et al., 2017). McInerney et al.
640 (2019) showed that the syrinx, hyoid, and larynx of Palaeognathae are less prone to
641 homoplastic evolution, thus, they might be more valuable for morphology-based
642 classification of Palaeognathae. Similarly, future eggshell studies may concentrate on finding

643 less-homoplasy-prone morphological entities of eggshells.

644 (iii) Prismatic microstructure might be derived from rhea-style microstructure. Among non-
645 avian maniraptoran eggshell, *Elongatoolithus* exhibits a rhea-style microstructure but
646 *Prismatoolithus* presents an ostrich-style one (Figure 13). Intriguingly, the eggshell of
647 gigantic oviraptorosaur (Pu et al., 2017) *Macroelongatoolithus* has an intermediate AR
648 between *Elongatoolithus* and *Prismatoolithus* (Figure 15). It may represent the intermediate
649 stage between the two morphotypes that might be related with the gigantism of
650 oviraptorosaur. Although correlation is not very clear, we would like to emphasize that thick
651 eggshell of ostrich and large moa are characterized by ostrich-style microstructure (hence,
652 high AR) and the thickest elephant bird eggshell also has high AR (Figure 15). Investigating
653 the relationship between the egg size, eggshell thickness, and AR of extinct maniraptoran
654 eggshell from more future findings may provide further insight into the evolution and
655 function of eggshell microstructure.

656 (iv) There are thin 'ratite-morphotype' fossil eggshells from the Upper Cretaceous deposits
657 (discussed in Choi and Lee, 2019). Considering the estimation that Palaeognathae and
658 Neognathae diverged in the Early Cretaceous (Lee et al., 2014; Yonezawa et al., 2017; Figure
659 13), at least some of Late Cretaceous 'ratite-morphotype' eggshell might belong to early-
660 diverging (and volant) Palaeognathae. For example, the European ootaxa *Sankofa pyrenaica*
661 (López-Martínez and Vicens, 2012), *Pseudogeckoolithus* cf. *nodosus*, and *P*. aff. *tirboulensis*
662 (Choi et al., 2020) have remarkable rhea-style microstructure. Although, here again, the
663 possibility of homoplasy should not be overlooked, further studies on Cretaceous materials
664 may provide new indirect evidence on the presence of Palaeognathae in the Cretaceous. In
665 fact, the presence of Neognathae in Late Cretaceous was confirmed by body fossils from
666 Maastrichtian (Late Cretaceous) deposits in Antarctica (Clarke et al., 2005) and Europe (Field

667 et al., 2020), indirectly supporting the presence of Palaeognathae in the Late Cretaceous. If
668 some Late Cretaceous rhea-style 'ratite-morphotype' eggshells turn out to be true palaeognath
669 eggshell, our interpretation (Figure 14) will be further supported with evidence.

670 (v) The ancestral state reconstruction of MD exemplifies the importance of fossils in
671 ancestral reconstructions, especially when focusing on early nodes with a high discrepancy
672 between extant and extinct species (e.g. Finarelli and Flynn, 2006; Li et al., 2008; Cascini et
673 al., 2019; Soul and Wright, 2021). Maddison et al. (1984) pointed out that, ideally, at least
674 two outgroups are necessary to unambiguously polarize characters of ingroup taxa. In our
675 study, the only outgroup for extant palaeognath eggshells is *Lithornis* eggshell. However, at
676 least some rhea-style fossil eggshells from the Upper Cretaceous deposits (e.g.
677 *Pseudogeckoolithus*) are characterized by Type 2 MD, which is also observed in *Troodon* and
678 enantiornithine eggshells (Figure 13; Choi et al., 2019, 2020). If these rhea-style eggshells are
679 confirmed as true palaeognath eggshells and can be included in the future ancestral
680 reconstruction analysis, the ancestral state interpretation might be affected. With an additional
681 outgroup down the phylogenetic tree of Palaeognathae, a better interpretation would be
682 possible.

683 (vi) The current parataxonomic classification usually used by palaeontologists is a
684 compromise between the Linnean rank system (e.g. oofamily. oogenus, and oospecies;
685 Mikhailov et al., 1996) and Hennigian cladistic approach (e.g. Varricchio and Jackson, 2004;
686 Grellet-Tinner et al., 2006; Zelenitsky and Therrien, 2008). It is similar to a philosophy of
687 evolutionary taxonomists who asserted that classification should find a balance between the
688 overall similarity and genealogical history (Wiley and Lieberman, 2011, p. 3). They defined
689 groups based on criteria (e.g. diagnosis) rather than common ancestry. We agree that naming
690 a fossil egg with binomial nomenclature and diagnosis has clear merits for stratigraphic

691 purposes and communications among researchers (Mikhailov, 2014). However, to guarantee
692 the objectivity and reproducibility of the classification, we also agree that cladistic approach
693 should be preferred over somewhat arbitrary similarity-based classification.

694 Nevertheless, the current cladistic approach for palaeoology is not without weaknesses.
695 When a character of two or more different egg types is similar, they are coded into a same
696 state (e.g. '0' or '1'). The presumption of this step is that the shared character state is a shared
697 homolog (Wiley and Lieberman, 2011, p. 13). Again, without the assurance that the same
698 character state is not a homoplasy, the presumption can collapse, and the resultant cladogram
699 can be a 'contaminated' result. That being said, homoplasies can be still useful for
700 ootaxonomy because homoplasies may separately contribute to defining two or more
701 monophyletic ootaxa. Wiley and Lieberman (2011, p. 119) stated "… some homoplasies,
702 taken together, are homoplastic; but taken separately, each may be independent taxic
703 homologies of the monophyletic groups with which they are associated as a diagnostic
704 property". In palaeognath eggshells, for example, roughly defined 'prismatic shell units' of
705 ostrich and thick moa eggshells are homoplastic. However, if the similar features of
706 'prismatic shell units' of both eggshells are used as their respective synapomorphy, the
707 homoplasies will become new respective synapomorphies of the members of a formerly
708 'polyphyletic group' (i.e. ostrich + moa).

709

710 Future research suggestions

711 The abundance of palaeognath eggshells in Cenozoic deposits makes it a biostratigraphically
712 meaningful fossil (Stidham, 2004; Harrison and Msuya, 2005), but their microstructure and
713 crystallography have rarely been studied. Palaeognath eggshells are widely distributed in
714 Cenozoic deposits with palaeontological or archaeological significance across Africa, Asia,

715 Europe, and Oceania. The eggshells have been conventionally differentiated into 'struthionid'
716 and 'aepyornithid' types based on the shape of pore openings (Sauer, 1972). This simple
717 criterion has been widely adopted in subsequent studies (Sauer and Rothe, 1972; Stern et al.,
718 1994; Harrison and Msuya, 2005; Donaire and López-Martínez, 2009; Patnaik et al., 2009;
719 Wang et al., 2011; Pickford, 2014; Blinkhorn et al., 2015; Field, 2020; Mikhailov and
720 Zelenkov, 2020). However, Hirsch et al. (1997, p. 363) stated that "The 'struthionid' and
721 'aepyornithid' pore system … should not be used solely in the identification and
722 classification of eggshell". Furthermore, slit-like (= 'aepyornithid') and circular pores (=
723 'struthionid') coexist in some Neogene palaeognath eggshell fragments (Bibi et al., 2006;
724 Pickford, 2014) and Quaternary moa eggshells (Gill, 2007, 2021). Potentially, the two
725 different pores may represent just different parts of the egg, at least in some species (Bibi et
726 al., 2006). Instead, we suggest that microstructural and crystallographic approaches presented
727 in this study would provide a better basis for identifying and archiving poorly understood
728 Cenozoic palaeognath eggshells.

729 Palaeoenvironmental information can be acquired from eggshells (Stern et al., 1994;
730 Montanari, 2018; Niespolo et al., 2020, 2021). Because Cenozoic palaeoenvironmental or
731 geological events that might have influenced the evolution of Palaeognathae are
732 comparatively well understood (Mitchell et al., 2014; Claramunt and Cracraft, 2015; Grealy
733 et al., 2017; Yonezawa et al., 2017; Crouch and Clarke, 2019; Figure 13), further analytical
734 investigation on Cenozoic palaeognath eggshells with proper geological and climatological
735 contexts may shed light on the palaeoenvironmental settings of fossil localities and their
736 effects in the evolution of Palaeognathae and its eggshells.

737 Zooarchaeology (or anthrozoology) is an additional serendipitous field that can be
738 benefited by thorough understandings of palaeognath eggshells. Palaeognath eggs were not

739 only important food resource for hunter-gatherers (Oskam et al., 2011; Collins and Steele,
740 2017; Diehl et al., 2022) but were also used for cultural purposes such as ornaments or
741 storage containers (Texier et al., 2010; Langley, 2018; Wilkins et al., 2021; Miller and Wang,
742 2022), thereby, they are common in archaeological sites. Because chronological and
743 palaeoenvironmental information inscribed in palaeognath eggshells in archaeological sites
744 are available through isotopic analyses (Sharp et al., 2019; Niespolo et al., 2020, 2021),
745 detailed microstructural information for those eggshells may provide more colourful
746 implications (e.g. identification, harvest timing of egg, and biostratigraphy) about the
747 interactions between early human, specific palaeognath avifauna, palaeoenvironments, and
748 the precise age of palaeognath eggshell materials (e.g. Harrison and Msuya, 2005; Loewy et
749 al., 2020; Niespolo et al., 2021; Douglass et al., 2021a, b). For this, a solid understanding for
750 microstructural evolution of modern palaeognath eggshells can be a helpful basis.

751

752 **Materials and Methods**

753 Materials

754 Eggshells of all major clades of modern Palaeognathae were analysed (at least ten species
755 including some that became extinct in Holocene): ostrich (*Struthio camelus*), rhea (*Rhea* sp.),
756 emu (*Dromaius novaehollandiae*), cassowary (*Casuarius casuarius*), kiwi (*Apteryx mantelli*),
757 elephant bird (Aepyornithidae), at least two species of moa (*Dinornis novaezealandiae* and
758 either *Euryapteryx curtus* or *Pachyornis geranoides*; see Appendix 1; Gill, 2010, 2021;
759 Huynen et al., 2010), and two species of tinamou (*Eudromia elegans* and *Nothoprocta*
760 *perdicaria*). The materials represent the personal collection of YNL (ostrich, rhea, emu,
761 elephant bird, and Chilean tinamou [*N. perdicaria*]); personal collection of MEH
762 (cassowary); sourced from the Rainbow Springs Kiwi Sanctuary in Rotorua, New Zealand

(kiwi); sourced from the Bronx Zoo, New York (elegant crested tinamou [*E. elegans*]); and sourced from the Auckland War Memorial Museum in Auckland, New Zealand (moa). An eggshell of Paleocene palaeognath *Lithornis celetius* (YPM 16961) was analysed to acquire the data of fossil palaeognath eggshell. This material was excavated from the Fort Union Formation, Montana (Weaver et al., 2021), and its polarized light microscopic and scanning electron microscopic micrographs were presented in Houde (1988) and Grellet-Tinner and Dyke (2005), respectively. This material was provided by Yale Peabody Museum of Natural History (New Haven, CT, USA).

Eggshells of five species of Neognathae, of which EBSD results were not available or insufficiently reported elsewhere, were analysed to provide information of non-palaeognath Neornithes (see Choi et al., 2019, table 1). The eggshells of three species were presented in the main text (Figure 13): common pheasant (Galliformes: *Phasianus colchicus*), northern goshawk (Accipitriformes: *Accipiter gentilis*), and European green woodpecker (Piciformes: *Picus viridis*). Japanese quail (Galliformes: *Coturnix japonica*) and common murre (Charadriiformes: *Uria aalge*) eggshells are shown in the Appendix 1—figures 5 and 7, respectively. The common pheasant and Japanese quail eggshells were purchased from a local market; eggshells of northern goshawk were provided by a private collector; European green woodpecker eggs were provided by the Delaware Museum of Natural History (Wilmington, DE, USA) and common murre eggshells were provided by Erpur Hansen (South Iceland Nature Research Center).

Four Late Cretaceous non-avian maniraptoran dinosaur eggshells were analysed to provide broad overview of eggshell evolution (Figures 13, 15, 16; Appendix 1—figures 9–12). Three oospecies (parataxonomic classification of fossil eggshell) are presented in the main text: *Prismatoolithus levis, Elongatoolithus* oosp., and *Macroelongatoolithus xixiaensis* (or *M.*

787 *carlylei sensu* Simon et al., 2018). *Prismatoolithus levis* is an ootaxon of *Troodon formosus*
788 (Troodontidae; Varricchio et al., 2002) and the materials are from an egg that contains an
789 embryo (MOR 246; Horner and Weishampel, 1988; Varricchio et al., 2002; Choi et al., 2022).
790 *Elongatoolithus* (MPC-D 100/1047) and *Macroelongatoolithus* (SNUVP 201801) are
791 oviraptorosaur eggshells (Norell et al., 1994; Bi et al., 2021; Xing et al., 2022) and
792 *Macroelongatoolithus* was laid by a giant oviraptorosaur (Pu et al., 2017). We also presented
793 EBSD image of *Triprismatoolithus stephensi* (ES 101; Appendix 1—figure 12). The egg-
794 layer of *T. stephensi* is unknown but suggested to be laid by a theropod dinosaur (Jackson and
795 Varricchio, 2010; Agnolin et al., 2012). We further propose maniraptoran affinity of *T.*
796 *stephensi* based on the existence of a SqZ, a diagnostic character of maniraptoran eggshells
797 (Choi et al., 2019).

798

799 EBSD

800 The methodology of EBSD analysis followed established protocols of Moreno-Azanza et al.
801 (2013) and Choi et al. (2019) except for a newly adopted aspect ratio analysis. See Appendix
802 1 for details. The data were presented in inverse pole figure, Euler, grain boundary mappings,
803 and misorientation distribution histograms. We had taken more than three maps and
804 misorientation distribution from a single eggshell, and results from the most well-prepared
805 parts of the eggshell were presented.

806 In this study, aspect ratio mapping (Koblischka-Veneva et al., 2010) was introduced, which
807 was successfully used to analyse the grain shape of brood parasitic and host eggshells (López
808 et al., 2021). In this method, a calcite grain is approximated as an ellipse. Based on the ratio
809 of long to short axes of the ellipse, the grain is assigned to a colour level. This way, the aspect

ratio of calcite grains can be quantitatively presented. We measured aspect ratio of all calcite grains in the maps. However, grains that are out of 50th percentile in area are presented in aspect ratio histograms. This step was necessary because smaller grains usually have a rounder shape and are quantitatively dominant compared to larger and more representative grains.

Data analysis

All statistical analyses were performed in R 4.1.2 (R Core Team, 2022) on each of two distinct calibrated phylogenies for Palaeognathae, taken respectively from Yonezawa et al. (2017) and Kimball et al. (2019). Log-transformed mean values were compiled for misorientation and aspect ratio, and used to perform ancestral state reconstructions on both phylogenetic trees for each trait – i.e. four distinct reconstructions (n = 12 for all analyses). We assigned the three moa eggshell types to the species *Dinornis novaezealandiae*, *Euryapteryx curtus*, and *Pachyornis geranoides*, respectively (electronic supplementary material, text S1). Trees from Yonezawa et al. (2017) and Kimball et al. (2019) did not sample the three moa species in our dataset, but did sample their respective sister groups among moa (Baker et al., 2005, Bunce et al., 2009; Huynen and Lambert, 2014), allowing us to use their respective calibrations for each of them without altering the topology of either tree. Prior to each reconstruction, we estimated phylogenetic signal using Pagel's lambda (Pagel, 1999) in 'phytools' (Revell, 2012) to estimate how strongly the trait of interest follows a Brownian Motion model on the phylogeny of interest. In addition, we fitted different evolutionary models to the data and estimated their goodness of fit based on Akaike Information Criterion corrected for small sample sizes (AICc – Burnham and Anderson 2002), using *fitContinuous* in 'geiger' (Pennell et al., 2014b) and *modSel.geiger* in 'windex'

(Arbuckle and Minter, 2015), respectively. The fitted models (see e.g. Mitchell et al., 2017) include Brownian Motion (BM), Ornstein-Uhlenbeck (OU, single-optimum), Early Burst, Linear Trend, Lambda, and White Noise (i.e. a non-phylogenetic model). We did not test for more complex models (i.e. OU with multiple optima and/or selective regimes), as these are prone to high type I error for small sample sizes (Cooper et al., 2016).

For both trees, misorientation showed a high phylogenetic signal (Yonezawa: $\lambda = 0.999$; Kimball: $\lambda = 0.987$), with a BM model being selected as the best fit among tested evolutionary models. We thus performed ancestral reconstructions of misorientation following a maximum likelihood BM model using *contMap* in 'phytools' (Revell, 2012, 2013). Conversely, aspect ratio presented a low phylogenetic signal (Yonezawa: $\lambda = 0.625$; Kimball: $\lambda < 0.001$) and a White Noise model was always selected as the best fit. For the tree from Yonezawa et al. (2017), the BM model was selected as the second-to-best model with $\Delta AICc < 2$, indicating it to be as good as the best model (Burnham and Anderson, 2002; Richards, 2005; Symonds and Moussalli, 2011); we thus also used *contMap* to reconstruct ancestral states of aspect ratio on this tree. For the tree from Kimball et al. (2019), however, the BM model was selected as the second-to-best model with $\Delta AICc > 2$. This suggests that any optimization of aspect ratio on this tree would not reflect a true evolutionary pattern for our sample; we therefore did not perform this ancestral reconstruction.

Acknowledgements

We thank Yong Park for extracting data; Matt Rayner, Ruby Moore, Vanessa Rhue, Daniel Brinkman, Brian Gill, Daniel Hanley, Erpur Hansen, Jungwoo Lee, and Jiwon Keum for sourcing eggshell materials.

Additional information

Funding

SC was supported by the Basic Science Program through the National Research Foundation of Korea funded by Ministry of Education (2020R1A6A3A03038316); MEH was supported by the Humboldt Foundation, Germany; LJL was supported by the Howard Hughes Medical Institute through the Science Education Program (GT10473); YNL was supported by the National Research Foundation of Korea (2019R1A2B5B02070240).

Author contributions

Seung Choi, Conceptualization, Methodology, Investigation, Data Curation, Writing—original draft, Writing—review & editing, Visualization, Funding acquisition; Mark E Hauber, Conceptualization, Validation, Resources, Writing—review & editing, Supervision, Funding acquisition; Lucas J Legendre, Methodology, Formal analysis, Data curation, Writing—original draft, Writing—review & editing, Visualization, Funding acquisition; Noe-Heon Kim, Investigation, Writing—review & editing; Yuong-Nam Lee, Resources, Writing—review & editing, Supervision, Funding acquisition; David J Varricchio, Validation, Resources, Writing—review & editing, Supervision, Project administration, Funding acquisition

Author ORCIDs

SC, 0000-0002-9013-2909; MEH, 0000-0003-2014-4928; LJL, 0000-0003-1343-8725; NHK,

879 0000-0002-3553-3718; YNL, 0000-0003-1067-6074; DJV, 0000-0002-0594-0929

880

881 Data availability

882 All EBSD data generated or analysed during this study were uploaded in Dryad.

883

884 References

885 Abourachid A, Castro I, Provini P. 2019. How to walk carrying a huge egg? Trade-offs
886 between locomotion and reproduction explain the special pelvis and leg anatomy in kiwi
887 (Aves; *Apteryx* spp.). *Journal of Anatomy* **235**:1045–1056. DOI:
888 https://doi.org/10.1111/joa.13072

889 Agnolin FL, Powell JE, Novas FE, Kundrát M. 2012. New alvarezsaurid (Dinosauria,
890 Theropoda) from uppermost Cretaceous of north-western Patagonia with associated eggs.
891 *Cretaceous Research* **35**:33–56. DOI: https://doi.org/10.1016/j.cretres.2011.11.014

892 Almeida FC, Porzecanski AL, Cracraft JL, Bertelli S. 2022. The evolution of tinamous
893 (Palaeognathae: Tinamidae) in light of molecular and combined analyses. *Zoological*
894 *Journal of the Linnean Society* **195**:106–124. DOI:
895 https://doi.org/10.1093/zoolinnean/zlab080

896 Altimiras J, Lindgren I, Giraldo-Deck LM, Matthei A, Garitano-Zavala Á. 2017. Aerobic
897 performance in tinamous is limited by their small heart. A novel hypothesis in the
898 evolution of avian flight. *Scientific Reports* **7**:15964. DOI: https://doi.org/10.1038/s41598-
899 017-16297-2

900 Ar A, Rahn H, Paganelli CV. 1979. The avian egg: Mass and strength. *Condor* **81**:331–337.

DOI: https://doi.org/10.2307/1366955

Arbuckle K, Minter A. 2015. windex: analyzing convergent evolution using the Wheatsheaf index in R. *Evolutionary Bioinformatics* **11**:11–14. DOI: https://doi.org/10.4137/EBO.S20968

Bailleul AM, Li Z. 2021. DNA staining in fossil cells beyond the Quaternary: Reassessment of the evidence and prospects for an improved understanding of DNA preservation in deep time. *Earth-Science Reviews* **216**:103600. DOI: https://doi.org/10.1016/j.earscirev.2021.103600

Bi S, Amiot R, Peyre de Fabrègues C, Pittman M, Lamanna MC, Yu Y, Yu C, Yang T, Zhang S, Zhao Q, Xu X. 2021. An oviraptorid preserved atop an embryo-bearing egg clutch sheds light on the reproductive biology of non-avialan theropod dinosaurs. *Science Bulletin* **66**:947–954. DOI: https://doi.org/10.1016/j.scib.2020.12.018

Bibi F, Shabel AB, Kraatz BP, Stidham TA. 2006. New fossil ratite (Aves: Palaeognathae) eggshell discoveries from the Late Miocene Baynunah Formation of the United Arab Emirates, Arabian Peninsula. *Palaeontologia Electronica* **9**:2A.

Birchard GF, Deeming DC. 2009. Avian eggshell thickness: scaling and maximum body mass in birds. *Journal of Zoology* **279**:95–101. DOI: https://doi.org/10.1111/j.1469-7998.2009.00596.x

Blinkhorn J, Achyuthan H, Petraglia MD. 2015. Ostrich expansion into India during the Late Pleistocene: Implications for continental dispersal corridors. *Palaeogeography, Palaeoclimatology, Palaeoecology* **417**:80–90. DOI: https://doi.org/10.1016/j.palaeo.2014.10.026

Botfalvai G, Csiki-Sava Z, Grigorescu D, Vasile Ş. 2017. Taphonomical and palaeoecological

924 investigation of the Late Cretaceous (Maastrichtian) Tuştea vertebrate assemblage
925 (Romania; Haţeg Basin) - insights into a unique dinosaur nesting locality.
926 *Palaeogeography, Palaeoclimatology, Palaeoecology* **468**:228–262. DOI:
927 http://doi.org/10.1016/j.palaeo.2016.12.003

928 Brusatte SL, O'Connor JK, Jarvis ED. 2015. The origin and diversification of birds. *Current*
929 *Biology* **25**:R888–R898. DOI: https://doi.org/10.1016/j.cub.2015.08.003

930 Bunce M, Worthy TH, Phillips MJ, Holdaway RN, Willerslev E, Haile J, Shapiro B, Scofield
931 RP, Drummond A, Kamp PJJ, Cooper A. 2009. The evolutionary history of the extinct
932 ratite moa and New Zealand Neogene paleogeography. *Proceedings of the National*
933 *Academy of Sciences* **106**:20646–20651. DOI: https://doi.org/10.1073/pnas.0906660106

934 Burnham KP, Anderson DR. 2002. *Model Selection and Multimodel Inference: A Practical*
935 *Information-Theoretic Approach*. Second edition. New York, NY: Springer. DOI:
936 https://doi.org/10.1007/b97636

937 Cascini M, Mitchell KJ, Cooper A, Phillips MJ. 2019. Reconstructing the evolution of giant
938 extinct kangaroos: comparing the utility of DNA, morphology, and total evidence.
939 *Systematic Biology* **68**:520–537. DOI: https://doi.org/10.1093/sysbio/syy080

940 Choi S, Lee Y-N. 2019. Possible Late Cretaceous dromaeosaurid eggshells from South
941 Korea: A new insight into dromaeosaurid oology. *Cretaceous Research* **103**:104167. DOI:
942 https://doi.org/10.1016/j.cretres.2019.06.013

943 Choi S, Han S, Lee Y-N. 2019. Electron backscatter diffraction (EBSD) analysis of
944 maniraptoran eggshells with important implications for microstructural and taphonomic
945 interpretations. *Palaeontology* **62**:777–803. DOI: https://doi.org/10.1111/pala.12427

946 Choi S, Moreno-Azanza M, Csiki-Sava Z, Prondvai E, Lee Y-N. 2020. Comparative

947 crystallography suggests maniraptoran theropod affinities for latest Cretaceous European
948 'geckoid' eggshell. *Papers in Palaeontology* **6**:265–292. DOI:
949 https://doi.org/10.1002/spp2.1294

950 Choi S, Park Y, Kweon JJ, Kim S, Jung H, Lee SK, Lee Y-N. 2021. Fossil eggshells of
951 amniotes as a paleothermometry tool. *Palaeogeography, Palaeoclimatology,*
952 *Palaeoecology* **571**:110376. DOI: https://doi.org/10.1016/j.palaeo.2021.110376

953 Choi S, Barta DE, Moreno-Azanza M, Kim N-H, Shaw CA, Varricchio DJ. 2022.
954 Microstructural description of the maniraptoran egg *Protoceratopsidovum*. *Papers in*
955 *Palaeontology* **8**:e1430. DOI: https://doi.org/10.1002/spp2.1430

956 Claramunt S, Cracraft J. 2015. A new time tree reveals Earth history's imprint on the
957 evolution of modern birds. *Science Advances* **1**:e1501005. DOI:
958 https://doi.org/10.1126/sciadv.1501005

959 Clarke JA, Tambussi CP, Noriega JI, Erickson GM, Ketcham RA. 2005. Definitive fossil
960 evidence for the extant avian radiation in the Cretaceous. *Nature* **433**:305–308. DOI:
961 https://doi.org/10.1038/nature03150

962 Cloutier A, Sackton TB, Grayson P, Clamp M, Baker AJ, Edwards SV. 2019. Whole-genome
963 analyses resolve the phylogeny of flightless birds (Palaeognathae) in the presence of an
964 empirical anomaly zone. *Systematic Biology* **68**, 937–955. DOI:
965 https://doi.org/10.1093/sysbio/syz019

966 Collins B, Steele TE. 2017. An often overlooked resource: Ostrich (*Struthio* spp.) eggshell in
967 the archaeological record. *Journal of Archaeological Science: Reports* **13**:121–131. DOI:
968 https://doi.org/10.1016/j.jasrep.2017.03.036

969 Cooper N, Thomas GH, Venditti C, Meade A, Freckleton RP. 2016. A cautionary note on the
970 use of Ornstein Uhlenbeck models in macroevolutionary studies. *Biological Journal of the*
971 *Linnean Society* **118**:64–77. DOI: https://doi.org/10.1111/bij.12701

972 Cracraft J. 1974. Phylogeny and evolution of the ratite birds. *Ibis* **116**:494–521. DOI:
973 https://doi.org/10.1111/j.1474-919X.1974.tb07648.x

974 Crouch NMA, Clarke JA. 2019. Body size evolution in palaeognath birds is consistent with
975 Neogene cooling-linked gigantism. *Palaeogeography, Palaeoclimatology, Palaeoecology*
976 **532**:109224. DOI: https://doi.org/10.1016/j.palaeo.2019.05.046

977 Darlim G, Lee MSY, Walter J, Rabi M. 2022. The impact of molecular data on the
978 phylogenetic position of the putative oldest crown crocodilian and the age of the clade.
979 *Biology Letters* **18**:20210603. DOI: https://doi.org/10.1098/rsbl.2021.0603

980 Dauphin Y, Cuif J-P, Salomé M, Susini J, Williams CT. 2006. Microstructure and chemical
981 composition of giant avian eggshells. *Analytical and Bioanalytical Chemistry* **386**:1761–
982 1771. DOI: https://doi.org/10.1007/s00216-006-0784-8

983 de Pinna MCC. 1991. Concepts and tests of homology in the cladistic paradigm. *Cladistics*
984 **7**:367–394. DOI: https://doi.org/10.1111/j.1096-0031.1991.tb00045.x

985 Deeming DC. 2018. Effect of composition on shape of bird eggs. *Journal of Avian Biology*
986 **49**:e01528. DOI: https://doi.org/10.1111/jav.01528

987 Diehl RJ, Keller HM, Hodgkins J. 2022. Towards an interpretive framework for heated
988 ostrich eggshell: an actualistic study. *Journal of Archaeological Science: Reports*
989 **43**:103465. DOI: https://doi.org/10.1016/j.jasrep.2022.103465

990 Donaire M, López-Martínez N. 2009. Porosity of Late Paleocene *Ornitholithus* eggshells

(Tremp Fm, south-central Pyrenees, Spain): Palaeoclimatic implications. *Palaeogeography, Palaeoclimatology, Palaeoecology* **279**:147–159. DOI: https://doi.org/10.1016/j.palaeo.2009.05.011

Douglass K, Bulathsinhala P, Feo TJ, Tighe T, Whittaker S, Brand Z, James H, Rick T. 2021a. Modeling avian eggshell microstructure to predict ontogenetic age and reveal patterns of human-avifauna interaction. *Journal of Archaeological Science* **133**:105442. DOI: https://doi.org/10.1016/j.jas.2021.105442

Douglass K, Gaffney D, Feo TJ, Bulathsinhala P, Mack AL, Spitzer M, Summerhayes GR. 2021b. Late Pleistocene/Early Holocene sites in the montane forests of New Guinea yield early record of cassowary hunting and egg harvesting. *Proceedings of the National Academy of Sciences* **118**:e2100117118. DOI: https://doi.org/10.1073/pnas.2100117118

During MAD, Smit J, Voeten DFAE, Berruyer C, Tafforeau P, Sanchez S, Stein KHW, Verdegaal-Warmerdam SJA, van der Lubbe JHJL. 2022. Mesozoic terminated in boreal spring. *Nature* **603**:91–94. DOI: https://doi.org/10.1038/s41586-022-04446-1

Edwards SV, Naeem S. 1993. The phylogenetic component of cooperative breeding in perching birds. *The American Naturalist* **141**:754–789. DOI: https://doi.org/10.1086/285504

Field DJ. 2020. Preliminary paleoecological insights from the Pliocene avifauna of Kanapoi, Kenya: Implications for the ecology of *Australopithecus anamensis*. *Journal of Human Evolution* **140**:102384. DOI: https://doi.org/10.1016/j.jhevol.2017.08.007

Field DJ, Benito J, Chen A, Jagt JWM, Ksepka DT. 2020. Late Cretaceous neornithine from Europe illuminates the origins of crown birds. *Nature* **579**:397–401. DOI: https://doi.org/10.1038/s41586-020-2096-0

1014 Finarelli JA, Flynn JJ. 2006. Ancestral state reconstruction of body size in the Caniformia
1015 (Carnivora, Mammalia): the effects of incorporating data from the fossil record.
1016 *Systematic Biology* **55**:301–313. DOI: https://doi.org/10.1080/10635150500541698

1017 Gill BJ. 2007. Eggshell characteristics of moa eggs (Aves: Dinornithiformes). *Journal of the*
1018 *Royal Society of New Zealand* **37**:139–150. DOI:
1019 https://doi.org/10.1080/03014220709510542

1020 Gill BJ. 2010. Regional comparisons of the thickness of moa eggshell fragments (Aves:
1021 Dinornithiformes). *Records of the Australian Museum* **62**:115–122. DOI:
1022 https://doi.org/10.3853/j.0067-1975.62.2010.1535

1023 Gill BJ. 2021. Thickness histograms of Holocene fossil eggshell fragments indicate diversity
1024 and relative abundance of moas (Aves: Dinornithiformes) at North Island sites. *New*
1025 *Zealand Journal of Zoology*. DOI: https://doi.org/10.1080/03014223.2021.1970585

1026 Gould SJ, Eldredge N. 1993. Punctuated equilibrium comes of age. *Nature* **366**:223–227.
1027 DOI: https://doi.org/10.1038/366223a0

1028 Grealy A, Phillips M, Miller G, Gilbert MTP, Rouillard J-M, Lambert D, Bunce M, Haile J.
1029 2017. Eggshell palaeogenomics: Palaeognath evolutionary history revealed through
1030 ancient nuclear and mitochondrial DNA from Madagascan elephant bird (*Aepyornis* sp.)
1031 eggshell. *Molecular Phylogenetics and Evolution* **109**:151–163. DOI:
1032 https://doi.org/10.1016/j.ympev.2017.01.005

1033 Grellet-Tinner G. 2006. Phylogenetic interpretation of eggs and eggshells: implications for
1034 phylogeny of Palaeognathae. *Alcheringa* **30**:141–182. DOI:
1035 https://doi.org/10.1080/03115510608619350

1036 Grellet-Tinner G, Dyke GJ. 2005. The eggshell of the Eocene bird *Lithornis*. *Acta*

Palaeontologica Polonica **50**:831–835.

Grellet-Tinner G, Chiappe L, Norell M, Bottjer D. 2006. Dinosaur eggs and nesting behaviors: A paleobiological investigation. *Palaeogeography Palaeoclimatology Palaeoecology* **232**:294–321. DOI: https://doi.org/10.1016/j.palaeo.2005.10.029

Grellet-Tinner G, Murelaga X, Larrasoaña JC, Silveira LF, Olivares M, Ortega LA, Trimby PW, Pascual A. 2012. The first occurrence in the fossil record of an aquatic avian twig-nest with Phoenicopteriformes eggs: Evolutionary implications. *PLoS ONE* **7**:e46972. DOI: https://doi.org/10.1371/journal.pone.0046972

Grellet-Tinner G, Spooner NA, Worthy TH. 2016. Is the "*Genyornis*" egg of a mihirung or another extinct bird from the Australian dreamtime? *Quaternary Science Reviews* **133**:147–164. DOI: https://doi.org/10.1016/j.quascirev.2015.12.011

Grellet-Tinner G, Lindsay S, Thompson MB. 2017. The biomechanical, chemical and physiological adaptations of the eggs of two Australian megapodes to their nesting strategies and their implications for extinct titanosaur dinosaurs. *Journal of Microscopy* **267**:237–249. DOI: https://doi.org/10.1111/jmi.12572

Grigorescu D. 2017. The 'Tuştea puzzle' revisited: Late Cretaceous (Maastrichtian) *Megaloolithus* eggs associated with *Telmatosaurus* hatchlings in the Haţeg Basin. *Historical Biology* **29**:627–640. DOI: http://doi.org/10.1080/08912963.2016.1227327

Harrison T, Msuya CP. 2005. Fossil struthionid eggshells from Laetoli, Tanzania: Taxonomic and biostratigraphic significance. *Journal of African Earth Sciences* **41**:303–315. DOI: https://doi.org/10.1016/j.jafrearsci.2005.07.001

Harshman J, Braun EL, Braun MJ, Huddleston CJ, Bowie RCK, Chojnowski JL, Hackett SJ, Han K-L, Kimball RT, Marks BD, Miglia KJ, Moore WS, Reddy S, Sheldon FH,

1060 Steadman DW, Steppan SJ, Witt CC, Yuri T. 2008. Phylogenomic evidence for multiple
1061 losses of flight in ratite birds. *Proceedings of the National Academy of Sciences* **105**,
1062 13462–13467. DOI: https://doi.org/10.1073/pnas.0803242105

1063 Hauber ME. 2014. *The Book of Eggs: A Life-Size Guide to the Eggs of Six Hundred of the*
1064 *World's Bird Species*. Chicago, IL: University of Chicago Press.

1065 Herrel A, Vanhooydonck B, van Damme R. 2004. Omnivory in lacertid lizards: Adaptive
1066 evolution or constraint? *Journal of Evolutionary Biology* **17**:974–984. DOI:
1067 https://doi.org/10.1111/j.1420-9101.2004.00758.x

1068 Hirsch KF, Kihm AJ, Zelenitsky DK. 1997. New eggshell of ratite morphotype with
1069 predation marks from the Eocene of Colorado. *Journal of Vertebrate Paleontology*
1070 **17**:360–369. DOI: https://doi.org/10.1080/02724634.1997.10010980

1071 Horner JR, Weishampel DB. 1988. A comparative embryological study of two ornithischian
1072 dinosaurs. *Nature* **332**:256–257. DOI: https://doi.org/10.1038/332256a0

1073 Houde P. 1988. *Paleognathous Birds from the Early Tertiary of the Northern Hemisphere*.
1074 Cambridge, MA: Nuttall Ornithological Club.

1075 Huynen L, Gill BJ, Millar CD, Lambert DM. 2010. Ancient DNA reveals extreme egg
1076 morphology and nesting behavior in New Zealand's extinct moa. *Proceedings of the*
1077 *National Academy of Sciences* **107**:16201–16206. DOI:
1078 https://doi.org/10.1073/pnas.0914096107

1079 Huynen L, Lambert DM. 2014. Complex species status for extinct moa (Aves:
1080 Dinornithiformes) from the genus *Euryapteryx*. *PLoS ONE* **9**:e90212. DOI:
1081 https://doi.org/10.1371/journal.pone.0090212

1082 Jackson FD, Varricchio DJ. 2010. Fossil eggs and eggshell from the lowermost Two
1083 Medicine Formation of western Montana, Sevenmile Hill locality. *Journal of Vertebrate*
1084 *Paleontology* **30**:1142–1156. DOI: https://doi.org/10.1080/02724634.2010.483537

1085 Jarvis ED, Mirarab S, Aberer AJ, Li B, Houde P, Li C, Ho SYW, Faircloth BC, Nabholz B,
1086 Howard JT, Suh A, Weber CC, da Fonseca RR, Li J, Zhang F, Li H, Zhou L, Narula N, Liu
1087 L, Ganapathy G, Boussau B, Bayzid MS, Zavidovych V, Subramanian S, Gabaldón T,
1088 Capella-Gutiérrez S, Huerta-Cepas J, Rekepalli B, Munch K, Schierup M, Lindow B,
1089 Warren WC, Ray D, Green RE, Bruford MW, Zhan X, Dixon A, Li S, Li N, Huang Y,
1090 Derryberry EP, Bertelsen MF, Sheldon FH, Brumfield RT, Mello CV, Lovell PV, Wirthlin
1091 M, Schneider MPC, Prosdocimi F, Samaniego JA, Vargas Velazquez AM, Alfaro-Núñez A,
1092 Campos PF, Petersen B, Sicheritz-Ponten T, Pas A, Bailey T, Scofield P, Bunce M,
1093 Lambert DM, Zhou Q, Perelman P, Driskell AC, Shapiro B, Xiong Z, Zeng Y, Liu S, Li Z,
1094 Liu B, Wu K, Xiao J, Yinqi X, Zheng Q, Zhang Y, Yang H, Wang J, Smeds L, Rheindt FE,
1095 Braun M, Fjelda J, Orlando L, Barker FK, Jønsson KA, Johnson W, Koepfli K-P, O'Brien
1096 S, Haussler D, Ryder OA, Rahbek C, Willerslev E, Graves GR, Glenn TC, McCormack J,
1097 Burt D, Ellegren H, Alström P, Edwards SV, Stamatakis A, Mindell DP, Cracraft J, Braun
1098 EL, Warnow T, Jun W, Gilbert MTP, Zhang G. 2014. Whole-genome analyses resolve
1099 early branches in the tree of life of modern birds. *Science* **346**:1320–1331. DOI:
1100 https://doi.org/10.1126/science.1253451

1101 Jin X, Azuma Y, Jackson FD, Varricchio DJ. 2007. Giant dinosaur eggs from the Tiantai
1102 basin, Zhejiang Province, China. *Canadian Journal of Earth Sciences* **44**:81–88. DOI:
1103 https://doi.org/10.1139/e06-077

1104 Juang J-Y, Chen P-Y, Yang D-C, Wu S-P, Yen A, Hsieh H-I. 2017. The avian egg exhibits
1105 general allometric invariances in mechanical design. *Scientific Reports* **7**:14205. DOI:

https://doi.org/10.1038/s41598-017-14552-0

Kimball RT, Oliveros CH, Wang N, White ND, Barker FK, Field DJ, Ksepka DT, Chesser RT, Moyle RG, Braun MJ, Brumfield RT, Faircloth BC, Smith BT, Braun EL. 2019. A phylogenomic supertree of birds. *Diversity* **11**:109. DOI: https://doi.org/10.3390/d11070109

Koblischka-Veneva A, Koblischka MR, Mücklich F. 2010. Advanced microstructural analysis of ferrite materials by means of electron backscatter diffraction (EBSD). *Journal of Magnetism and Magnetic Materials* **322**:1178–1181. DOI: https://doi.org/10.1016/j.jmmm.2009.06.073

Kulshreshtha G, D'Alba L, Dunn IC, Rehault-Godbert S, Rodriguez-Navarro AB, Hincke MT. 2022. Properties, genetics and innate immune function of the cuticle in egg-laying species. *Frontiers in Immunology* **13**:838525. DOI: https://doi.org/10.3389/fimmu.2022.838525

Langley MC. 2018. Explaining the lack of emu eggshell material culture in Australia: Experimental working and archaeological implications. *Journal of Archaeological Science: Reports* **17**:155–162. DOI: https://doi.org/10.1016/j.jasrep.2017.11.011

Lawver DR, Boyd CA. 2018. An avian eggshell from the Brule Formation (Oligocene) of North Dakota. *Journal of Vertebrate Paleontology* **38**:e1486848. DOI: https://doi.org/10.1080/02724634.2018.1486848

Lee MSY, Palci A. 2015. Morphological phylogenetics in the genomic age. *Current Biology* **25**:R922–R929. DOI: https://doi.org/10.1016/j.cub.2015.07.009

Lee MSY, Cau A, Naish D, Dyke GJ. 2014. Morphological clocks in paleontology, and a mid-Cretaceous origin of crown Aves. *Systematic Biology* **63**:442–449. DOI:

https://doi.org/10.1093/sysbio/syt110

Legendre LJ, Clarke JA. 2021. Shifts in eggshell thickness are related to changes in locomotor ecology in dinosaurs. *Evolution* **75**:1415–1430. DOI: https://doi.org/10.1111/evo.14245

Li G, Steel M, Zhang L. 2008. More taxa are not necessarily better for the reconstruction of ancestral character states. *Systematic Biology* **57**:647–653. DOI: https://doi.org/10.1080/10635150802203898

Livezey BC, Zusi RL. 2007. Higher-order phylogeny of modern birds (Theropoda, Aves: Neornithes) based on comparative anatomy. II. Analysis and discussion. *Zoological Journal of the Linnean Society* **149**:1–95. DOI: https://doi.org/10.1111/j.1096-3642.2006.00293.x

Loewy SL, Valdes J, Wang H, Ingram B, Miller NR, de la Cruz Medina K, Roberts A, Yanny S, Banner J, Feseha M, Todd L, Kappelman J. 2020. Improved accuracy of U-series and radiocarbon dating of ostrich eggshell using a sample preparation method based on microstructure and geochemistry: A study from the Middle Stone Age of Northwestern Ethiopia. *Quaternary Science Reviews* **247**:106525. DOI: https://doi.org/10.1016/j.quascirev.2020.106525

López AV, Bolmaro RE, Ávalos M, Gerschenson LN, Reboreda JC, Fiorini VD, Tartalini V, Risso P, Hauber ME. 2021. How do build a puncture- and breakage-resistant eggshell? Mechanical and structural analyses of avian brood parasites and their hosts. *Journal of Experimental Biology* **224**:jeb243016. DOI: https://doi.org/10.1242/jeb.243016

López-Martínez N, Vicens E. 2012. A new peculiar dinosaur egg, *Sankofa pyrenaica* oogen. nov. oosp. nov. from the Upper Cretaceous coastal deposits of the Aren Formation, south-

central Pyrenees, Lleida, Catalonia, Spain. *Palaeontology* **55**:325–339. DOI: https://doi.org/10.1111/j.1475-4983.2011.01114.x

Losos JB. 2011. Convergence, adaptation, and constraint. *Evolution* **65**:1827–1840. DOI: https://doi.org/10.1111/j.1558-5646.2011.01289.x

Maddison WP, Donoghue MJ, Maddison DR. 1984. Outgroup analysis and parsimony. *Systematic Zoology* **33**:83–103. DOI: https://doi.org/10.1093/sysbio/33.1.83

Mayr G, Zelenkov N. 2021. Extinct crane-like birds (Eogruidae and Ergilonithidae) from the Cenozoic of Central Asia are indeed ostrich precursors. *Ornithology* **138**:1–15. DOI: https://doi.org/10.1093/ornithology/ukab048

McInerney PL, Lee MSY, Clement AM, Worthy TH. 2019. The phylogenetic significance of the morphology of the syrinx, hyoid and larynx, of the southern cassowary, *Casuarius casuarius* (Aves, Palaeognathae). *BMC Evolutionary Biology* ***19***:233. DOI: https://doi.org/10.1186/s12862-019-1544-7

Mikhailov KE. 1997a. *Avian Eggshells: An Atlas of Scanning Electron Micrographs*. Tring, UK: British Ornithologists' Club.

Mikhailov KE. 1997b. Fossil and recent eggshell in amniotic vertebrates: Fine structure, comparative morphology and classification. *Special Papers in Palaeontology* **56**:1–80.

Mikhailov KE. 2014. Eggshell structure, parataxonomy and phylogenetic analysis: Some notes on articles published from 2002 to 2011. *Historical Biology* **26**:144–154. DOI: https://doi.org/10.1080/08912963.2013.829824

Mikhailov KE. 2019. Conservative nature of biomineral structures as a challenge for the cladistic method of phylogeny reconstruction (illustrated by two groups of dinosaur eggs).

Paleontological Journal **53**:551–565. DOI: https://doi.org/10.1134/S0031030119060066

Mikhailov KE, Zelenkov N. 2020. The late Cenozoic history of the ostriches (Aves: Struthionidae), as revealed by fossil eggshell and bone remains. *Earth-Science Reviews* **208**:103270. DOI: https://doi.org/10.1016/j.earscirev.2020.103270

Mikhailov KE, Bray ES, Hirsch KF. 1996. Parataxonomy of fossil egg remains (Veterovata): Principles and applications. *Journal of Vertebrate Paleontology* **16**:763–769. DOI: https://doi.org/10.1080/02724634.1996.10011364

Miller JM, Wang YV. 2022. Ostrich eggshell beads reveal 50,000-year-old social network in Africa. *Nature* **601**:234–239. DOI: https://doi.org/10.1038/s41586-021-04227-2

Mitchell J, Legendre LJ, Lefèvre C, Cubo J. 2017. Bone histological correlates of soaring and high-frequency flapping flight in the furculae of birds. *Zoology* **122**:90–99. DOI: https://doi.org/10.1016/j.zool.2017.03.004

Mitchell KJ, Llamas B, Soubrier J, Rawlence NJ, Worthy TH, Wood J, Lee MSY, Cooper A. 2014. Ancient DNA reveals elephant birds and kiwi are sister taxa and clarifies ratite bird evolution. *Science* **344**:898–900. DOI: https://doi.org/10.1126/science.1251981

Montanari S. 2018. Cracking the egg: The use of modern and fossil eggs for ecological, environmental and biological interpretation. *Royal Society Open Science* **5**:180006. DOI: https://doi.org/10.1098/rsos.180006

Moore LA. 2007. Population ecology of the southern cassowary *Casuarius casuarius johnsonii*, Mission Beach north Queensland. *Journal of Ornithology* **148**:357–366. DOI: https://doi.org/10.1007/s10336-007-0137-1

Moreno-Azanza M, Mariani E, Bauluz B, Canudo JI. 2013. Growth mechanisms in dinosaur

1196 eggshells: An insight from electron backscatter diffraction. *Journal of Vertebrate*
1197 *Paleontology* **33**:121–130. DOI: https://doi.org/10.1080/02724634.2012.710284

1198 Nesbitt SJ, Clarke JA. 2016. The anatomy and taxonomy of the exquisitely preserved Green
1199 River Formation (Early Eocene) lithornithids (Aves) and the relationships of
1200 Lithornithidae. *Bulletin of the American Museum of Natural History* **406**:1–91. DOI:
1201 https://doi.org/10.1206/0003-0090-406.1.1

1202 Niespolo EM, Sharp WD, Tryon CA, Faith JT, Lewis J, Ranhorn K, Mambelli S, Miller MJ,
1203 Dawson TE. 2020. Carbon, nitrogen, and oxygen isotopes of ostrich eggshells provide
1204 site-scale Pleistocene-Holocene paleoenvironmental records for eastern African
1205 archaeological sites. *Quaternary Science Reviews* **230**:106142. DOI:
1206 https://doi.org/10.1016/j.quascirev.2019.106142

1207 Niespolo EM, Sharp WD, Avery G, Dawson RE. 2021. Early, intensive marine resource
1208 exploitation by Middle Stone Age humans at Ysterfontein 1 rockshelter, South Africa.
1209 *Proceedings of the National Academy of Sciences* **118**:e2020042118. DOI:
1210 https://doi.org/10.1073/pnas.2020042118

1211 Norell MA, Clark JM, Dashzeveg D, Barsbold R, Chiappe LM, Davidson AR, McKenna MC,
1212 Perle A, Novacek MJ. 1994. A theropod dinosaur embryo and the affinities of the Flaming
1213 Cliffs dinosaur eggs. *Science* **266**:779–782. DOI:
1214 https://doi.org/10.1126/science.266.5186.779

1215 Norell MA, Wiemann J, Fabbri M, Yu C, Marsicano CA, Moore-Nall A, Varricchio DJ, Pol
1216 D, Zelenitsky DK. 2020. The first dinosaur egg was soft. *Nature* **583**:406–410. DOI:
1217 https://doi.org/10.1038/s41586-020-2412-8

1218 Oser SE, Chin K, Sertich JJW, Varricchio DJ, Choi S, Rifkin J. 2021. Tiny, ornamented eggs

1219 and eggshell from the Upper Cretaceous of Utah represent a new ootaxon with theropod
1220 affinities. *Scientific Reports* **11**:10021. DOI: https://doi.org/10.1038/s41598-021-89472-1

1221 Oskam CL, Jacomb C, Allentoft ME, Walter R, Scofield RP, Haile J, Holdaway RN, Bunce
1222 M. 2011. Molecular and morphological analyses of avian eggshell excavated from a late
1223 thirteenth century earth oven. *Journal of Archaeological Science* **38**:2589–2595. DOI:
1224 https://doi.org/10.1016/j.jas.2011.05.006

1225 Pagel M. 1999. Inferring the historical patterns of biological evolution. *Nature* **401**:877–884.
1226 DOI: https://doi.org/10.1038/44766

1227 Panhéleux M, Kälin O, Gautron J, Nys Y. 1999. Features of eggshell formation in guinea
1228 fowl: Kinetics of shell deposition, uterine protein secretion and uterine histology. *British*
1229 *Poultry Science* **40**:632–643. DOI: https://doi.org/10.1080/00071669987025

1230 Patnaik R, Sahni A, Cameron D, Pillans B, Chatrath P, Simons E, Williams M, Bibi F. 2009.
1231 Ostrich-like eggshells from a 10.1 million-yr-old Miocene ape locality, Haritalyangar,
1232 Himachal Pradesh, India. *Current Science* **96**:1485–1495.

1233 Patterson C. 1988. Homology in classical and molecular biology. *Molecular Biology and*
1234 *Evolution* **5**:603–625. DOI: https://doi.org/10.1093/oxfordjournals.molbev.a040523

1235 Pennell MW, Harmon LJ, Uyeda JC. 2014a. Is there room for punctuated equilibrium in
1236 macroevolution? *Trends in Ecology & Evolution* **29**:23–32. DOI:
1237 https://doi.org/10.1016/j.tree.2013.07.004

1238 Pennell MW, Eastman JM, Slater GJ, Brown JW, Uyeda JC, FitzJohn RG, Alfaro ME,
1239 Harmon LJ. 2014b. geiger v2.0: an expanded suite of methods for fitting
1240 macroevolutionary models to phylogenetic trees. *Bioinformatics* **30**:2216–2218. DOI:
1241 https://doi.org/10.1093/bioinformatics/btu181

1242 Phillips MJ, Gibb GC, Crimp EA, Penny D. 2010. Tinamous and moa flock together:
1243 Mitochondrial genome sequence analysis reveals independent losses of flight among
1244 ratites. *Systematic Biology* **59**:90–107. https://doi.org/10.1093/sysbio/syp079

1245 Pickford M. 2014. New ratite eggshells from the Miocene of Namibia. *Communications of*
1246 *the Geological Survey of Namibia* **15**:70–90.

1247 Prum RO, Berv JS, Dornburg A, Field DJ, Townsend JP, Lemmon EM, Lemmon AR. 2015. A
1248 comprehensive phylogeny of birds (Aves) using targeted next-generation DNA
1249 sequencing. *Nature* **526**:569–573. DOI: https://doi.org/10.1038/nature15697

1250 Pu H, Zelenitsky DK, Lü J, Currie PJ, Carpenter K, Xu L, Koppelhus EB, Jia S, Xiao L,
1251 Chuang H, Li T, Kundrát M, Shen C. 2017. Perinate and eggs of a giant caenagnathid
1252 dinosaur from the Late Cretaceous of central China. *Nature Communications* **8**:14952.
1253 DOI: https://doi.org/10.1038/ncomms14952

1254 Quental TB, Marshall CR. 2010. Diversity dynamics: Molecular phylogenies need the fossil
1255 record. *Trends in Ecology & Evolution* **25**:434–441. DOI:
1256 https://doi.org/10.1016/j.tree.2010.05.002

1257 Revell LJ. 2012. phytools: an R package for phylogenetic comparative biology (and other
1258 things). *Methods in Ecology and Evolution* **3**:217–223. DOI:
1259 https://doi.org/10.1111/j.2041-210X.2011.00169.x

1260 Revell LJ. 2013. Two new graphical methods for mapping trait evolution on phylogenies.
1261 *Methods in Ecology and Evolution* **4**:754–759. DOI: https://doi.org/10.1111/2041-
1262 210X.12066

1263 Richards SA. 2005. Testing ecological theory using the information-theoretic approach:
1264 examples and cautionary results. *Ecology* **86**:2805–2814. DOI: https://doi.org/10.1890/05-
1265 0074

1266 Sackton TB, Grayson P, Cloutier A, Hu Z, Liu JS, Wheeler NE, Gardner PP, Clarke JA, Baker
1267 AJ, Clamp M, Edwards SV. 2019. Convergent regulatory evolution and loss of flight in
1268 paleognathous birds. *Science* **364**:74–78. DOI: https://doi.org/10.1126/science.aat7244

1269 Saitta ET, Liang R, Lau MCY, Brown CM, Longrich NR, Kaye TG, Novak BJ, Salzberg SL,
1270 Norell MA, Abbott GD, Dickinson MR, Vinther J, Bull ID, Brooker RA, Martin P,
1271 Donohoe P, Knowles TDJ, Penkman KEH, Onstott T. 2019. Cretaceous dinosaur bone
1272 contains recent organic material and provides an environment conducive to microbial
1273 communities. *eLife* **8**:e46205. DOI: https://doi.org/10.7554/eLife.46205

1274 Sangster G, Braun EL, Johansson US, Kimball RT, Mayr G, Suh A. 2022. Phylogenetic
1275 definitions for 25 higher-level clade names of birds. *Avian Research* **13**:100027. DOI:
1276 https://doi.org/10.1016/j.avrs.2022.100027

1277 Sauer EGF. 1972. Ratite eggshells and phylogenetic questions. *Bonner Zoologische Beitrage*
1278 **23**:3–48.

1279 Sauer EGF, Rothe P. 1972. Ratite eggshells from Lanzarote, Canary Islands. *Science* **176**:43–
1280 45. DOI: https://doi.org/10.1126/science.176.4030.43

1281 Schönwetter, M. 1960–1978. *Handbuch der Oologie*. Berlin, Germany: Akademie Verlag.

1282 Shanahan T. 2011. Phylogenetic inertia and Darwin's higher law. *Studies in History and*
1283 *Philosophy of Biological and Biomedical Sciences* **42**:6068. DOI:
1284 https://doi.org/10.1016/j.shpsc.2010.11.013

1285 Sharp WD, Tryon CA, Niespolo EM, Fylstra ND, Tripathy-Lang A, Faith JT. 2019. ^{230}Th/U
1286 burial dating of ostrich eggshell. *Quaternary Science Reviews* **219**:263–276. DOI:
1287 https://doi.org/10.1016/j.quascirev.2019.06.037

1288 Simon DJ, Varricchio DJ, Jin X, Robison SF. 2018. Microstructural overlap of
1289 *Macroelongatoolithus* eggs from Asia and North America expands the occurrence of
1290 colossal oviraptorosaurs. *Journal of Vertebrate Paleontology* **38**:e1553046. DOI:
1291 https://doi.org/10.1080/02724634.2018.1553046

1292 Soul LC, Wright DF. 2021. *Phylogenetic Comparative Methods: A User's Guide for*
1293 *Paleontologists*. Cambridge, UK: Cambridge University Press. DOI:
1294 https://doi.org/10.1017/9781108894142

1295 Stein K, Prondvai E, Huang T, Baele J-M, Sander PM, Reisz R. 2019. Structure and
1296 evolutionary implications of the earliest (Sinemurian, Early Jurassic) dinosaur eggs and
1297 eggshells. *Scientific Reports* **9**:4494. DOI: https://doi.org/10.1038/s41598-019-40604-8

1298 Stern LA, Johnson GD, Chamberlain CP. 1994. Carbon isotope signature of environmental
1299 change found in fossil ratite eggshells from a South Asian Neogene sequence. *Geology*
1300 **22**:419–422. DOI: https://doi.org/10.1130/0091-7613(1994)022<0419:CISOEC>2.3.CO;2

1301 Stidham TA. 2004. Extinct ostrich eggshell (Aves: Struthionidae) from the Pliocene
1302 Chiwondo Beds, Malawi: implications for the potential biostratigraphic correlation of
1303 African Neogene deposits. *Journal of Human Evolution* **46**:489–496. DOI:
1304 https://doi.org/10.1016/j.jhevol.2004.02.002

1305 Stoddard MC, Yong EH, Akkaynak D, Sheard C, Tobias JA, Mahadevan L. 2017. Avian egg
1306 shape: Form, function, and evolution. *Science* **356**:1249–1254. DOI:
1307 https://doi.org/10.1126/science.aaj1945

1308 Symonds MRE, Moussalli A. 2011. A brief guide to model selection, multimodel inference
1309 and model averaging in behavioural ecology using Akaike's information criterion.
1310 *Behavioral Ecology and Sociobiology* **65**:13–21. DOI: https://doi.org/10.1007/s00265-
1311 010-1037-6

1312 Texier P-J, Porraz G, Parkington J, Rigaud J-P, Poggenpoel C, Miller C, Tribolo C,
1313 Cartwright C, Coudenneau A, Klein R, Steele T, Verna C. 2010. A Howiesons Poort
1314 tradition of engraving ostrich eggshell containers dated to 60,000 years ago at Diepkloof
1315 Rock Shelter, South Africa. *Proceedings of the National Academy of Sciences* **107**:6180–
1316 6185. DOI: https://doi.org/10.1073/pnas.0913047107

1317 Torres CR, Norell MA, Clarke JA. 2020. Estimating flight style of Early Eocene stem
1318 palaeognath bird *Calciavis grandei* (Lithornithidae). *The Anatomical Record* **303**:1035–
1319 1042. DOI: https://doi.org/10.1002/ar.24207

1320 Varricchio DJ, Jackson FD. 2004. A phylogenetic assessment of prismatic dinosaur eggs from
1321 the Cretaceous Two Medicine Formation of Montana. *Journal of Vertebrate Paleontology*
1322 **24**:931–937. DOI: https://doi.org/10.1671/0272-4634(2004)024[0931:APAOPD]2.0.CO;2

1323 Varricchio DJ, Horner JR, Jackson FD. 2002. Embryos and eggs for the Cretaceous theropod
1324 dinosaur *Troodon formosus*. *Journal of Vertebrate Paleontology* **22**:564–576. DOI:
1325 https://doi.org/10.1671/0272-4634(2002)022[0564:EAEFTC]2.0.CO;2

1326 Vieco-Galvez D, Castro I, Morel PCH, Chua WH, Loh M. 2021. The eggshell structure in
1327 *apteryx*; Form, function, and adaptation. *Ecology and Evolution* **11**:3184–3202. DOI:
1328 https://doi.org/10.1002/ece3.7266

1329 Wang S, Hu Y, Wang L. 2011. New ratite eggshell material from the Miocene of Inner
1330 Mongolia, China. *Chinese Birds* **2**:18–26. DOI: https://doi.org/10.5122/cbirds.2011.0002

1331 Weaver LN, Tobin TS, Claytor JR, Wilson Deibel PK, Clemens WA, Wilson Mantilla GP.
1332 2022. Revised stratigraphic relationships within the lower Fort Union Formation (Tullock
1333 Member, Garfield County, Montana, U.S.A.) provide a new framework for examining post
1334 K-Pg mammalian recovery dynamics. *PALAIOS* **37**:104–127. DOI:
1335 https://doi.org/10.2110/palo.2021.011

1336 Weir JT, Haddrath O, Robertson HA, Colbourne RM, Baker AJ. 2016. Explosive ice age
1337 diversification of kiwi. *Proceedings of the National Academy of Sciences* **113**:E5580–
1338 E5587. DOI: https://doi.org/10.1073/pnas.1603795113

1339 Widrig K, Field DJ. 2022. The evolution and fossil record of palaeognathous birds
1340 (Neornithes: Palaeognathae). *Diversity* **14**:105. DOI: https://doi.org/10.3390/d14020105

1341 Wiens JJ. 2004. The role of morphological data in phylogeny reconstruction. *Systematic*
1342 *Biology* **53**:653–661. DOI: https://doi.org/10.1080/10635150490472959

1343 Wiley EO, Lieberman SB. 2011. *Phylogenetics: Theory and Practice of Phylogenetic*
1344 *Systematics*. 2nd ed. Hoboken, NJ: Wiley-Blackwell.

1345 Wilkins J, Schoville BJ, Pickering R, Gliganic L, Collins B, Brown KS, von der Meden J,
1346 Khumalo W, Meyer MC, Maape S, Blackwood AF, Hatton A. 2021. Innovative *Homo*
1347 *sapiens* behaviours 105,000 years ago in a wetter Kalahari. *Nature* **592**:248–252. DOI:
1348 https://doi.org/10.1038/s41586-021-03419-0

1349 Worthy TH, Tennyson AJD, Jones C, McNamara JA, Douglas BJ. 2007. Miocene waterfowl
1350 and other birds from Central Otago, New Zealand. *Journal of Systematic Palaeontology*
1351 **5**:1–39. DOI: https://doi.org/10.1017/S1477201906001957

1352 Worthy TH, Worthy JP, Tennyson AJD, Salisbury SW, Hand SJ, Scofield RP. 2013. Miocene
1353 fossils show that kiwi (*Apteryx*, Apterygidae) are probably not phyletic dwarves.

1354 Paleornithological Research: Proceedings of the 8th International Meeting of the Society
1355 of Avian Paleontology and Evolution. pp. 63–80. Naturhistorisches Museum Wien.

1356 Worthy TH, Hand SJ, Archer M. 2014. Phylogenetic relationships of the Australian Oligo–
1357 Miocene ratite *Emuarius gidju* Casuariidae. *Integrative Zoology* **9**:148–166. DOI:
1358 https://doi.org/10.1111/1749-4877.12050

1359 Worthy TH, Degrange FJ, Handley WD, Lee MSY. 2017. The evolution of giant flightless
1360 birds and novel phylogenetic relationships for extinct fowl (Aves, Galloanseres). *Royal*
1361 *Society Open Science* **4**:170975. DOI: https://doi.org/10.1098/rsos.170975

1362 Xing L, Niu K, Ma W, Zelenitsky DK, Yang T-R, Brusatte SL. 2022. An exquisitely
1363 preserved *in-ovo* theropod dinosaur embryo sheds light on avian-like prehatching postures.
1364 *iScience* **25**:103516. DOI: https://doi.org/10.1016/j.isci.2021.103516

1365 Yonezawa T, Segawa T, Mori H, Campos PF, Hongoh Y, Endo H, Akiyoshi A, Kohno N,
1366 Nishida S, Wu J, Jin H, Adachi J, Kishino H, Kurokawa K, Nogi Y, Tanabe H, Mukoyama
1367 H, Yoshida K, Rasoamiaramanana A, Yamagishi S, Hayashi Y, Yoshida A, Koike H,
1368 Akishinonomiya F, Willerslev E, Hasegawa M. 2017. Phylogenomics and morphology of
1369 extinct paleognaths reveal the origin and evolution of the ratites. *Current Biology* **27**:68–
1370 77. DOI: https://doi.org/10.1016/j.cub.2016.10.029

1371 Zelenitsky DK, Hills LV. 1996. An egg clutch of *Prismatoolithus levis* oosp. nov. from the
1372 Oldman Formation (Upper Cretaceous), Devil's Coulee, southern Alberta. *Canadian*
1373 *Journal of Earth Sciences* **33**:1127–1131. DOI: https://doi.org/10.1139/e96-085

1374 Zelenitsky DK, Modesto SP. 2003. New information on the eggshell of ratites (Aves) and its
1375 phylogenetic implications. *Canadian Journal of Zoology* **81**:962–970. DOI:
1376 https://doi.org/10.1139/Z03-076

1377 Zelenitsky DK, Therrien F. 2008. Phylogenetic analysis of reproductive traits of maniraptoran
1378 theropods and its implications for egg parataxonomy. *Palaeontology* **51**:807–816. DOI:
1379 https://doi.org/10.1111/j.1475-4983.2008.00770.x

1380 Zelenitsky DK, Modesto SP, Currie PJ. 2002. Bird-like characteristics of troodontid theropod
1381 eggshell. *Cretaceous Research* **23**:297–305. DOI: https://doi.org/10.1006/cres.2002.1010

Microstructural and crystallographic evolution of palaeognath (Aves) eggshells

Seung Choi[1,2*], Mark E Hauber[3], Lucas J Legendre[4], Noe-Heon Kim[5], Yuong-Nam Lee[5], David J Varricchio[1*]

[1]Department of Earth Sciences, Montana State University, Bozeman, Montana, United States; [2]Key Laboratory of Evolutionary Systematics of Vertebrates, Institute of Vertebrate Paleontology and Paleoanthropology, Chinese Academy of Sciences, Beijing, China; [3]Department of Evolution, Ecology, and Behavior, University of Illinois at Urbana-Champaign, Urbana-Champaign, Illinois, United States; [4]Department of Geological Sciences, University of Texas at Austin, Austin, Texas, United States; [5]School of Earth and Environmental Sciences, Seoul National University, Seoul, South Korea

APPENDIX 1

Supplementary Text 1. Moa eggshells used in this study were collected from the North Cape, northern end of North Island, New Zealand (see Gill 2010, fig. 1). The moa eggshells used in this study were given catalogue number LB8510 in Gill (2010) and we received thin (~0.90 mm), middle (~1.05 mm), and thick (~1.4 mm) eggshells from the Auckland War Memorial Museum. Gill (2010) provided a thickness histogram of North Cape moa eggshells and it showed a bimodal distribution (Gill 2010, fig. 3). It has "a spread of numerous thin eggshell fragments (mode at 0.90–0.94 mm) and a second spread of rarer thicker fragments (mostly 1.2–1.7 mm thick)" (Gill 2010, p. 117). The thicknesses of our three materials fall into thin and thick ranges of Gill (2010).

In North Cape, majority of moa bone fossils are attributable to *Euryapteryx curtus* and *Pachyornis geranoides* (Gill 2021), both of them are small- to medium-sized moa (Gill 2000; Bunce et al. 2009). The presence of large moa *Dinornis novaezealandiae* (Gill 2000; Bunce et al. 2009) was also reported from the North Cape based on body fossils (Gill 2010). Gill (2021) provided key to the identification of North Island moa eggshells. According to the key, moa eggshells thinner than 1.0 mm with slit-shaped pore depression absent or short most likely belong to *P. geranoides*, eggshells range from 1.0 to 1.3 mm with slit-shaped pore depression most likely belong to *Euryapteryx curtus*, and eggshells thicker than 1.3 mm with numerous and long slit-shaped pore-depression belong to *D. novaezealandiae*. According to these criteria, our thick eggshell unequivocally belongs to *D. novaezealandiae*. In the case of thin eggshell, *P. geranoides* is the most probable egg-layer because of the thickness (~0.90 mm) and near absence of slit-shaped pore depression. The middle eggshell probably belongs to *E. curtus* based on the thickness and pore structure. However, considering the variation of pore pattern and thickness within *Euryapteryx* eggshell (Gill 2021, fig. 1) the thin and middle eggshell may belong to a single species. Therefore, we conclude that our moa eggshell materials derived from *D. novaezealandiae* and at least one smaller species (*E. curtus* or *P. geranoides*). The presence of three species in the North Cape inferred from body fossil record and haplotype data (Gill 2010, 2021; Huynen et al. 2010) is consistent with palaeobiogeography of these taxa inferred from molecular phylogeny (Bunce et al. 2009).

It is noteworthy that Oskam et al. (2011) criticized the use of eggshell thickness as a diagnosis of egg-laying moa species because intraspecific thickness variation among a certain species' eggshell is rather large so that it is hard to differentiate different types of moa eggshells. This criticism is reasonable enough as admitted by Gill (2021), but the clear microstructural and crystallographic contrasts between the thin and thick moa eggshells used in this study (Figures 9–11) strongly support that our materials from the North Cape represent at least two different species of moa.

Supplementary Text 2. The eggshells were embedded in epoxy resin with a drop of hardener and let them consolidate in room temperature for one day. After that, they were cut to expose radial sections using a circular blade. The rough exposed sections were lapped using 400-, 1000- and 3000-grit aluminum compound by hand. Because complete polishing is crucial in EBSD analysis, the sections were polished by hand with 0.5 μm diamond paste for 20 minutes for each specimen. Finally, each specimen was polished with colloidal silica (0.06 μm) for 20 minutes using a turntable. The completed radial sections were coated with carbon. EBSD analyses were conducted using a FE-SEM (JEOL JSM-7100F) and its attached EBSD (Symmetry Detector; Oxford

Instrument), housed in the School of Earth and Environmental Sciences, Seoul National University. The accelerating voltage of FE-SEM was 15.0 kV. EBSD analysis was performed in working distance 15.0 mm; 70 degrees tilting of the specimen. The Kikuchi lines were indexed using AZtec software (Oxford Instrument) and step size ranged from 0.25 μm (in case of tinamou eggshell) to 3 μm (in case of elephant bird eggshell), depending on the thickness of the eggshells.

The acquired mapping images were enhanced to correct wild spikes and unindexed pixels. A wild spike is an erroneous pixel, which is surrounded by correctly indexed pixels. The wild spikes were all eliminated. An unindexed pixel (or zero solution) is a failed indexing caused by no input of clear crystallographic data (= Kikuchi line) or several nearby grains information overlapped in a pixel, thus the AZtec software failed to read a proper signal. Following the method of Choi et al. (2019), we treated the unindexed pixel as the same signal of surrounding pixels when an unindexed pixel is surrounded by at least six consistent signals.

The acquired EBSD data were presented in four different mappings (Figures 1–12; inverse pole figure [IPF], Euler, grain boundary [GB], and aspect ratio [AR]) and in misorientation histograms. In IPF mapping, c-axis orientation of calcite in the eggshell is presented using colour index. When the c-axis of the calcite grains lie perpendicular to the eggshell surface, the grain is coloured red. In contrast, when the c-axis of calcite grain lies parallel to the eggshell surface, it is coloured green or blue. In a Euler map, differently oriented calcite grains have different colours, thus it is easy to differentiate the individual calcite grains. In GB mapping, grain boundaries between the grains (i.e. misorientation) that are 5°–10°, 10°–20°, and >20° are marked with green, blue, and purples lines, respectively. The grain boundary information is used in constructing the misorientation histograms. In AR mapping, a calcite grain is approximated to an ellipse that has the most similar shape to the calcite grain. When the approximated ellipse is elongated, it is coloured green, yellow and even orange, but when an approximated ellipse is round, it is coloured blue. In making misorientation histograms, neighbour-pair and random-pair distributions were used. The former was acquired by selecting the adjacent pairs of grains and the angle between them are calculated, whilst the latter was calculated by using the randomly selected (hence, usually distant) grains. We selected 1000 randomly chosen grains in constructing the random-pair misorientation to be consistent with former studies that deals with misorientation of fossil and modern eggshells (Moreno-Azanza et al. 2013; Choi and Lee 2019; Choi et al. 2019, 2020, 2022).

Supplementary Text 3. Detailed description for EBSD maps of neognath eggshells

Common pheasant (*Phasianus colchicus*) and Japanese quail (*Coturnix japonica*) (Figures S4, S5): Both species belong to Galliformes and the microstructures and crystallography are similar enough to be described together. As in chicken and duck eggshells (Choi et al. 2019), the vertical alignment of c-axis is not as strong as that of palaeognath eggshells. The ML is wedge-like and the prismatic calcites extend to SqZ and EZ. The boundaries between the ML and SqZ, SqZ and EZ are gradual. As in ostrich-style palaeognath eggshells, a 'splaying' structure is very weak in SqZ. Low-angle GB are rare compared to palaeognath eggshells. ML and EZ have linear GB while SqZ has rugged GB. However, the difference in ruggedness between the layers is not prominent compared to that of palaeognath eggshells. These features are consistent with other galliform eggshells (chicken, Choi et al. 2019; megapode, Grellet-Tinner et al. 2017; turkey, Nys et al. 2004), but guineafowl eggshell has prominent rugged GB in SqZ as in rhea-style palaeognath eggshell (Nys et al. 2004).

Northern goshawk (*Accipiter gentilis*) (Figure S6): The goshawk eggshell has exotic microstructure. The ML is composed of wedge-like calcite. The boundary between the ML and SqZ is gradual. The SqZ seems to be thin while EZ is thick based on grain boundary condition. In outer EZ, the calcite grains are characterized by angular porosities. This feature has not been observed in other avian eggshell and needs further investigation of other accipitriform eggshells (see also Mikhailov 1997a). In addition, the porous EZ is overlain by another layer that is not indexed by EBSD. It means that this layer is not composed of calcite, but other biominerals. Preliminary energy-dispersive X-ray spectroscopy (EDS) analysis showed that Si is enriched in this layer. However, the origin and function of this layer is beyond the focus of current study. Low-angle GB are rarely seen. ML is composed of linear GB. The rugged GB is located near the inner part of the eggshell, while linear GB occupy nearly outer half of the calcite eggshell. This result may imply that the SqZ occupies only a small portion of the eggshell and EZ is dominant in the eggshell. Also, the angular porosities mentioned above may be confined to the EZ. However, in most avian eggshells, the vesicles are usually located in SqZ, but in the northern goshawk

eggshell, vesicles are widely distributed to the outer end of calcitic eggshell so identifying SqZ and EZ are equivocal. Along with the non-calcite biominerals mentioned earlier, testing this hypothesis is an unexplored issue in Accipitriformes biology, but we will not investigate this issue in this study. See also Dalbeck and Cusack (2006) for EBSD imaging for eggshell of another Accipitriformes, *Aquila chrysaetos*.

Common murre (*Uria aalge*) (Figure S7): Compared to the other neognath eggshells, the common murre eggshell has prominent vertical c-axis alignment, similar to that of palaeognath eggshells. The ML is wedge-like. Similar to palaeognath eggshell, the boundary between the ML and SqZ is easily identified due to the 'splaying' microstructure of SqZ. The calcite in the EZ is massive. Overall, common murre eggshell is remarkably similar to Guineafowl (Numididae, Galliformes) eggshell (Nys et al. 2004). Both eggshells are dissimilar to typical 'prismatic neognath morphotype' (Mikhailov 1997b), but more like rhea-style palaeognath eggshell. Low-angle GB is usually confined to ML. In ML and EZ, GB are linear while in SqZ, GB are rugged.

European green woodpecker (*Picus viridis*) (Figure S8): The overall microstructure is strikingly similar to that of tinamou eggshells. It has relatively strong vertical c-axis alignment as palaeognath eggshells. The ML has needle-like structure although wedge-like structure is also observed. The boundary between the ML and SqZ is clear due to the contrasting microstructure. Grains are mostly irregular in SqZ. The EZ is composed of massive calcite grains. Mikhailov (1997a) already pointed out that eggshell of woodpecker (Neognathae) is similar to palaeognath eggshells. This observation can be further supported by the current study. Low-angle GB are concentrated on the ML. The GB configuration is similar to that of tinamou eggshell. The only minor difference is that the GB linearity in EZ is not as prominent as that of tinamou eggshells.

Supplementary Text 4. Detailed description for EBSD maps of non-avian maniraptoran eggshells

The microstructural and crystallographic features of oviraptorosaur (*Elongatoolithus* oosp. and *Macroelongatoolithus xixiaensis* [or *M. carlylei sensu* Simon et al. 2018]; Figures S9, S10) and troodontid eggshell (Figure S11) were fully described in Choi et al. (2019). Briefly, oviraptorosaur eggshells have rhea-style microstructure and crystallography except for the presence of needle-like ML and absence of EZ. This trait is more prominent for *Elongatoolithus*; *Macroelongatoolithus* is characterized by weakly developed, hidden prismatic structure (or cryptoprismatic structure *sensu* Jin et al. 2007). Oviraptorosaur eggshells have widespread low-angle GB, not confined to certain part of the eggshell. ML has linear GB, but in SqZ, GB becomes highly rugged. They do not have EZ that is characterized by linear GB. In contrast, troodontid eggshell (*Prismatoolithus levis*; Zelenitsky and Hills 1996; Varricchio et al. 2002; Varricchio and Jackson 2004; Funston and Currie 2018) has well-developed prismatic shell units. In addition, *P. levis* has EZ (Varricchio and Jackson 2004), a feature that is usually found in avian eggshell. Although the existence of EZ is still challenged (e.g. Mikhailov 2014), general consensus is that EZ exists in *P. levis* (Zelenitsky and Therrien 2008; Choi et al. 2019). Troodontid eggshell is characterized by linear GB in ML and EZ, but SqZ has very weakly developed rugged GB.

Triprismatoolithus stephensi (Figure S12): The overall microstructure is similar to that of *P. levis* in that prismatic shell units occupy the whole thickness of eggshell. The ML is wedge-like, and the boundary between the ML and SqZ is gradual. The existence of EZ can be identified by grain boundary condition and polarized light microscopic features (Jackson and Varricchio 2010; Varricchio and Jackson 2016). The overall GB configuration is similar to that of *P. levis*. Low-angle GB are rare. In ML and EZ, grain boundaries are linear but in SqZ, grain boundaries are rugged. However, the difference in ruggedness of SqZ and EZ is clearer compared to the *P. levis*.

Supplementary Text 5. Further information for aspect ratio

Because it is known that *Prismatoolithus levis* is characterized by very narrow shell units (Zelenitsky and Hills 1996; Varricchio et al. 2002; Varricchio and Jackson 2004), whereas the shell unit structure of oviraptorosaur *Macroelongatoolithus* (Pu et al. 2017) is rather controversial (Grellet-Tinner et al. 2006; Jin et al. 2007), we analysed AR of oviraptorosaur (*Elongatoolithus* and *Macroelongatoolithus*) and troodontid eggshells (*P. levis*). Intriguingly, *P. levis* shows very high AR following the AR of ostrich eggshell (Figure 15). Thus, both *P. levis*

and modern ostrich eggshell have very narrow and tall shell units and weakly developed 'splaying' microstructure. *Elongatoolithus* does not have high AR whereas *Macroelongatoolithus* shows higher AR. It strongly supports the view that the SqZ of *Macroelongatoolithus* can be best described by the term 'cryptoprismatic' (Jin et al. 2007) but 'aprismatic' may be still a reasonable term for *Elongatoolithus* (Grellet-Tinner and Chiappe 2004).

It was proposed that character states of ML, either needle-like or wedge-like, can be diagnosed by richness of low-angle GB (Choi et al. 2019). However, it can be better defined by the combination of AR and GB mappings of the ML (Figure S3). We suggest that density of calcite grains within a ML would be the most objective criterion. When the calcite grains of ML are confined to ML, the AR mapping provides most straightforward results: needle-like ML is characterized by the presence of high AR colour (e.g. *Reticuloolithus*, *Elongatoolithus*, kiwi, and tinamou eggshells). However, when the calcite grains of ML are not limited to ML, even wedge-like calcite grains show high AR colour (e.g. ostrich and thick moa eggshells). In this case, a wedge-like ML is composed of a small number of calcite grains, thus one can count the number of grains in a single ML. It will provide a way to circumvent the limitation of AR mapping in diagnosing wedge-like versus needle-like ML in ostrich-like eggshells. In sum, identifying needle- or wedge-like ML can be quantitatively done by counting calcite grains in ML in all cases; when the calcite grains are confined to ML and not extended to SqZ, AR mapping will provide simplest visual representation. Detailed elaboration of this approach will be presented in future research.

Supplementary Text S6. Alternative interpretation

The alternative interpretations presented here are based on the phylogeny of Cloutier et al. (2019) and Sackton et al. (2019) (Figures S14–S16). Only those differences from the main text are discussed herein: (i) the tinamou and moa are nested in a more inclusive position of the tree and rhea is assigned to a less inclusive position. Still, three tinamou-style and two ostrich-style microstructures might have been derived from rhea-style microstructure. (ii) Unfortunately, the rate of evolutionary change cannot be inferred in this interpretation because speciation timeline estimates have not been made in Cloutier et al. (2019) nor Sackton et al. (2019).

Supplementary Figures

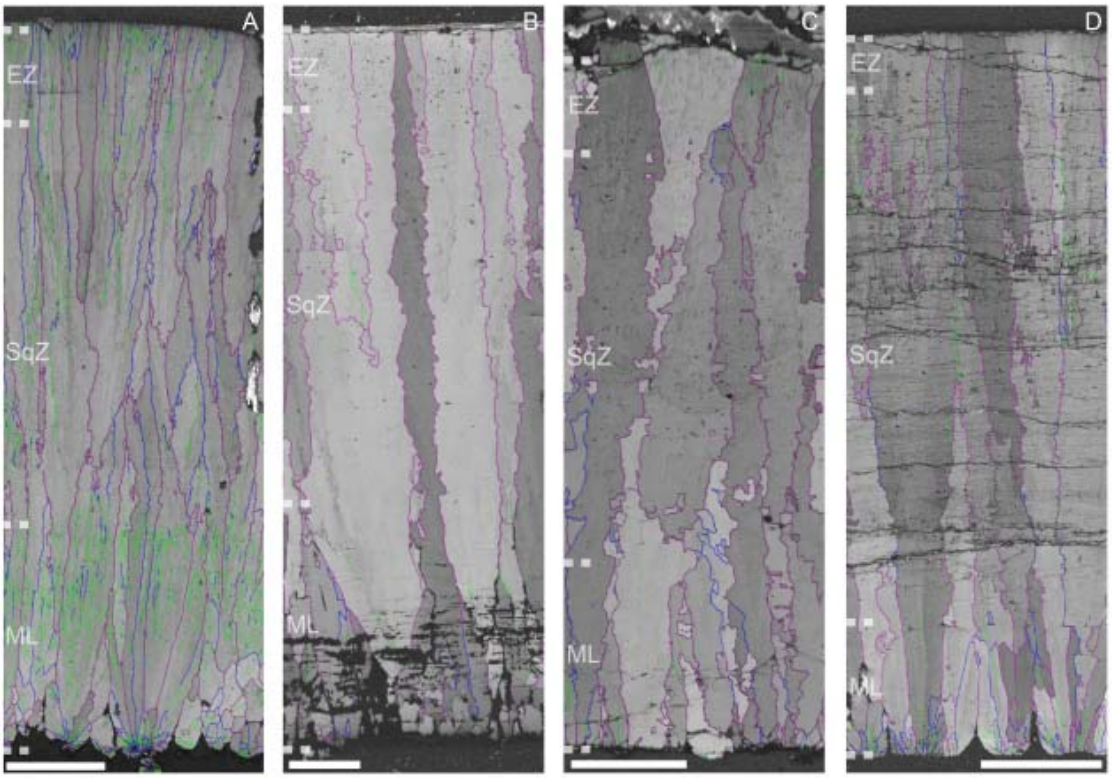

Fig. S1. Composite GB mappings of fossil and modern eggshells that have prismatic shell unit structure. (A) Ostrich, (B) *Prismatoolithus levis*, (C) *Triprismatoolithus stephensi*, and (D) thick moa eggshell. In *P. levis* and *T. stephensi* (B,C), GB becomes slightly more linear in outer parts of eggshell, which have been suggested as EZ (Varricchio and Jackson 2004; Jackson and Varricchio 2010). In ostrich and thick moa eggshell (A,D), the difference in linearity is much more subtle. Scale bars equal 250 μm (A); 100 μm (B–D).

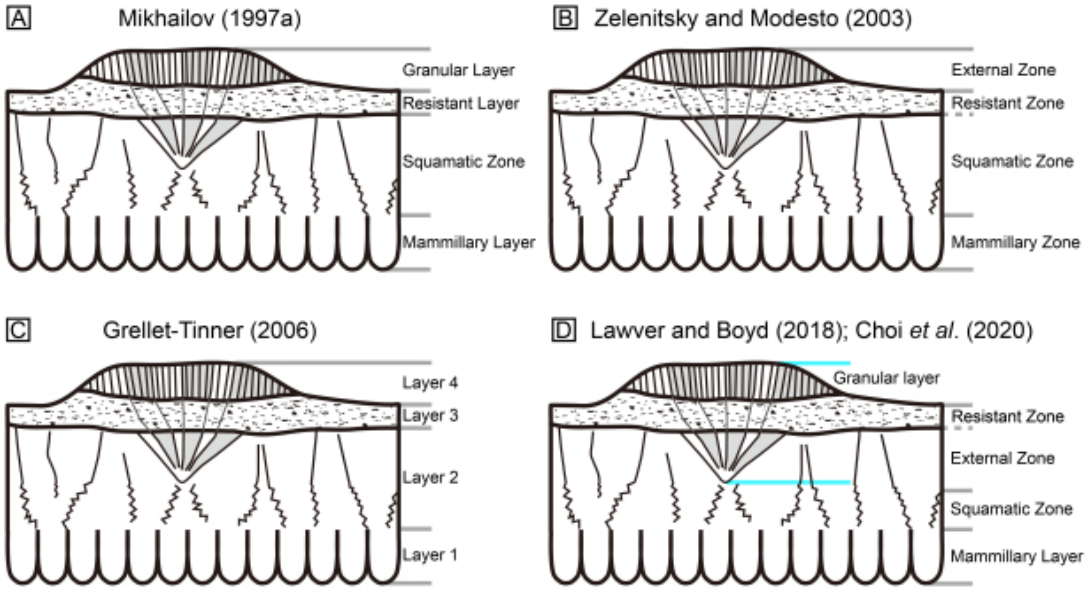

Fig. S2. Previous and current interpretations on the microstructure of casuariid eggshells. (A,C) Mikhailov (1997a) and Grellet-Tinner (2006) suggested four layers. (B) Zelenitsky and Modesto (2003) suggested that compact calcified part of the eggshell is composed of SqZ and Resistant Zone is an extension of SqZ. In their view, ornamentation is a homologous structure to EZ that is usually present in all avian eggshell (except for passerine; Mikhailov 1997a). (D) Lawver and Boyd (2018) pointed out that ornamentation has its 'root' inside compact calcified eggshell. It was confirmed in Choi et al. (2020) and this study. In addition, based on the GB condition of EZ, which is characterized by linear line, Choi et al. (2020) further suggested that outer compact calcified part of the eggshell is EZ, not SqZ as suggested by Zelenitsky and Modesto (2003). In our view, therefore, ornamentation is not homologous to EZ of most avian eggshells, but is an autapomorphic character of MRCA of emu and cassowary.

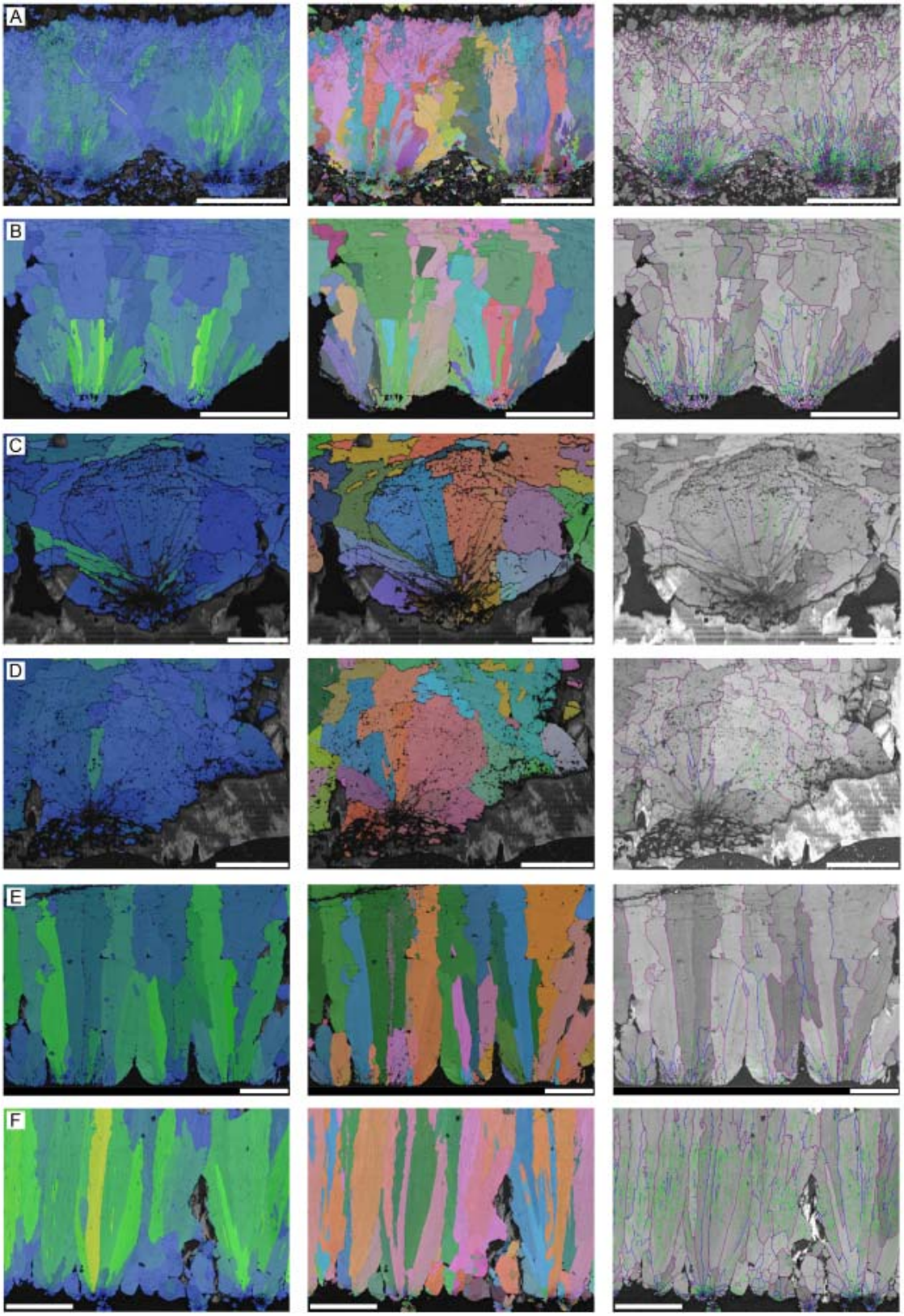

Fig. S3. Mammillary layers of (A) *Reticuloolithus*, (B) *Elongatoolithus*, (C) tinamou, (D) kiwi, (E) thick moa, and (F) ostrich eggshells presented in AR, Euler, and GB mappings. When ML is confined to certain region of

eggshell (A–D) AR mappings effectively show the needle-like calcite grains, which is a useful character state for fossil eggshell classification. However, when the calcite grain in ML is not limited within the ML, even wedge-like ML can have high AR (E,F). In these cases, measuring the density of calcite grains in the ML can provide a quantitative approach to diagnose needle-like versus wedge-like states in ML. Scale bars equal 250 μm (A,F); 100 μm (B,E); 50 μm (D); 25 μm (C).

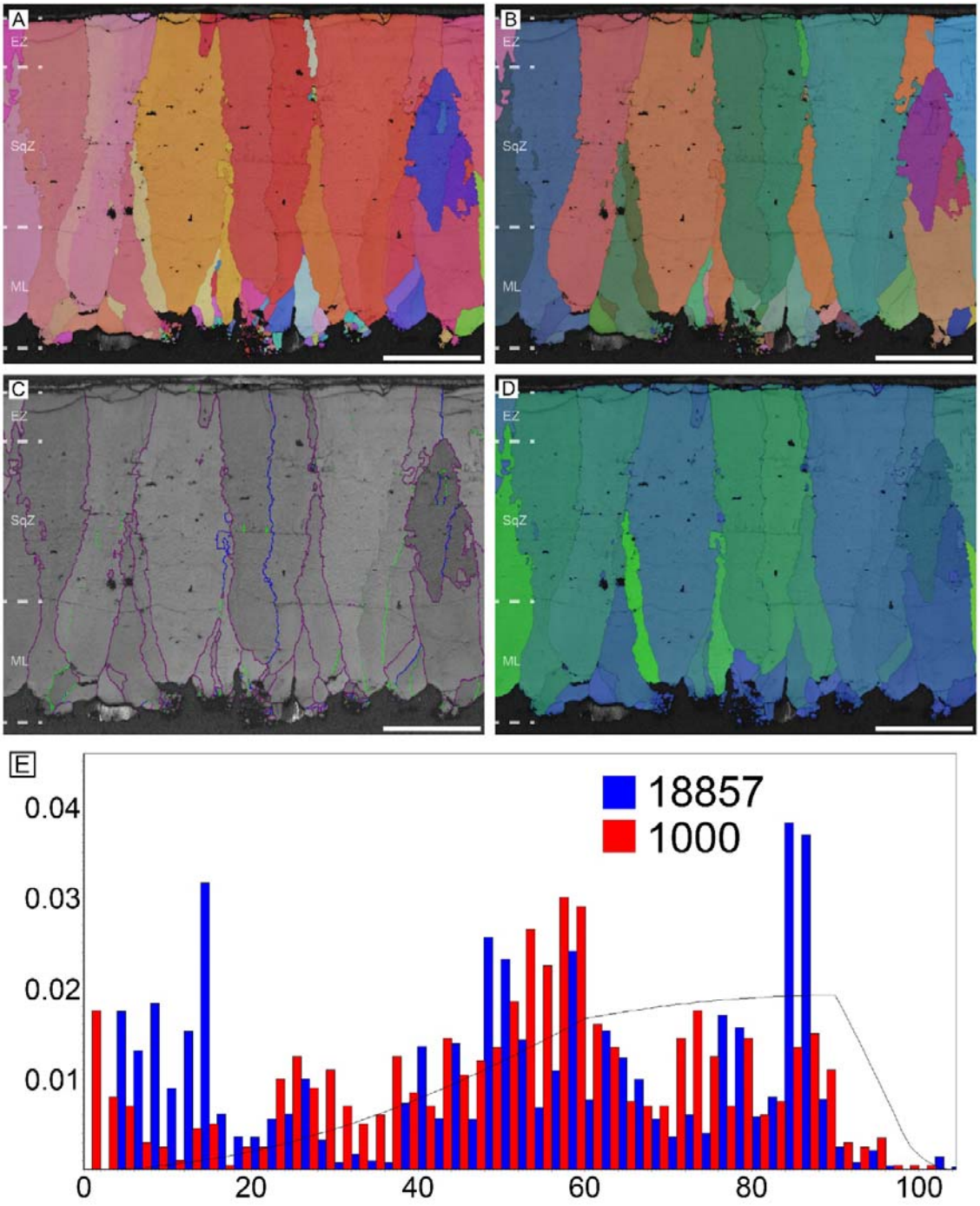

Fig. S4. Common pheasant eggshell. Scale bars equal 100 μm.

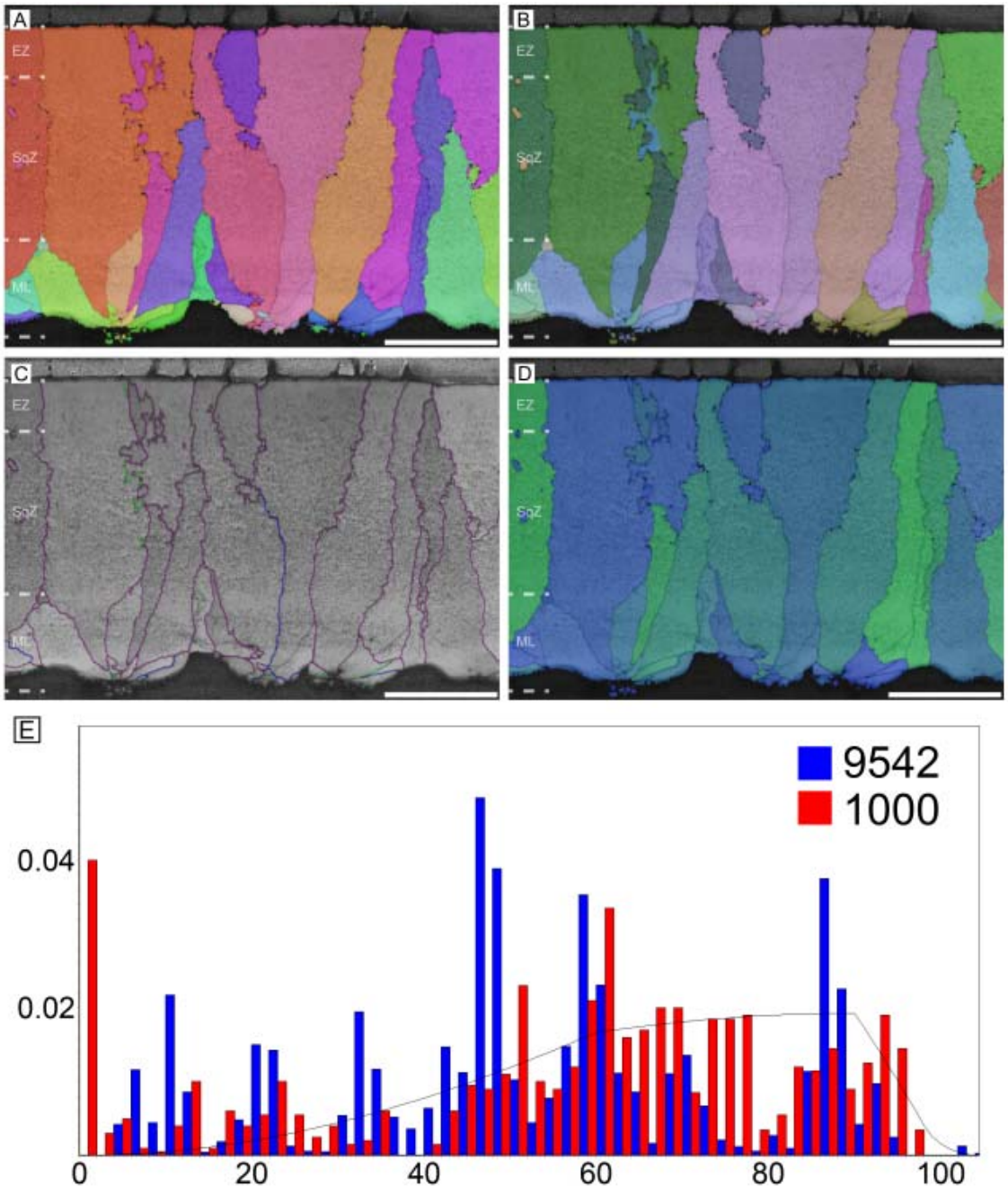

Fig. S5. Japanese quail eggshell. Scale bars equal 50 µm.

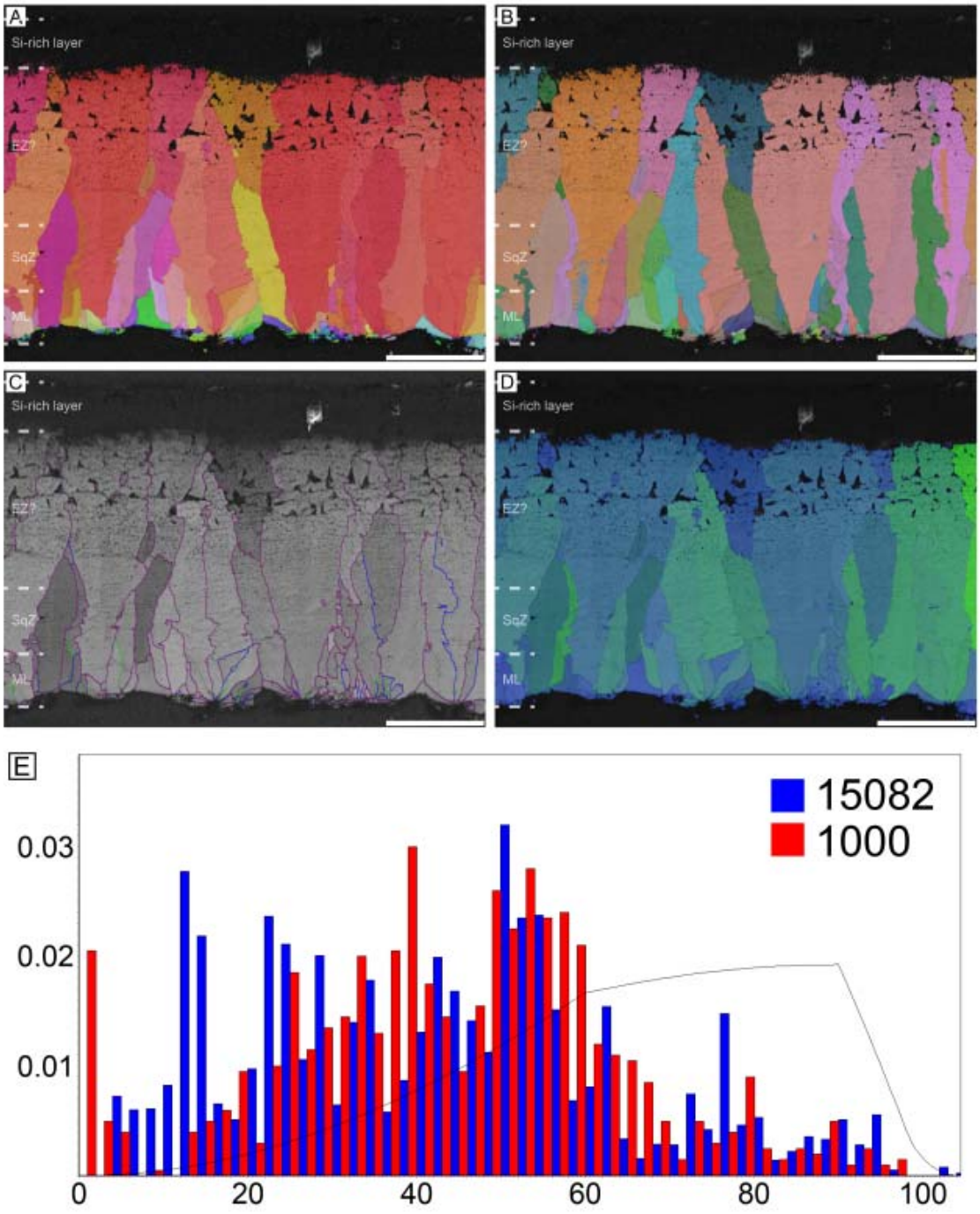

Fig. S6. Northern goshawk pheasant eggshell. Scale bars equal 100 μm.

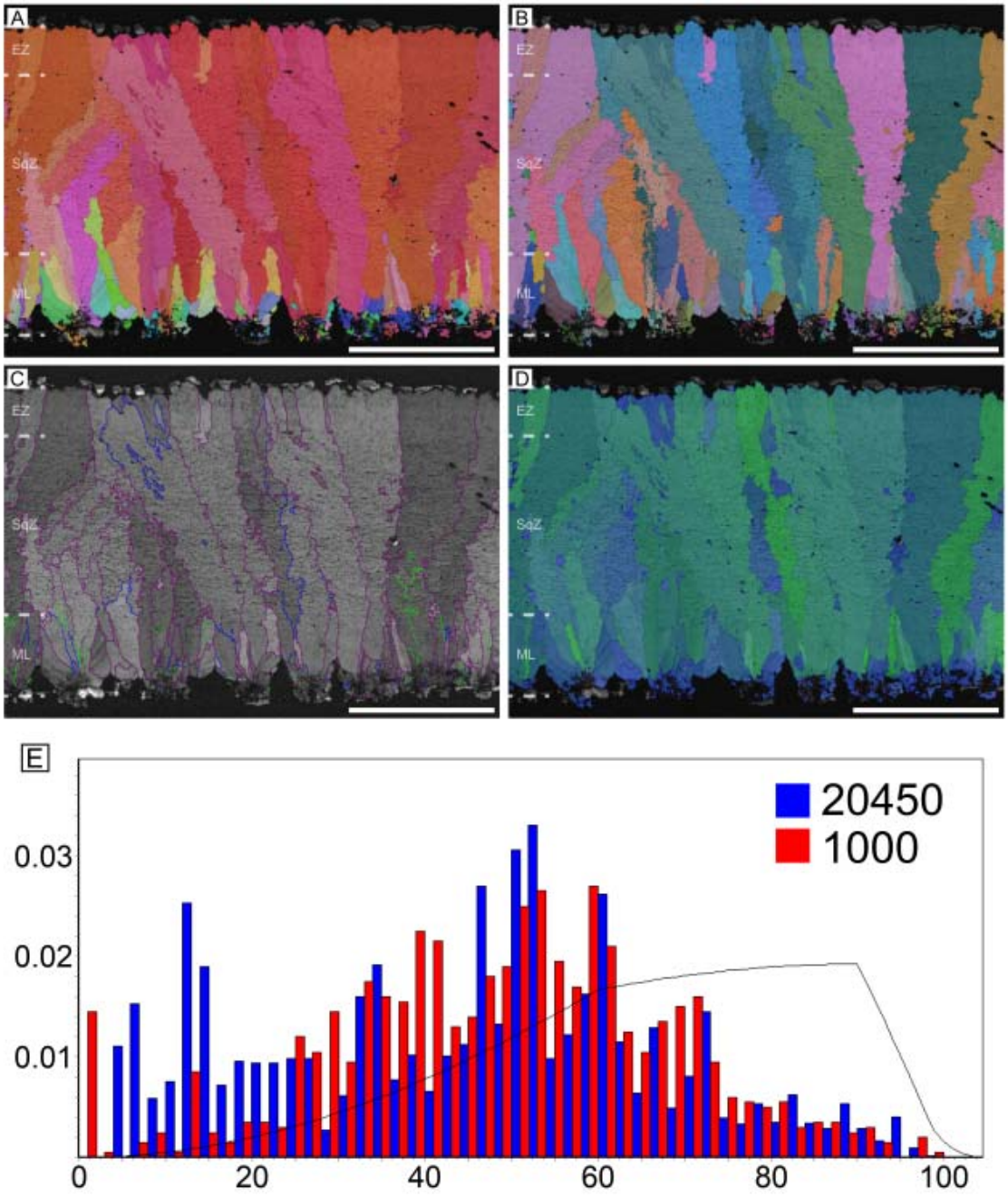

Fig. S7. Common murre eggshell. Scale bars equal 250 µm.

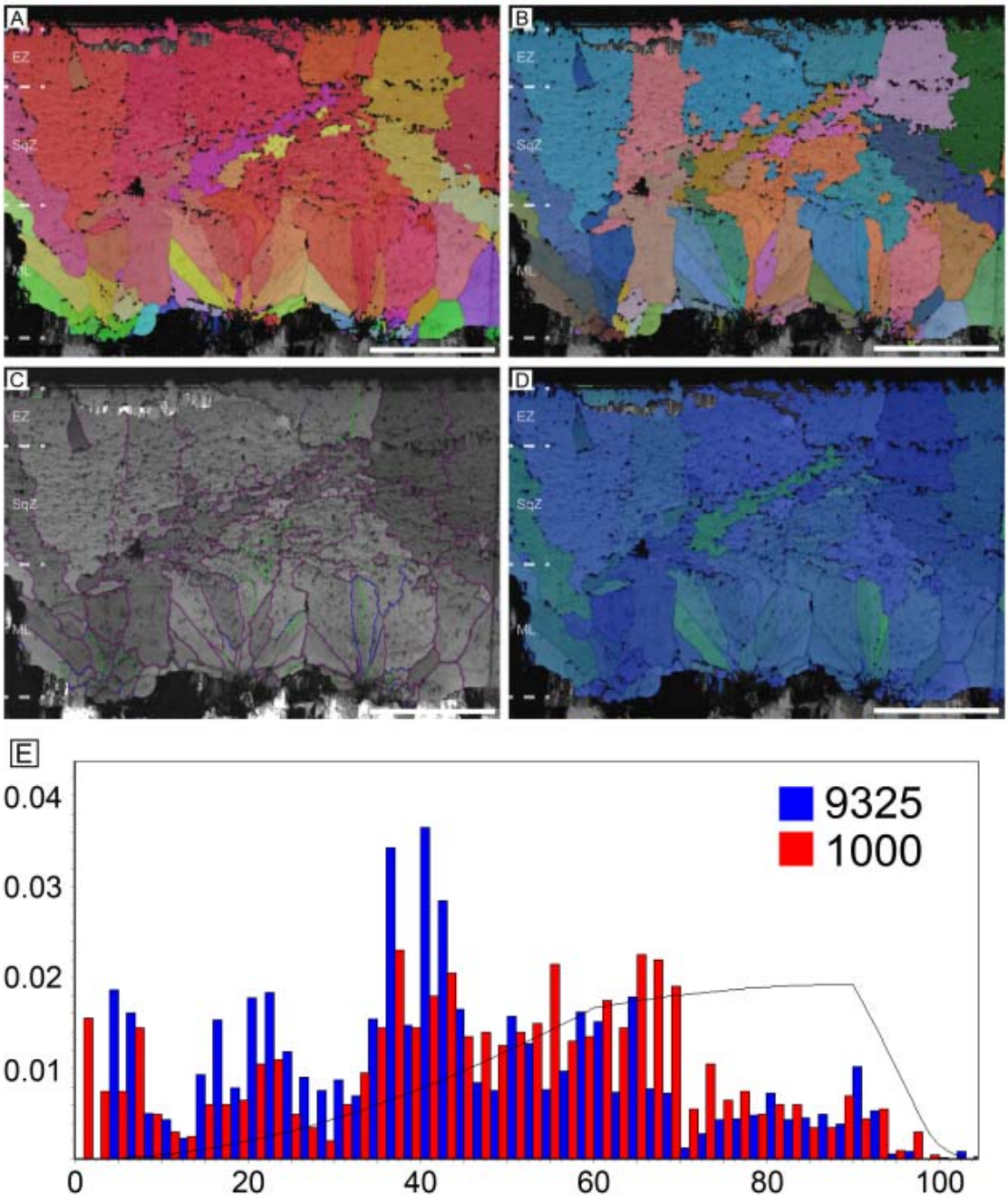

Fig. S8. European green woodpecker eggshell. Scale bars equal 50 µm.

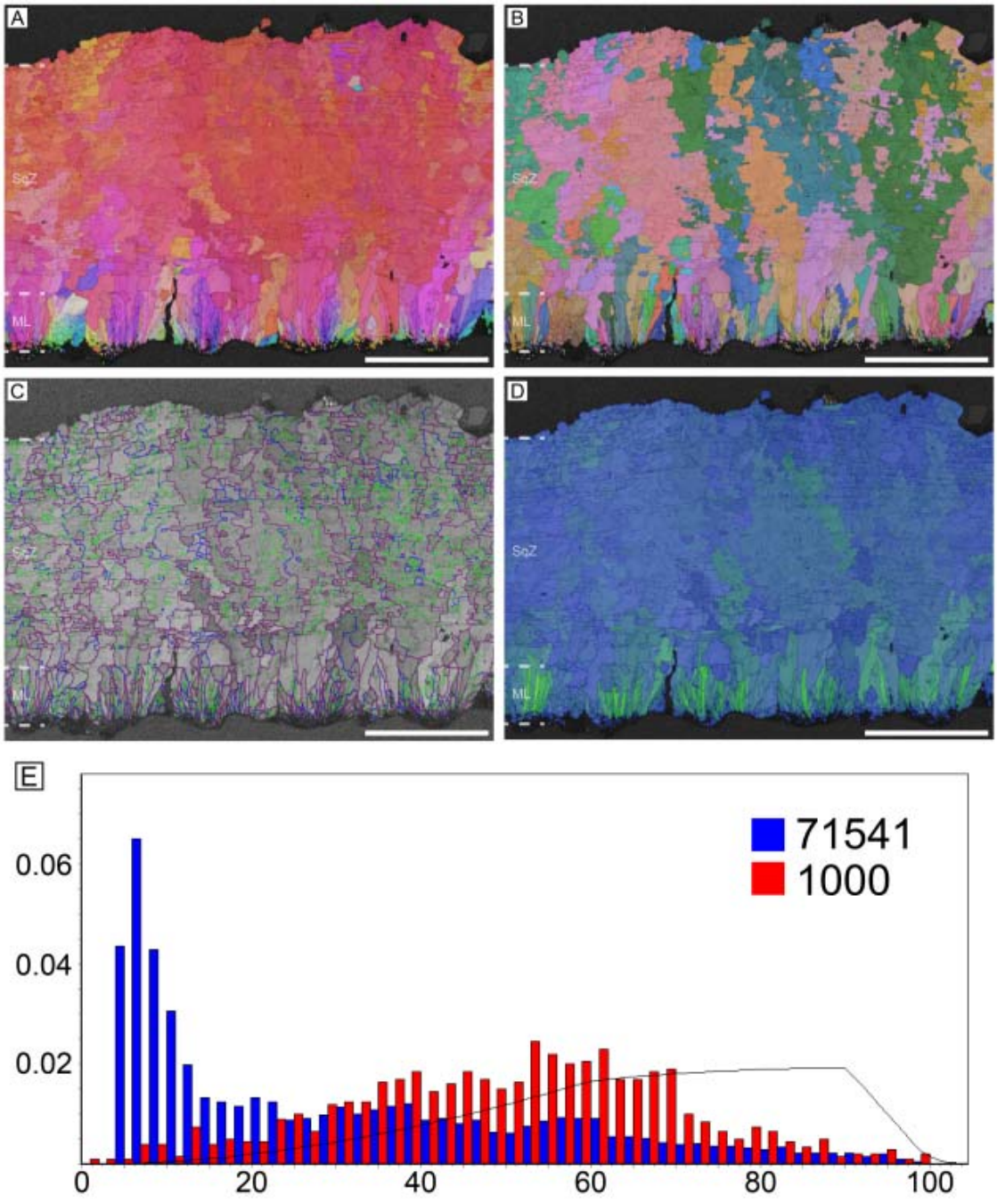

Fig. S9. *Elongatoolithus* oosp. (see also Choi et al. 2019). Scale bars equal 250 μm.

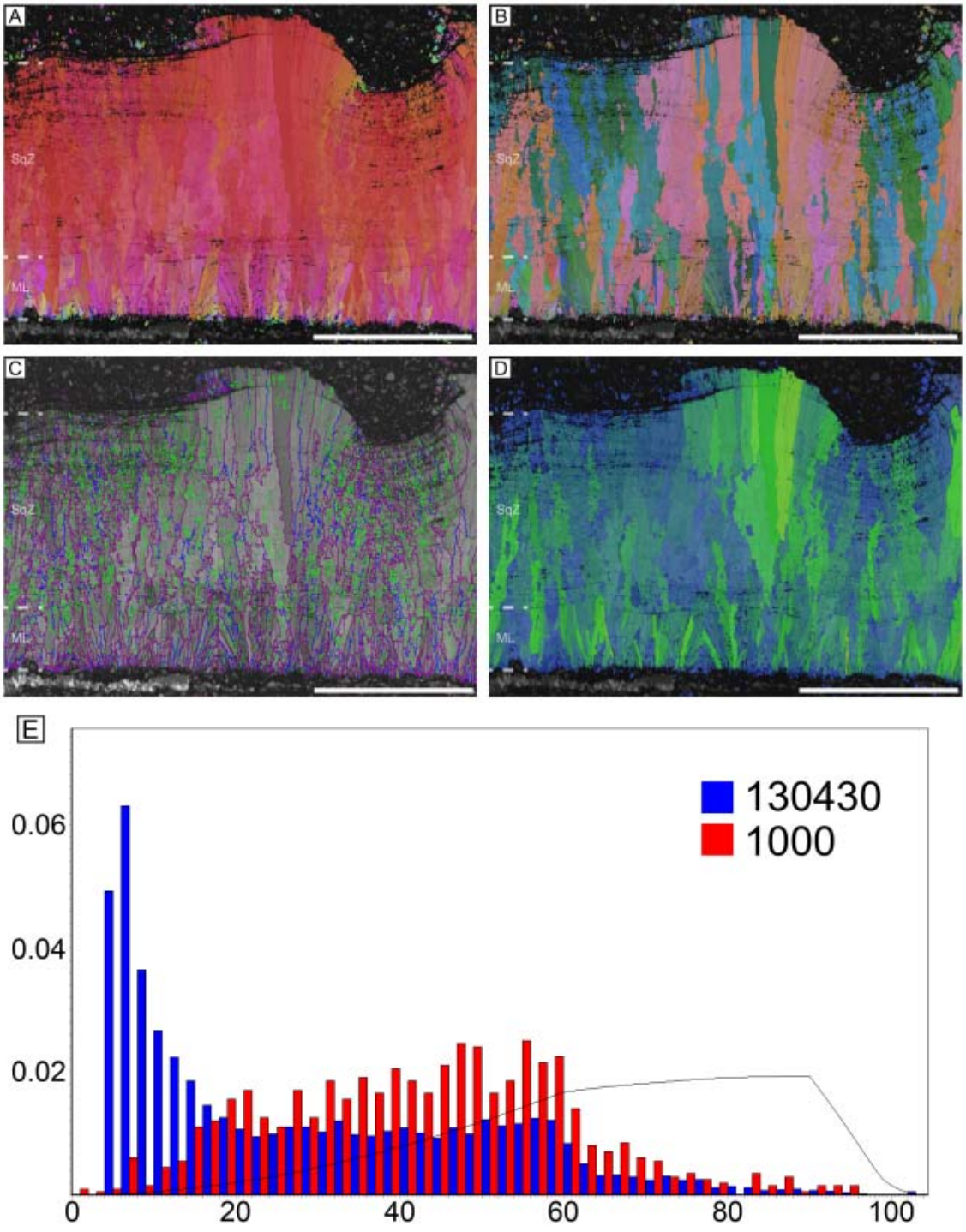

Fig. S10. *Macroelongatoolithus xixiaensis (*or *M. carlylei*) (see also Huh et al. 2014; Choi et al. 2019). Scale bars equal 1000 μm.

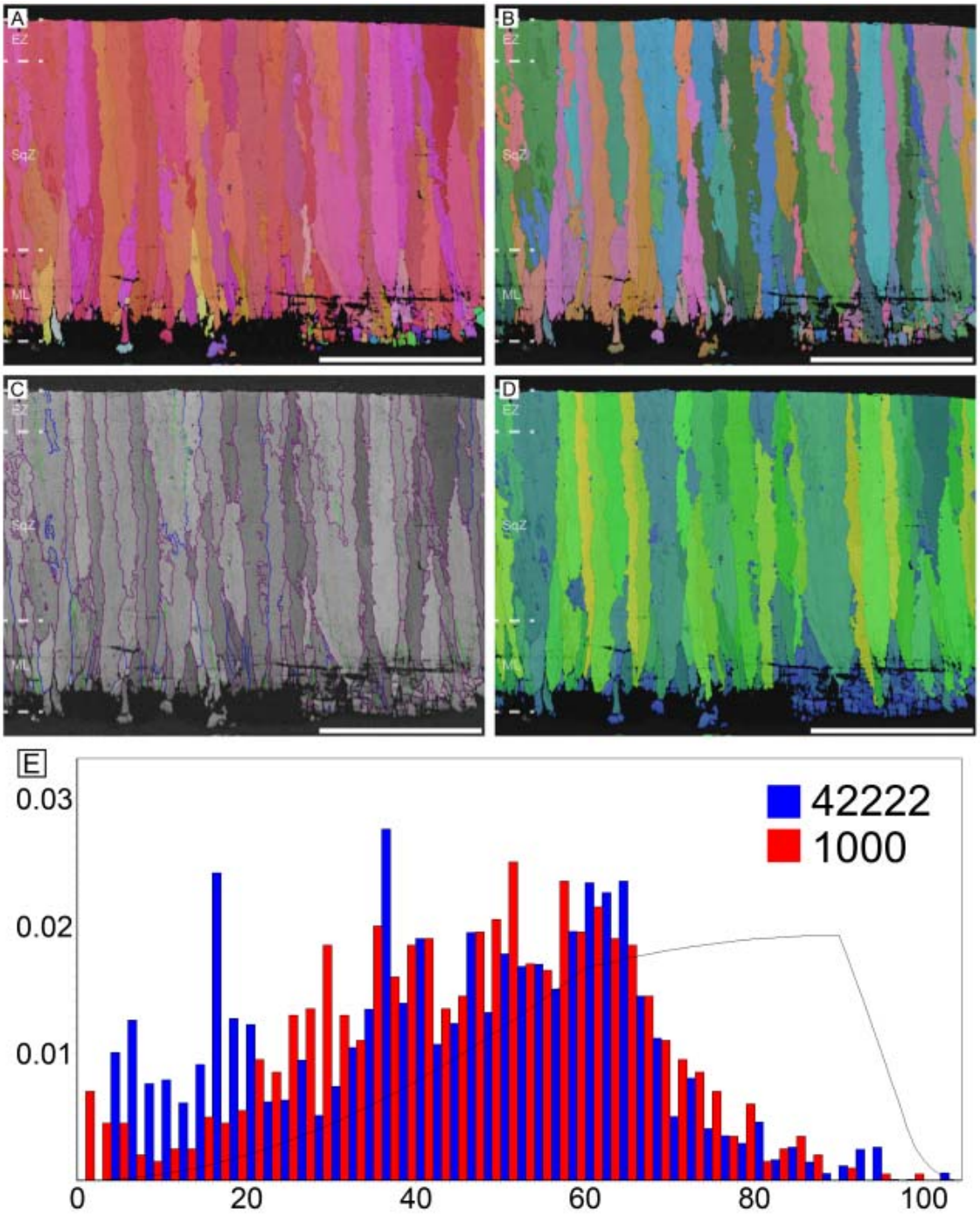

Fig. S11. *Prismatoolithus levis* (see also Varricchio et al. 2002; Varricchio and Jackson 2004). Scale bars equal 500 μm.

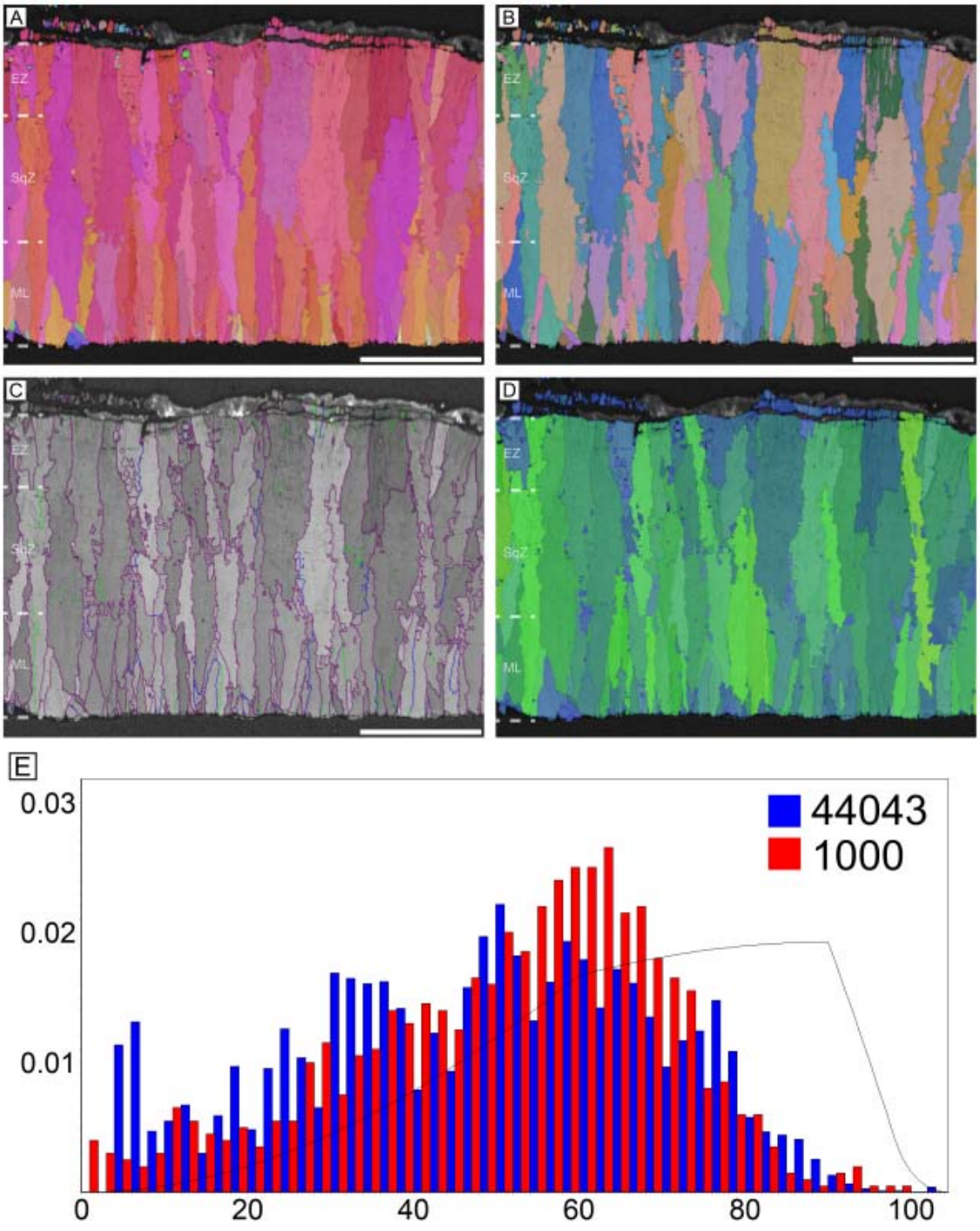

Fig. S12. *Triprismatoolithus stephensi* (see also Jackson and Varricchio 2010; Yang et al. 2018). Scale bars equal 250 μm.

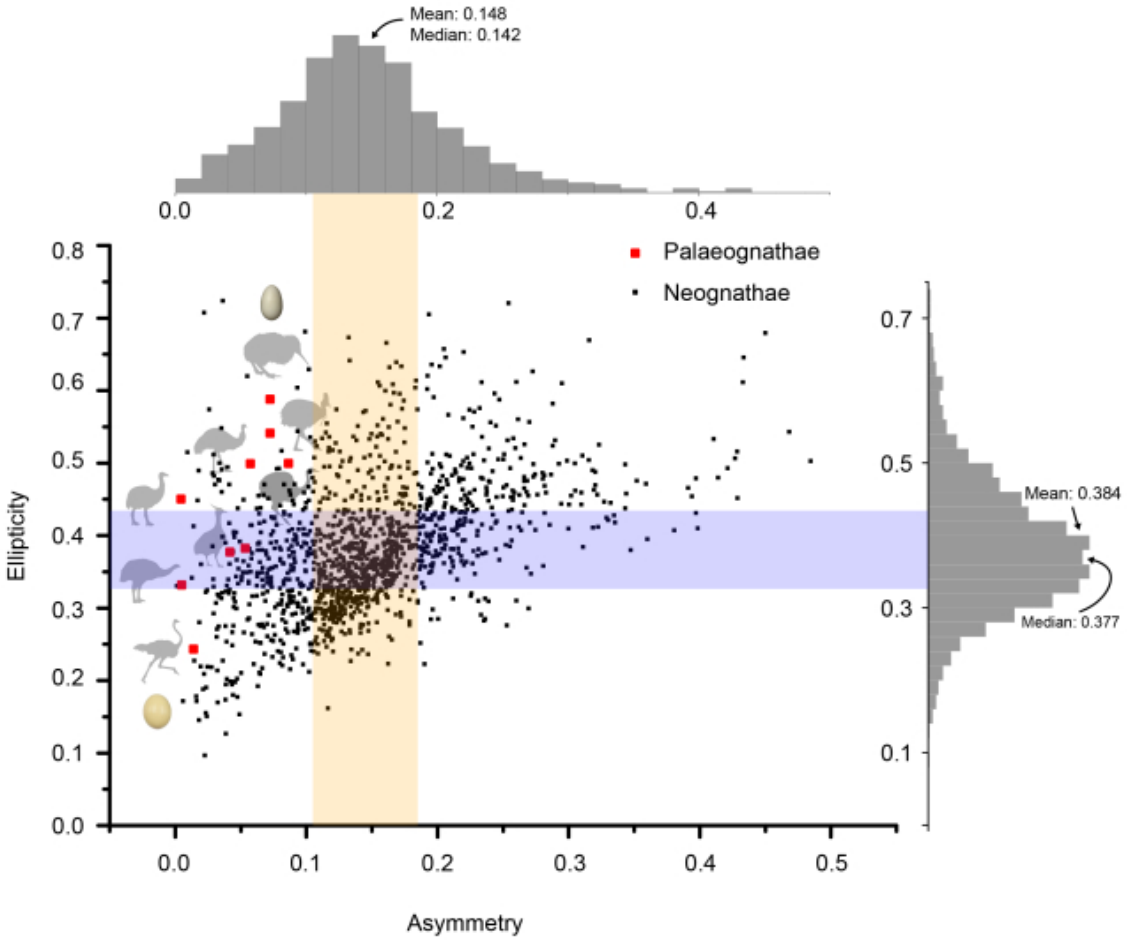

Fig. S13. Ellipticity and asymmetry of palaeognath eggs. Note that ellipticity of palaeognath eggs are not confined to certain range. Kiwi egg has maximum ellipticity and ostrich egg has minimum ellipticity. However, in case of asymmetry, palaeognath eggs have low asymmetry compared to neognath eggs. Coloured ranges mark interquartile ranges of both indices. Modified from Stoddard et al. (2017).

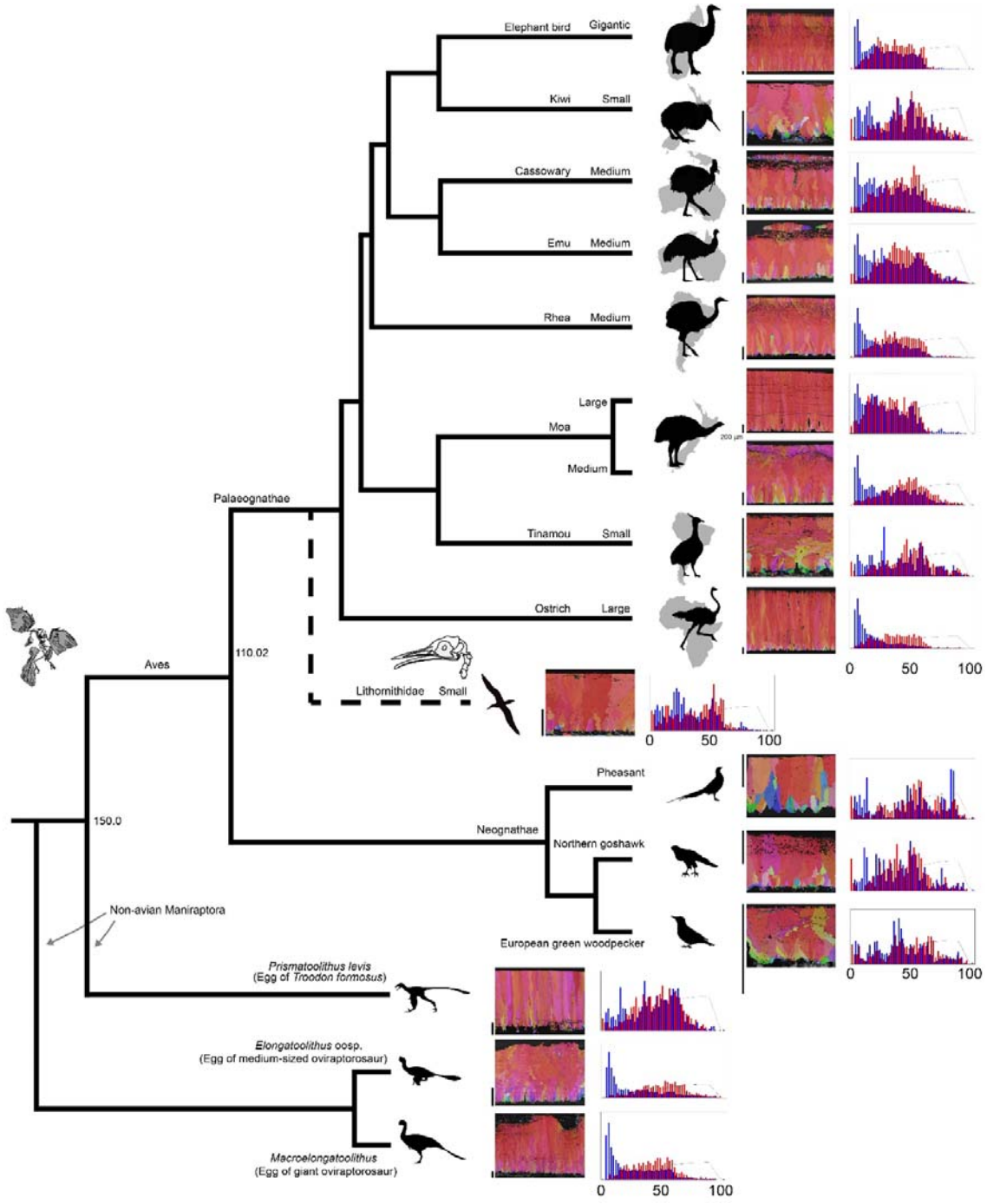

Fig. S14. Alternative interpretation of phylogeny of Palaeognathae with IPF mapping and MD. After Cloutier et al. (2019) and Sackton et al. (2019).

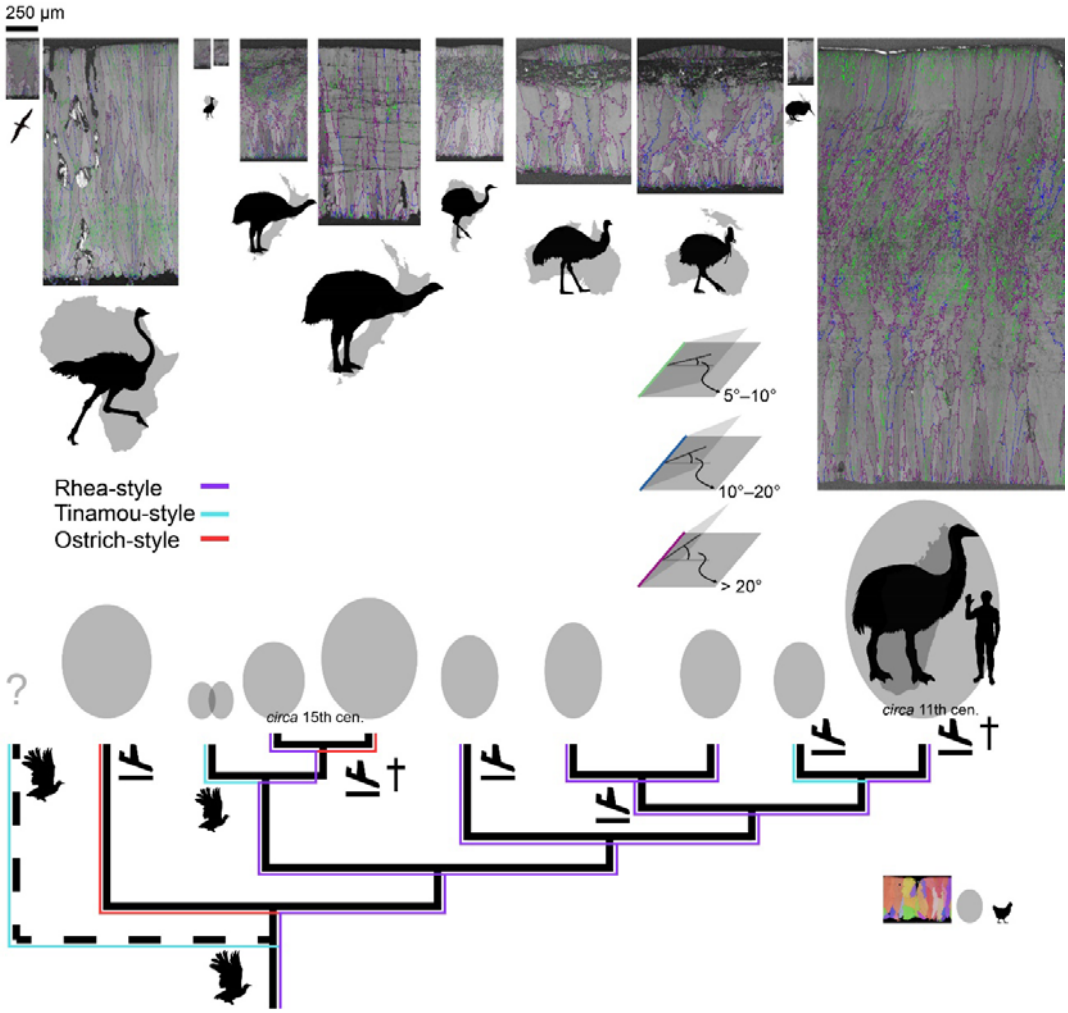

Fig. S15. Alternative interpretation of phylogeny of Palaeognathae with GB mapping, egg size, and thickness of eggshells. After Cloutier et al. (2019) and Sackton et al. (2019).

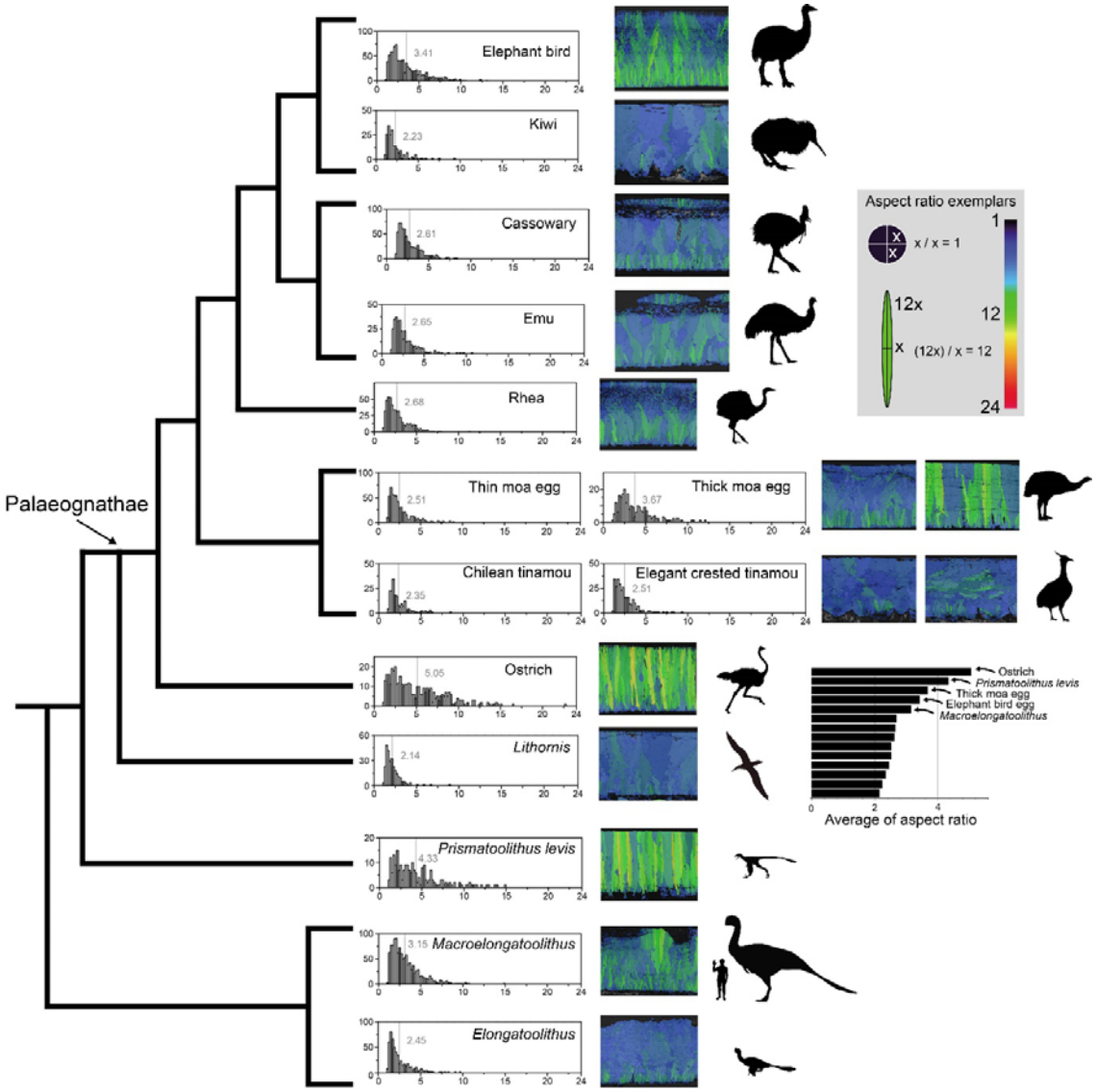

Fig. S16. Alternative interpretation of phylogeny of Palaeognathae with AR mapping. After Cloutier et al. (2019) and Sackton et al. (2019).

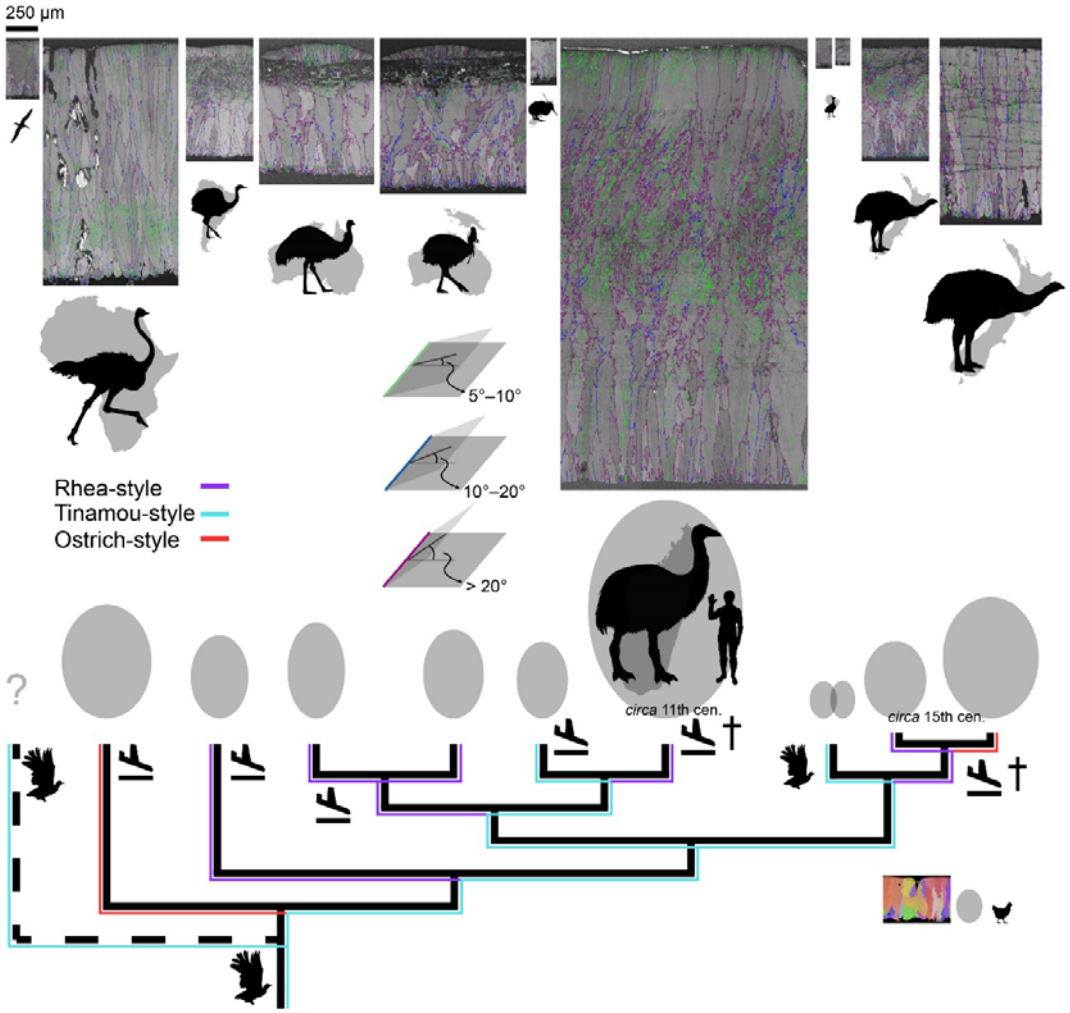

Fig. S17. An alternative interpretation of evolution of palaeognath eggshells assuming that all tinamou-style eggshells are homologous to one another. In this case, rhea-style eggshells might have been independently evolved at least four times.

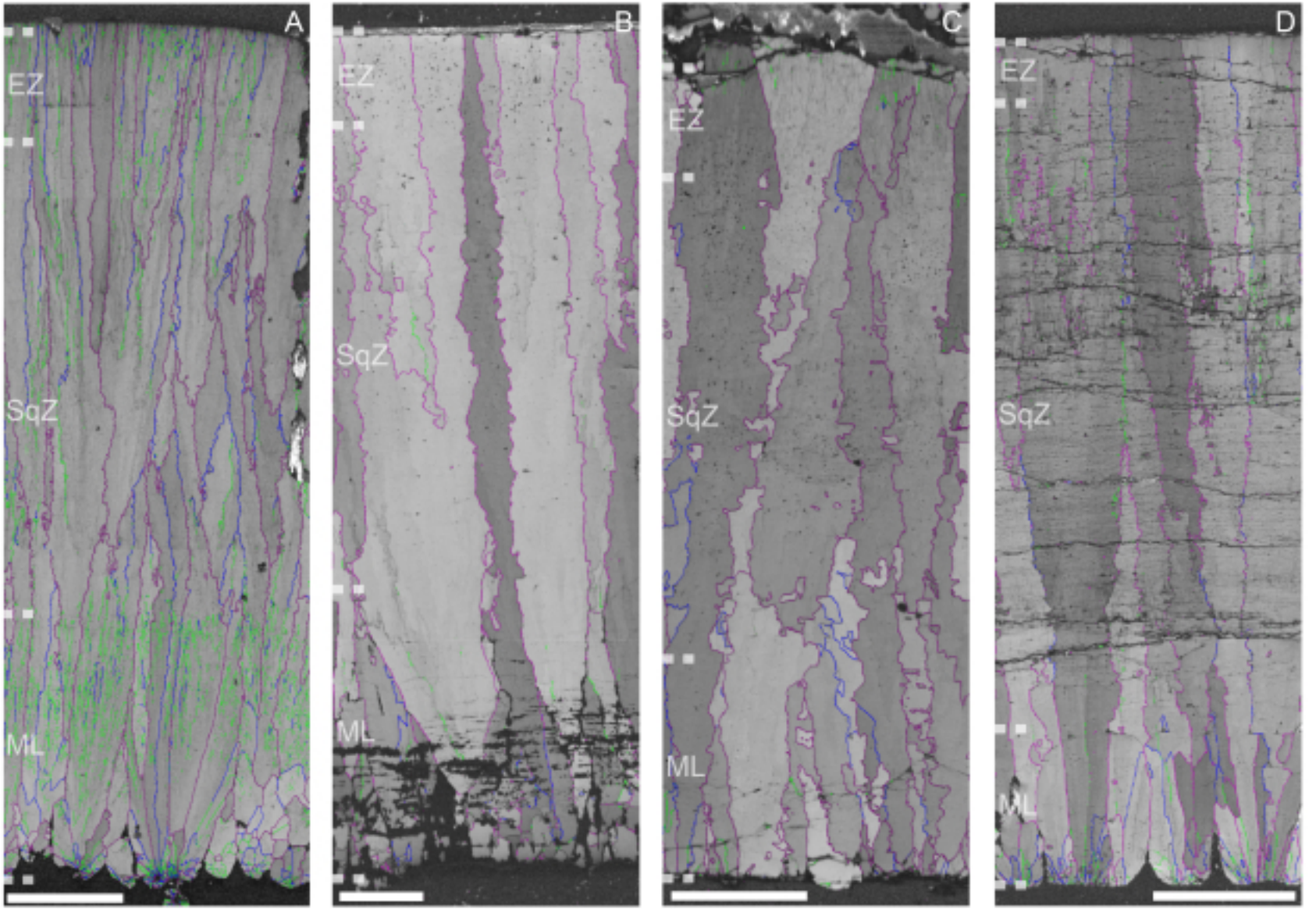
A
EZ
SqZ
ML
B
EZ
SqZ
ML
C
EZ
SqZ
ML
D
EZ
SqZ
ML

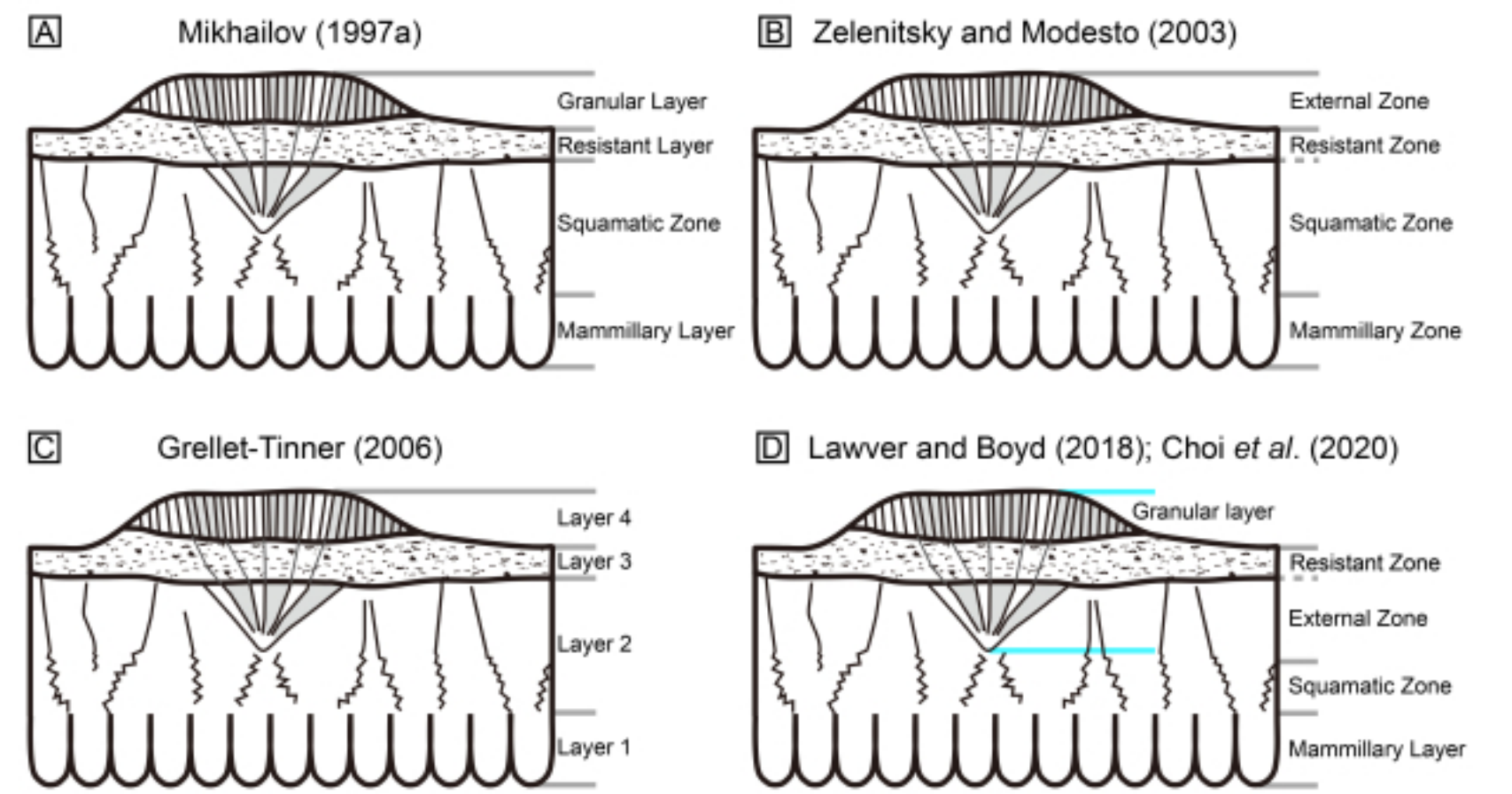
A
Mikhailov (1997a)
Granular Layer
Resistant Layer
Squamatic Zone
Mammillary Layer
B
Zelenitsky and Modesto (2003)
External Zone
Resistant Zone
Squamatic Zone
Mammillary Zone
C
Grellet-Tinner (2006)
Layer 4
Layer 3
Layer 2
Layer 1
D
Lawver and Boyd (2018); Choi et al. (2020)
Granular layer
Resistant Zone
External Zone
Squamatic Zone
Mammillary Layer

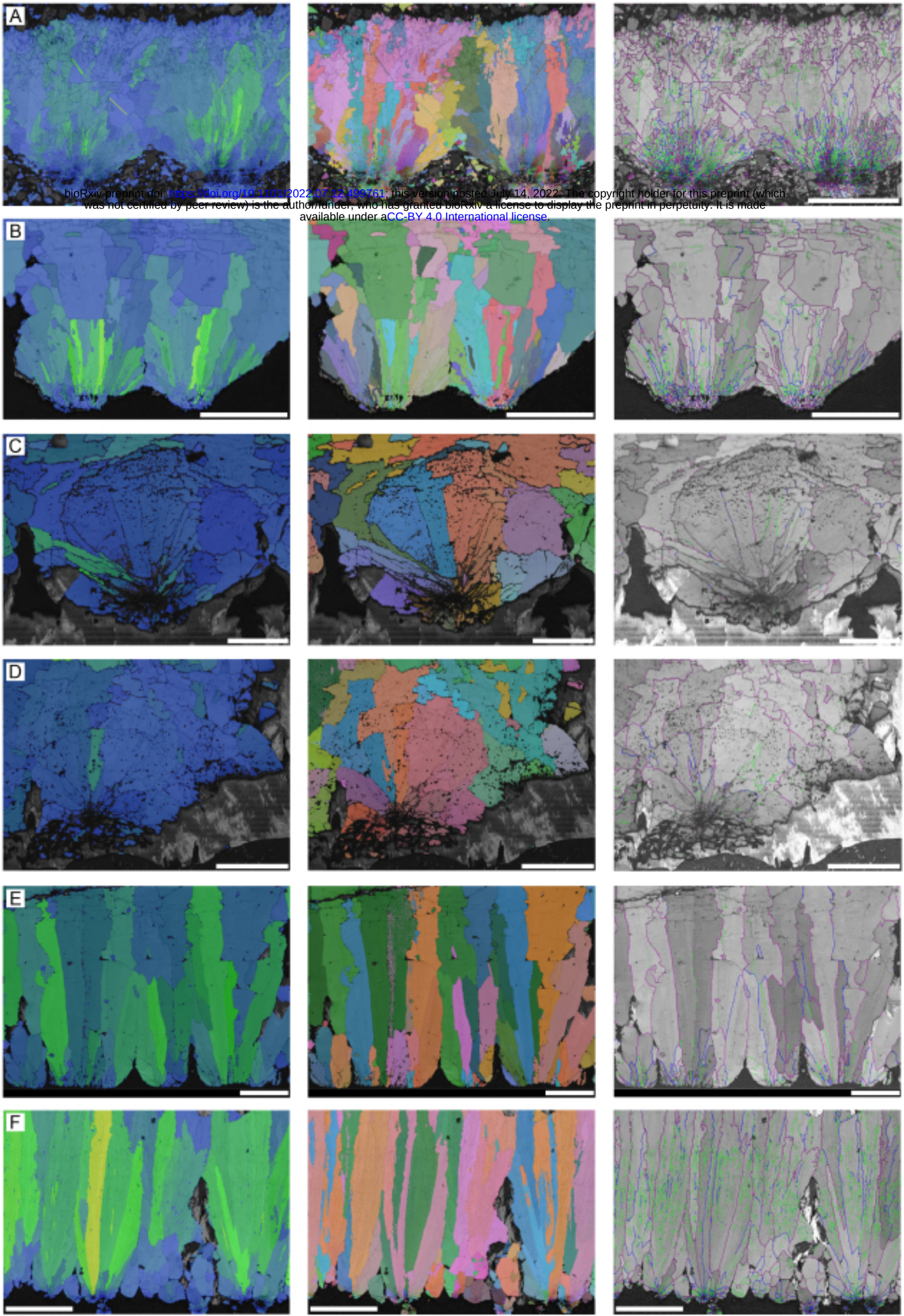

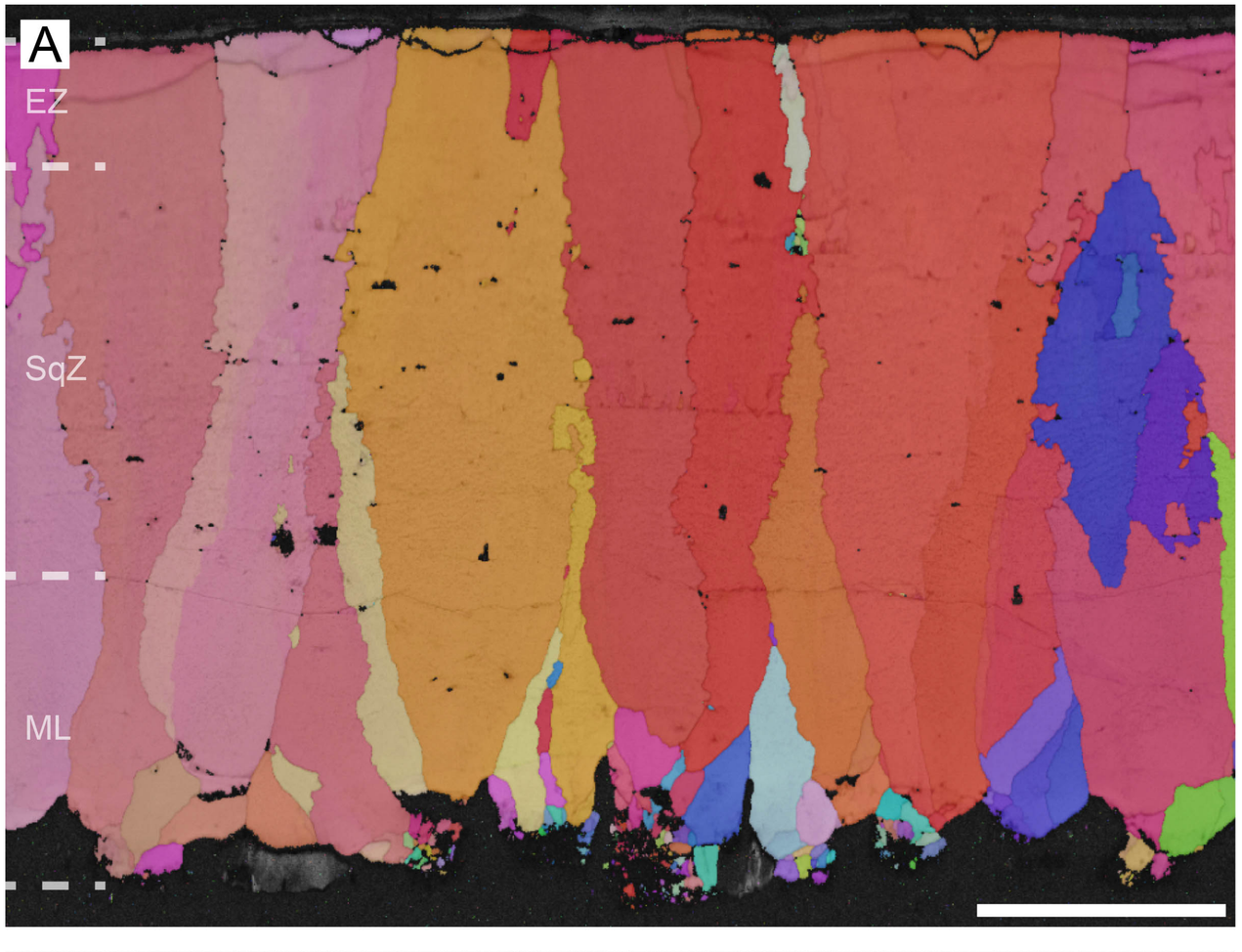

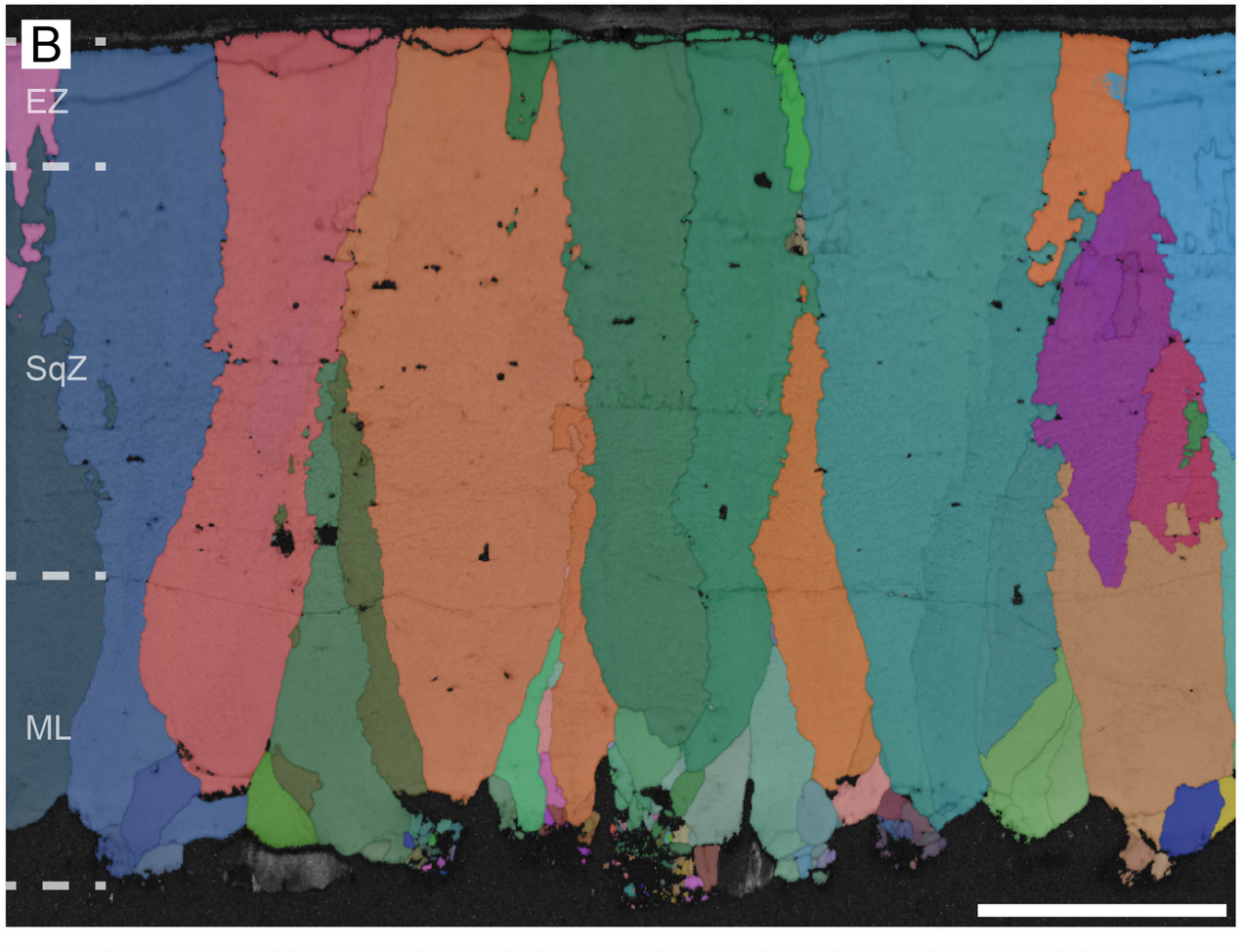

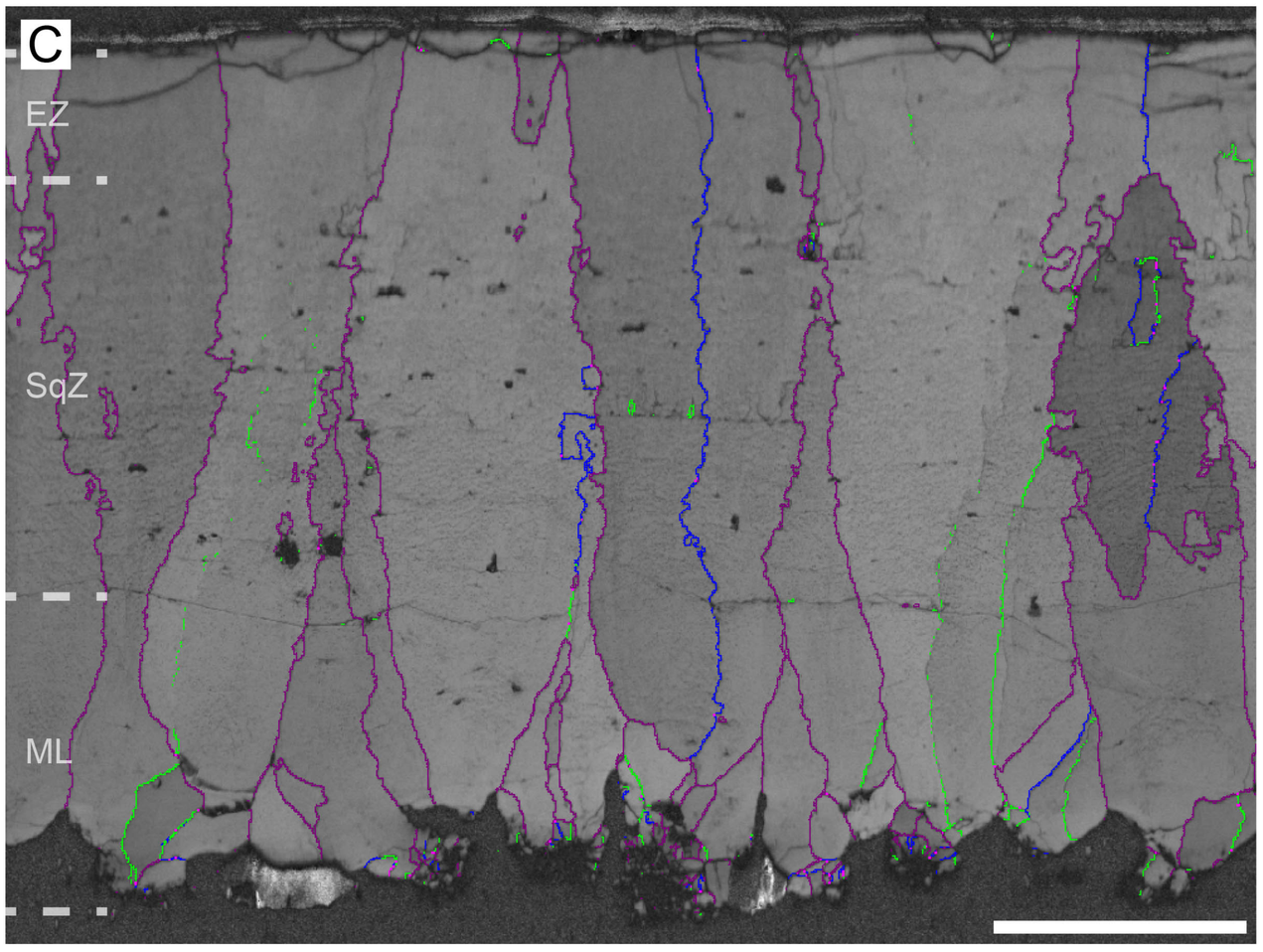

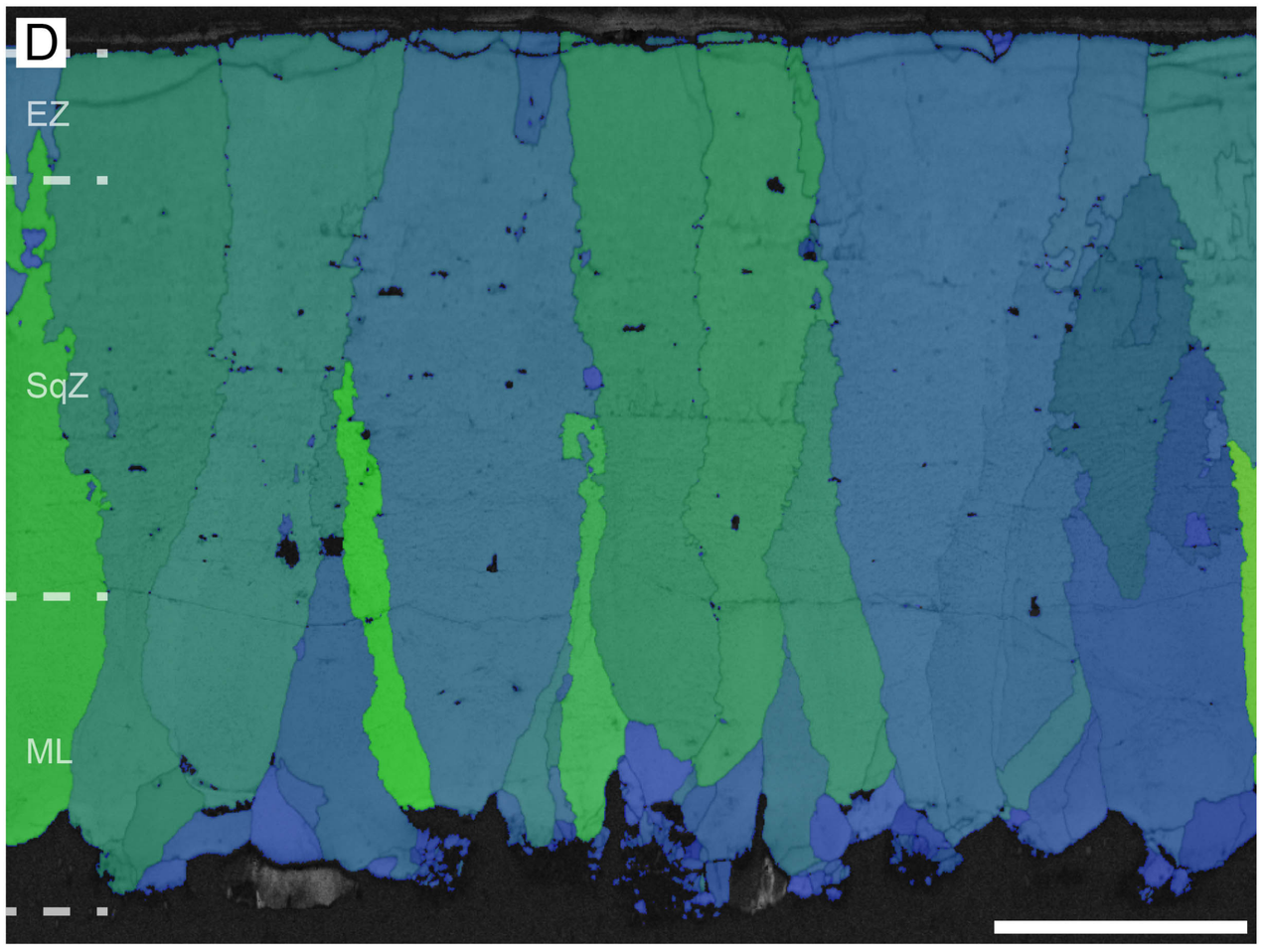

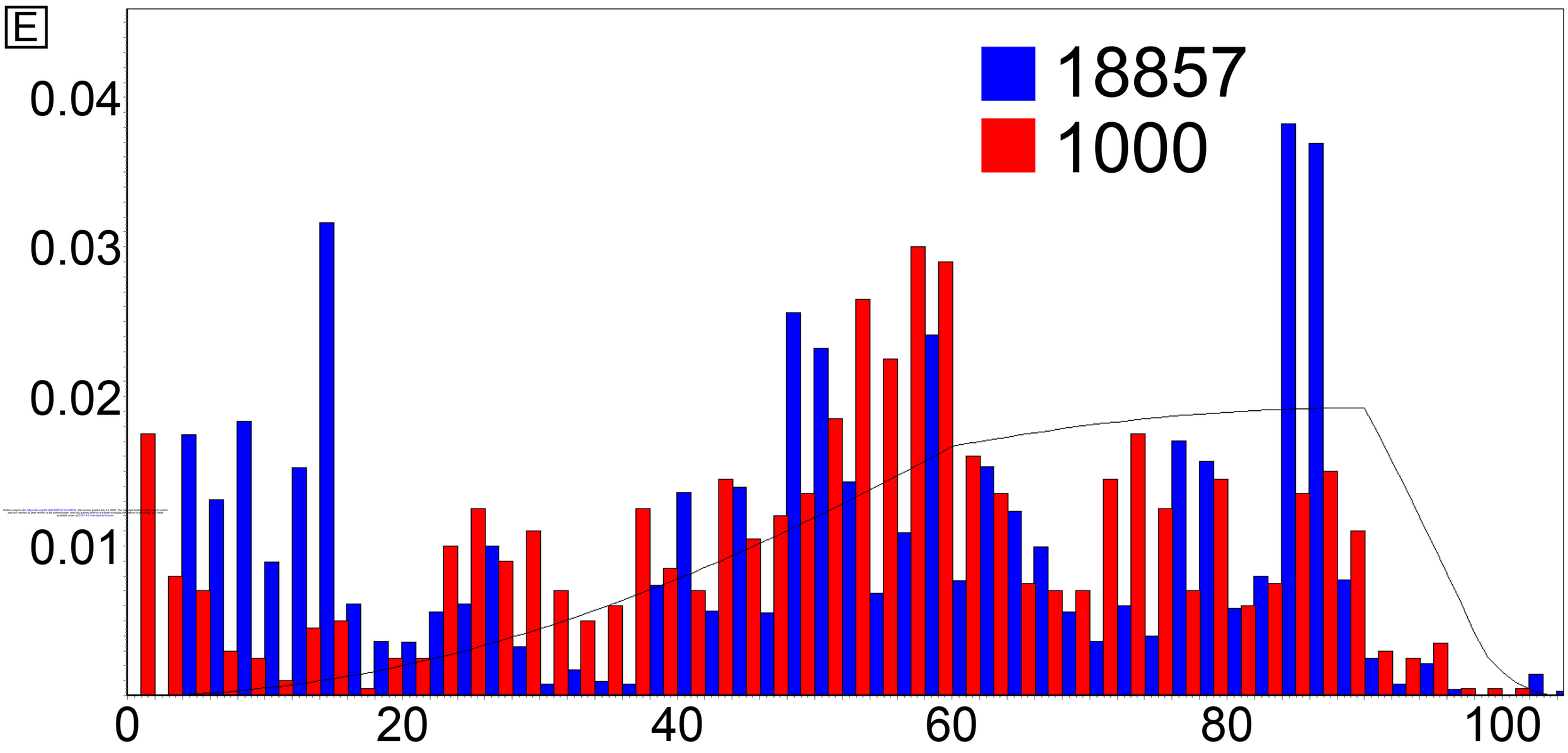

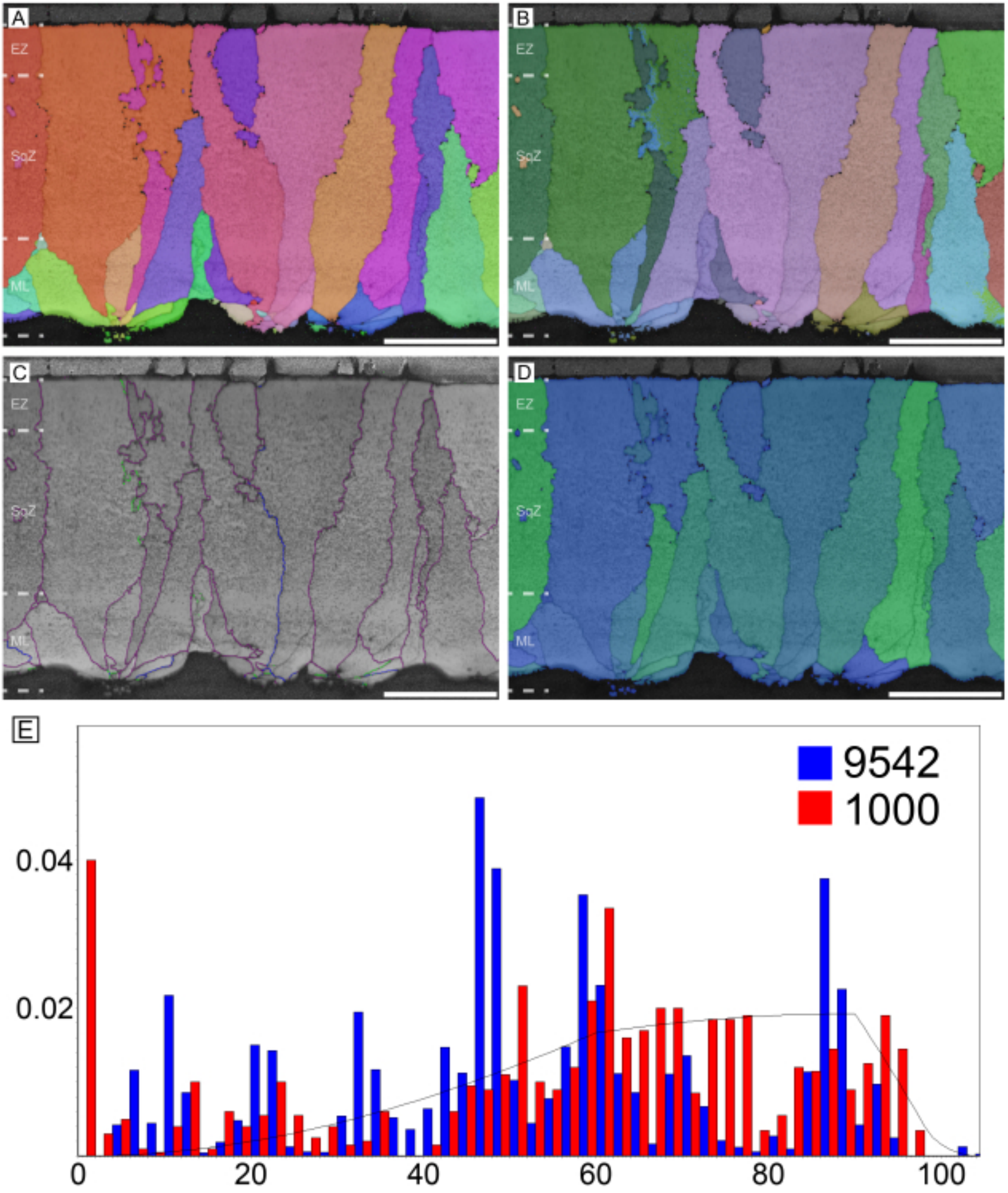
A
EZ
SoZ
ML
B
EZ
SoZ
ML
C
EZ
SoZ
ML
D
EZ
SoZ
ML
E
9542
1000
0.04
0.02
0
20
40
60
80
100

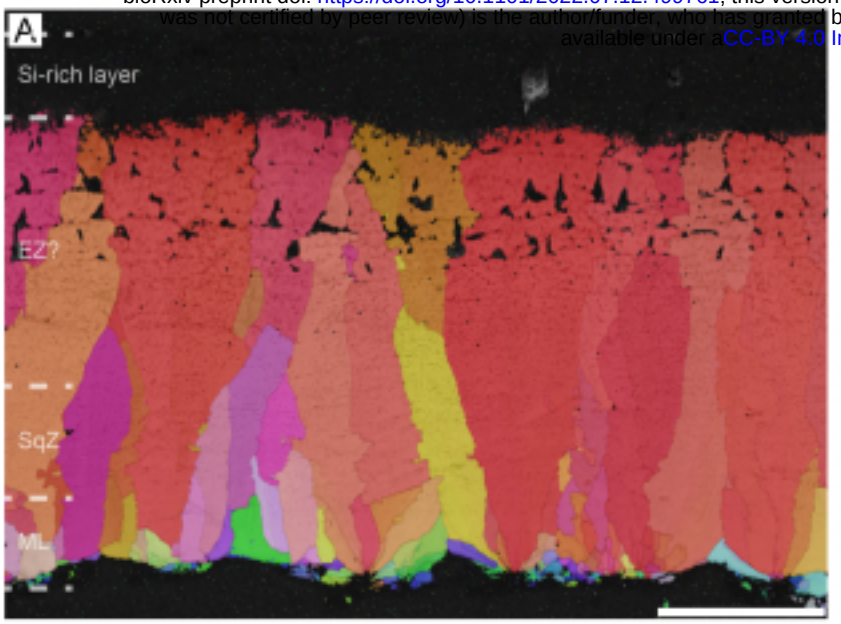

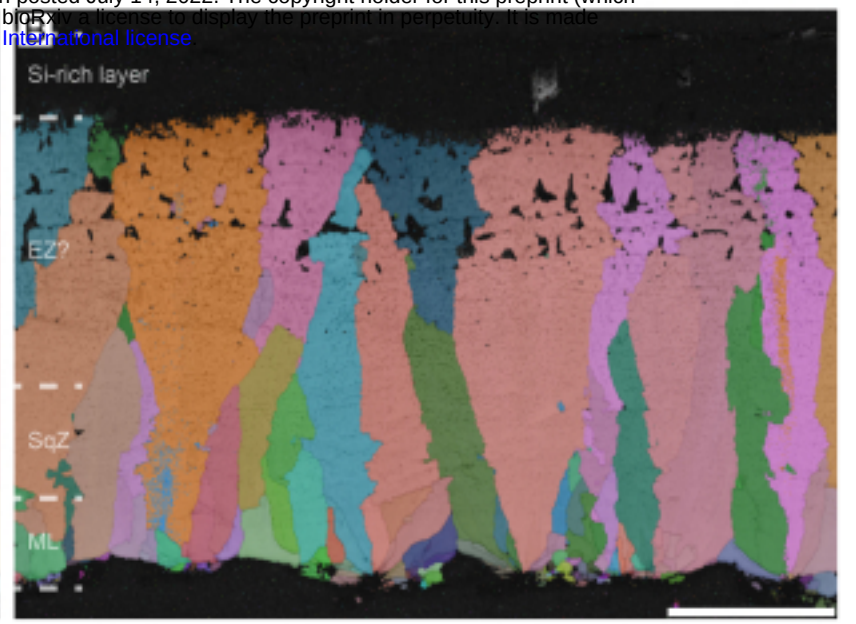

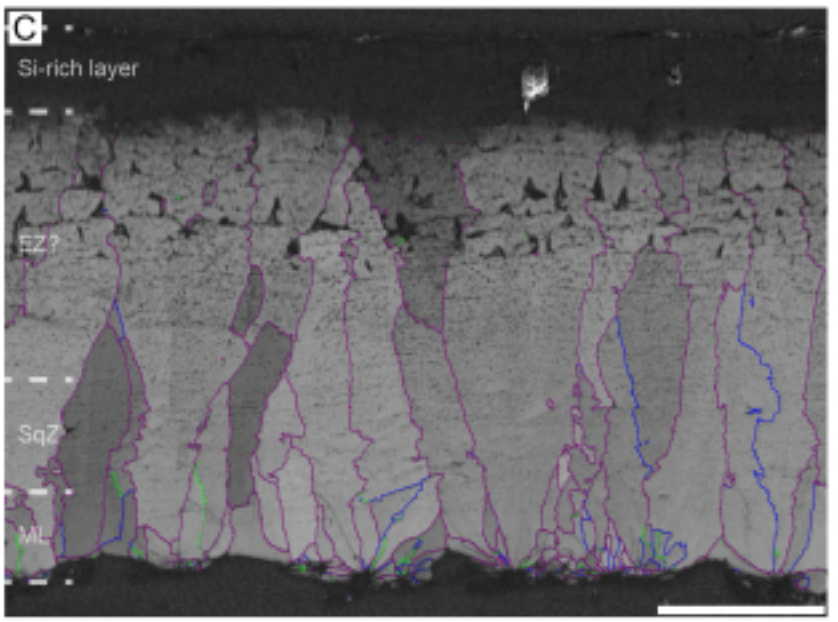

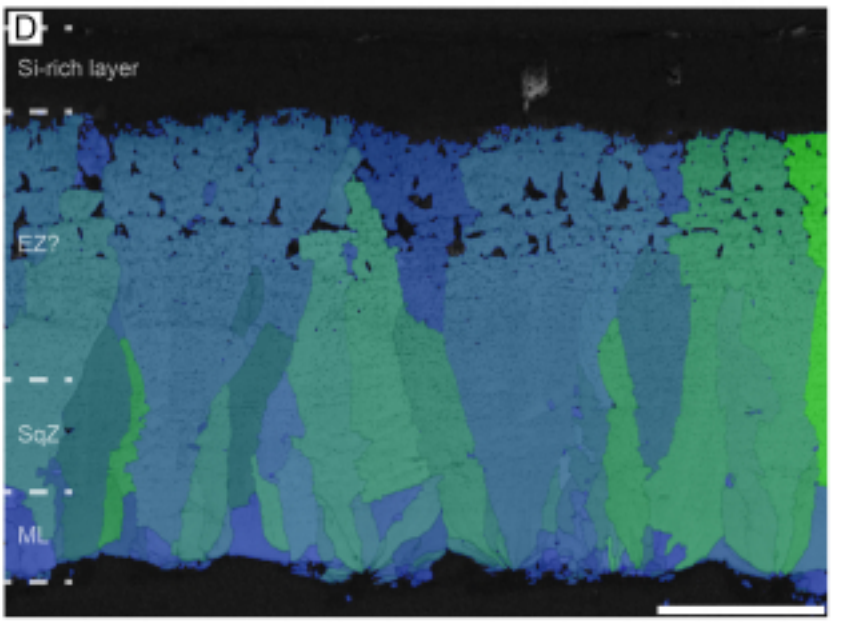

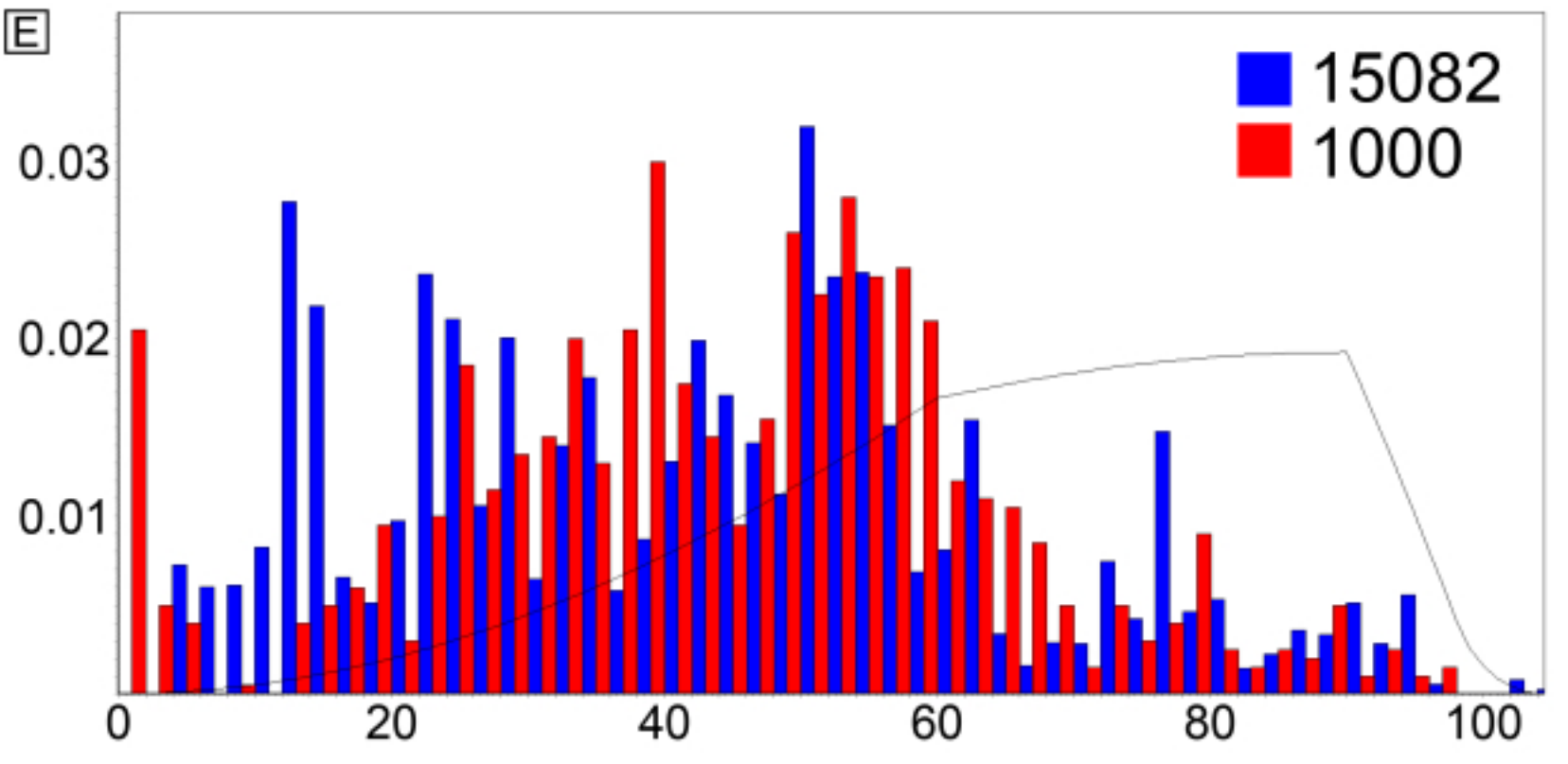

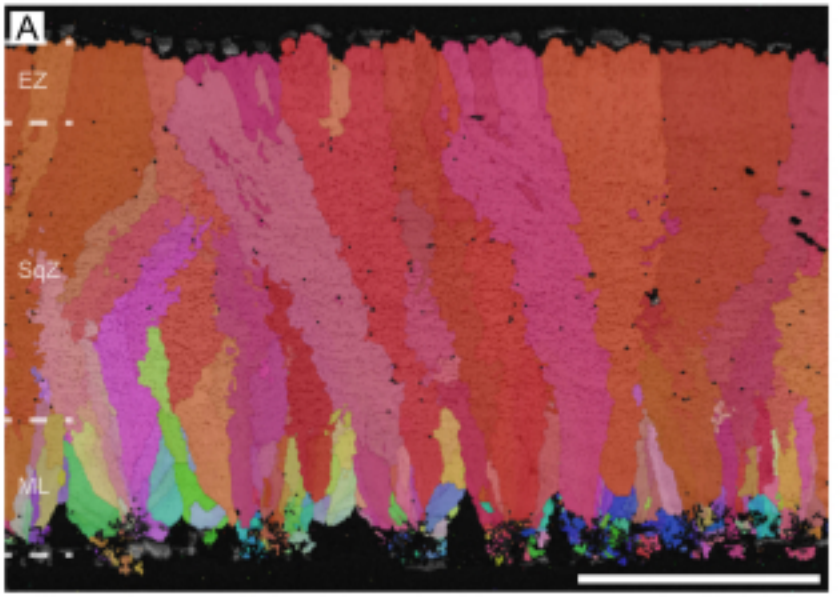
A
EZ
SqZ
ML

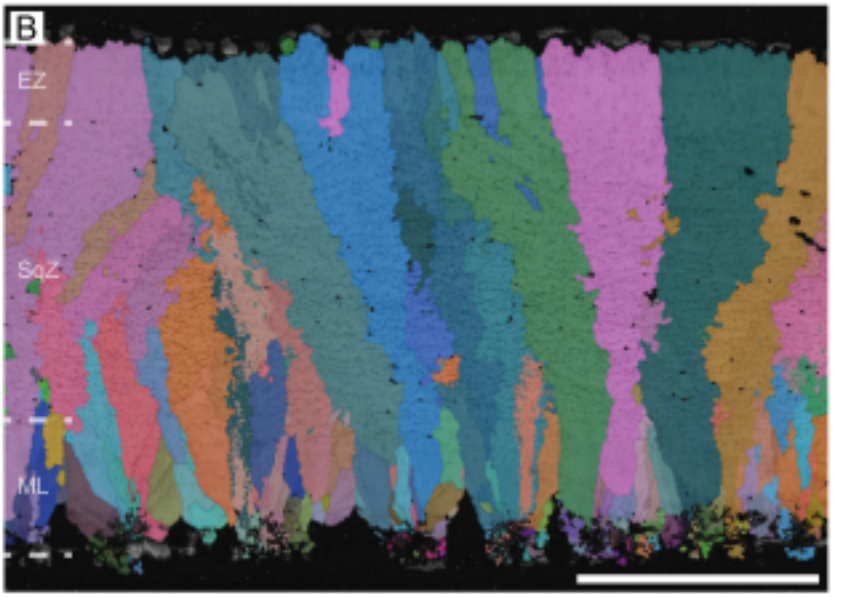
B
EZ
SqZ
ML

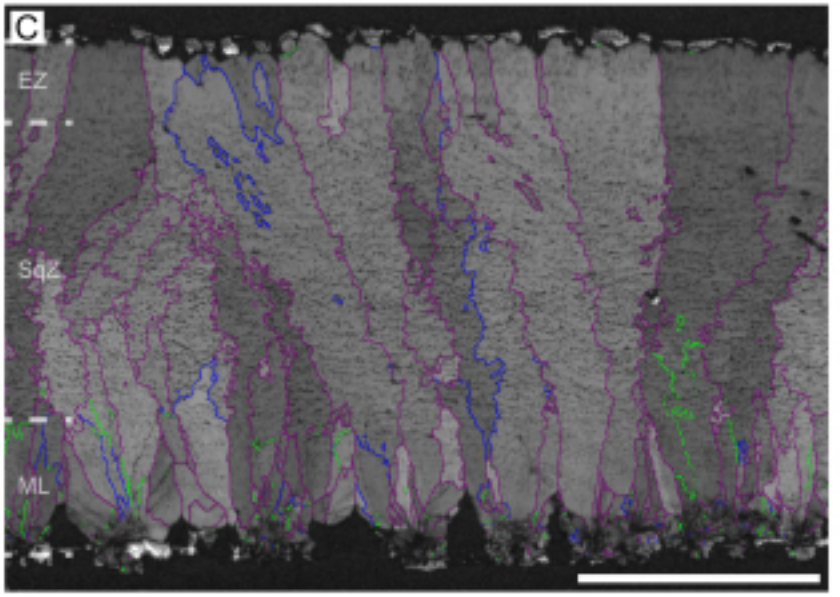
C
EZ
SqZ
ML

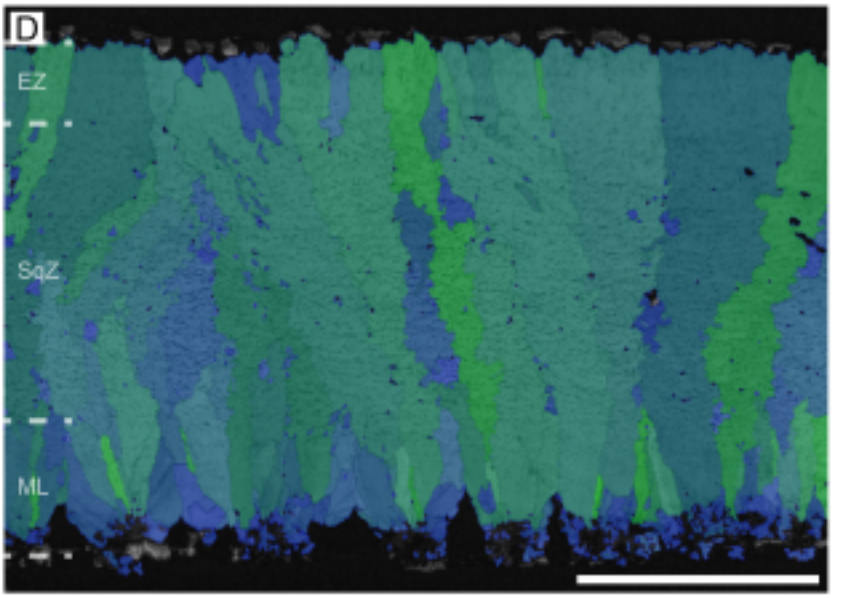
D
EZ
SqZ
ML

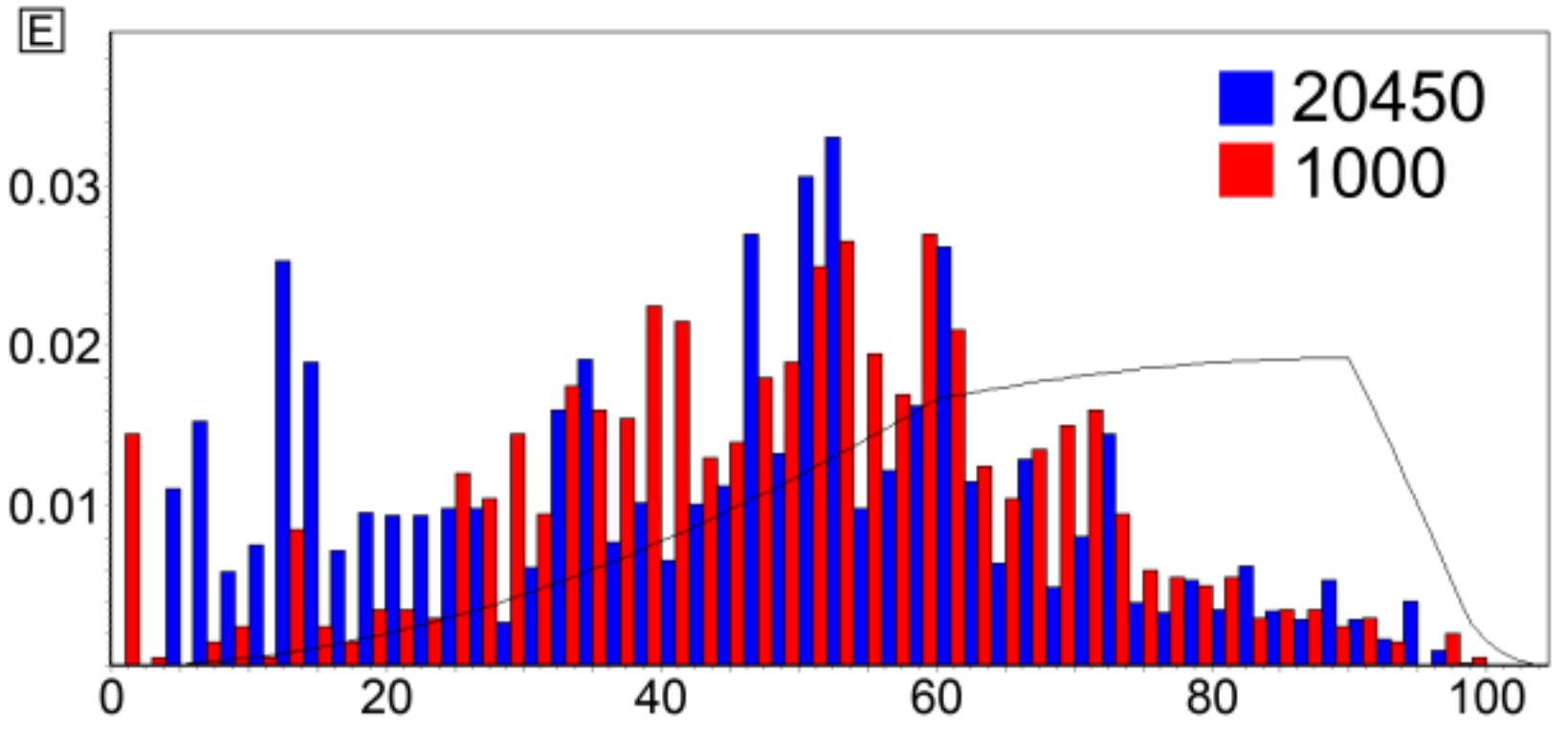
E
20450
1000
0.03
0.02
0.01
0
20
40
60
80
100

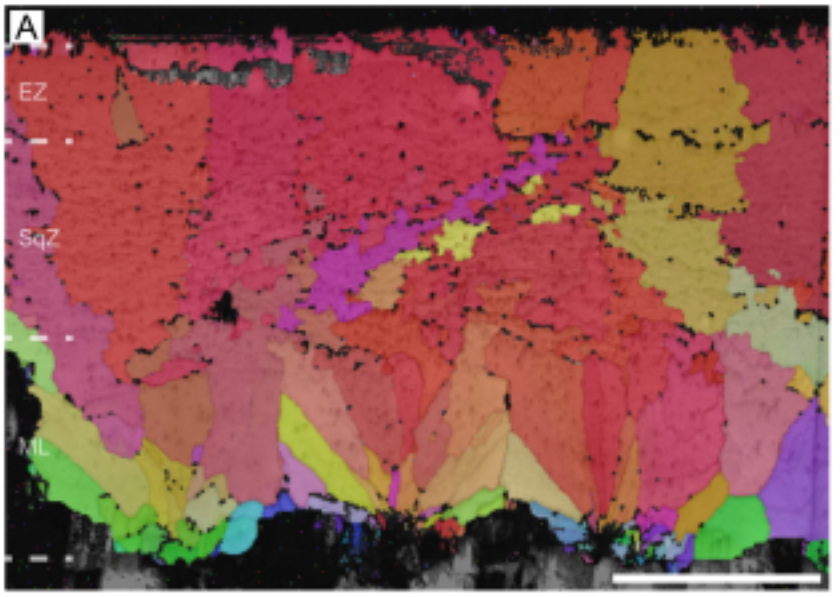
A
EZ
SqZ
ML

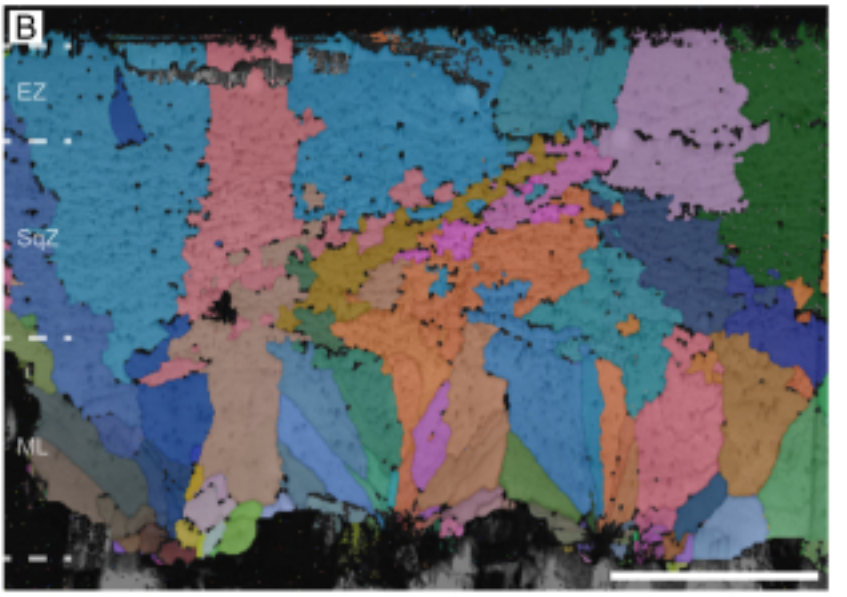
B
EZ
SqZ
ML

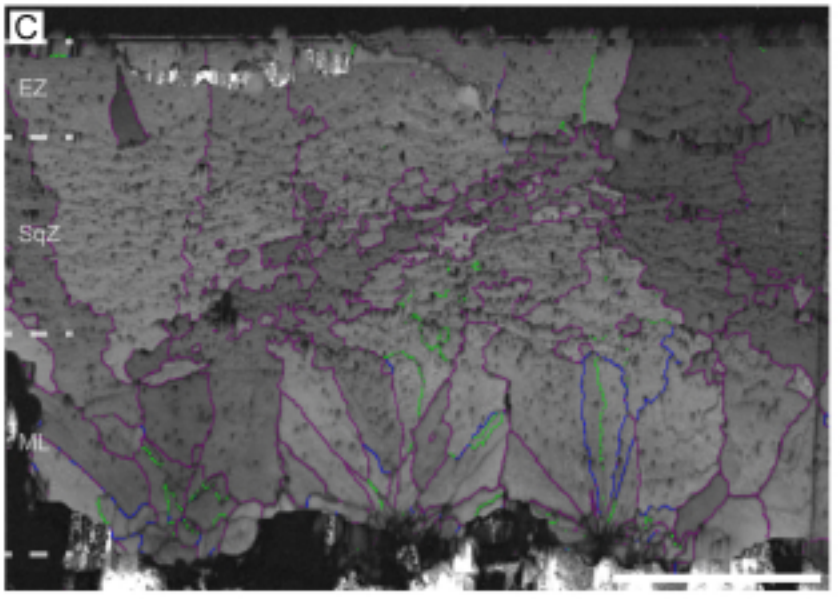
C
EZ
SqZ
ML

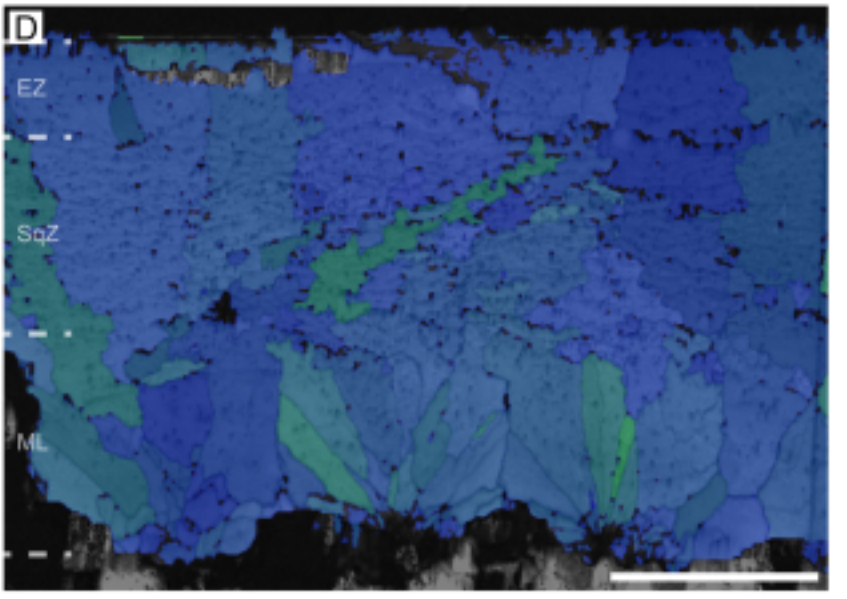
D
EZ
SqZ
ML

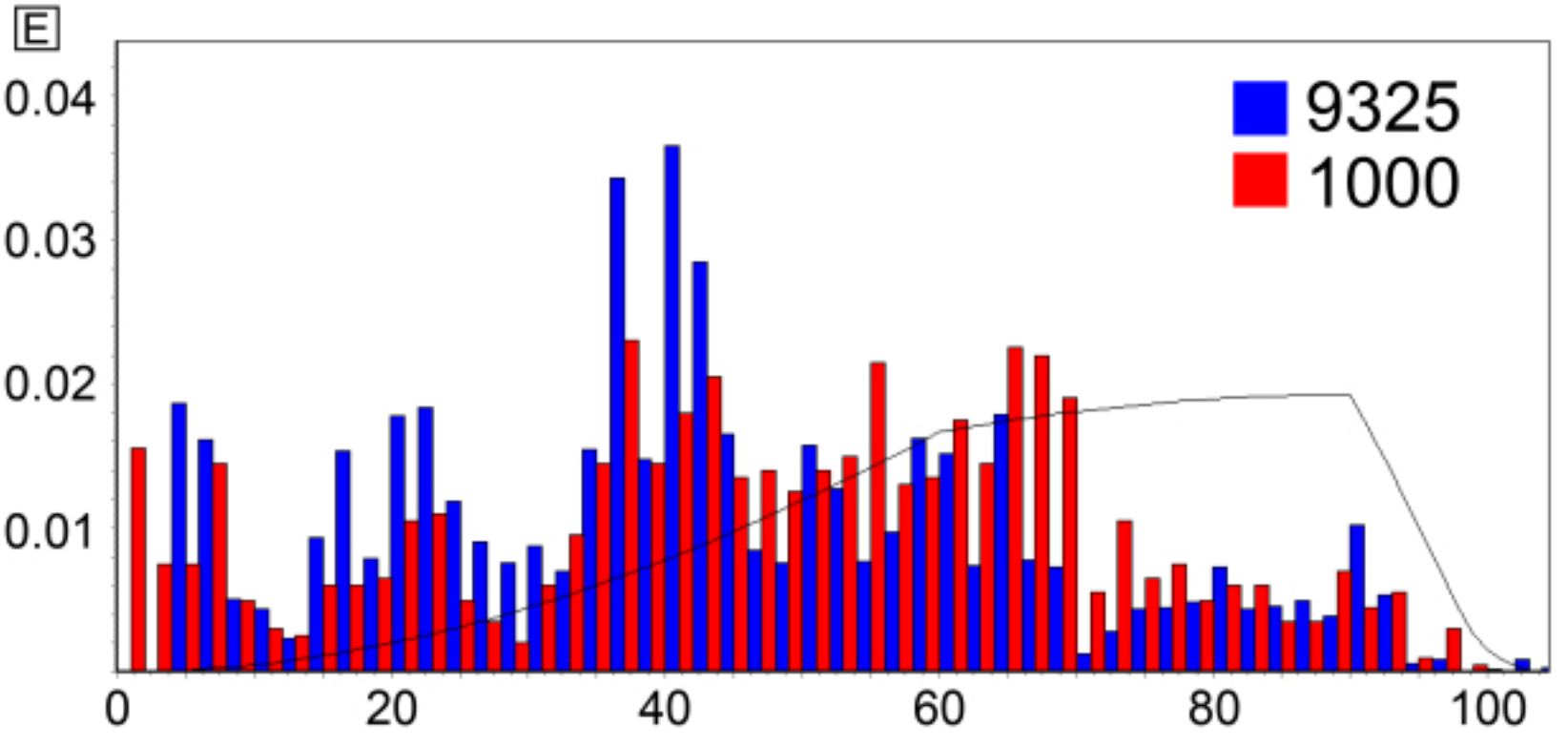
E
0.04
0.03
0.02
0.01
0
20
40
60
80
100
9325
1000

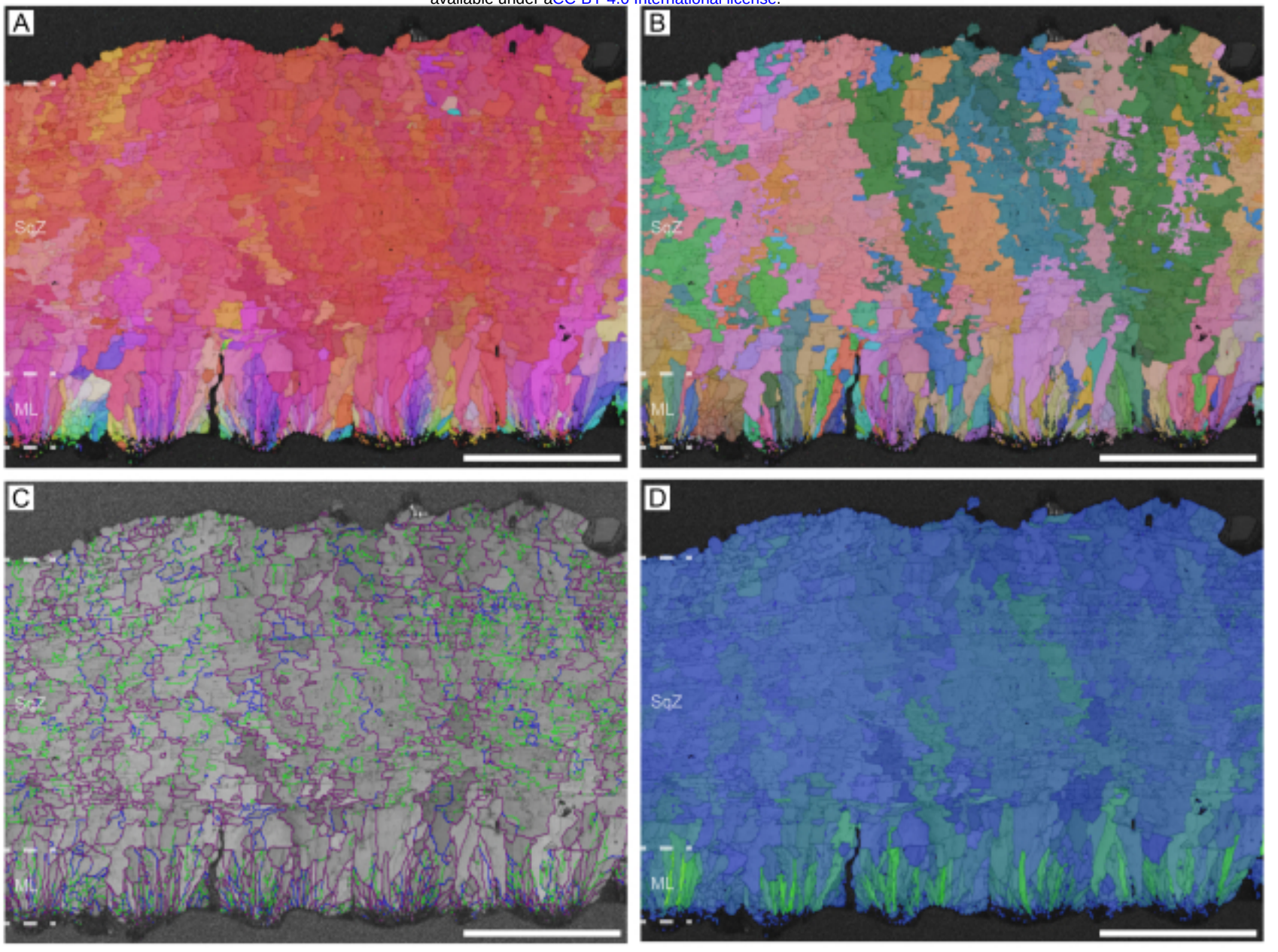

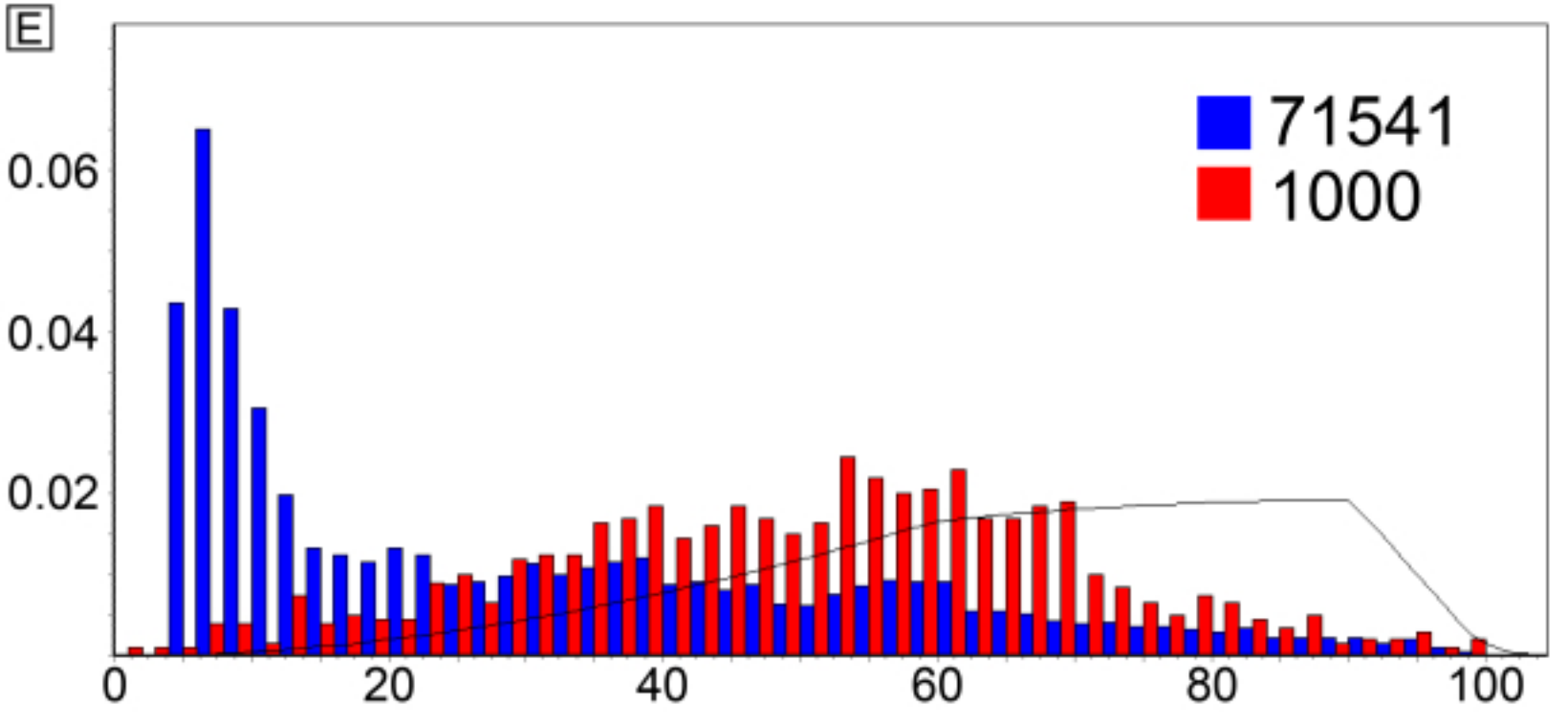

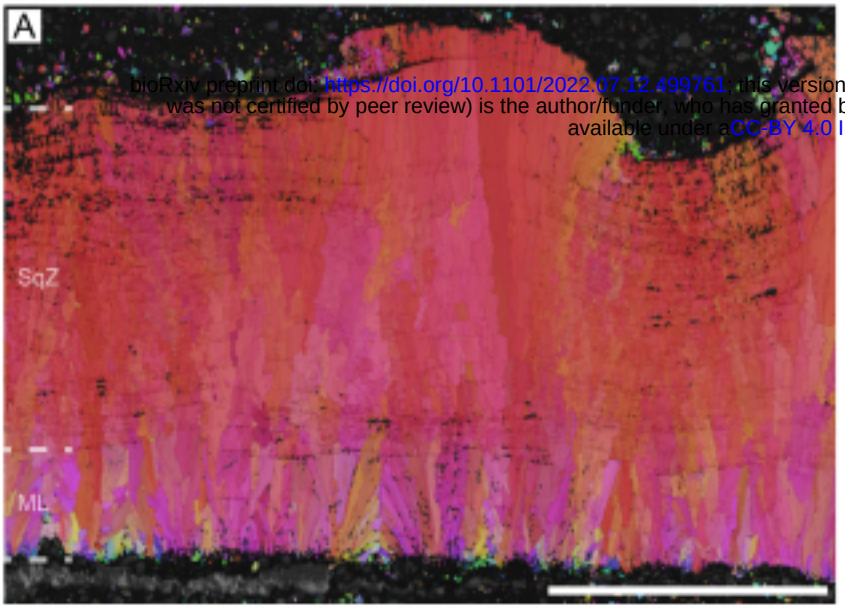

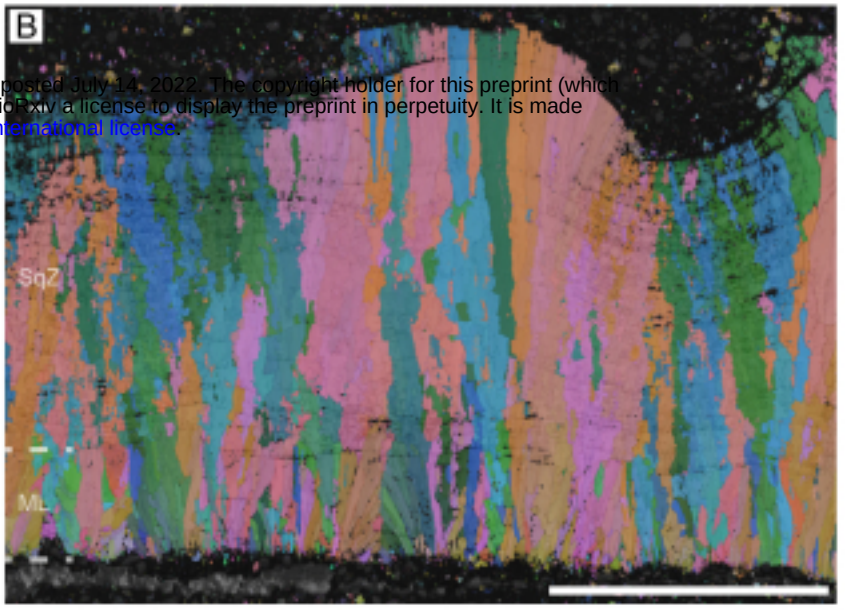

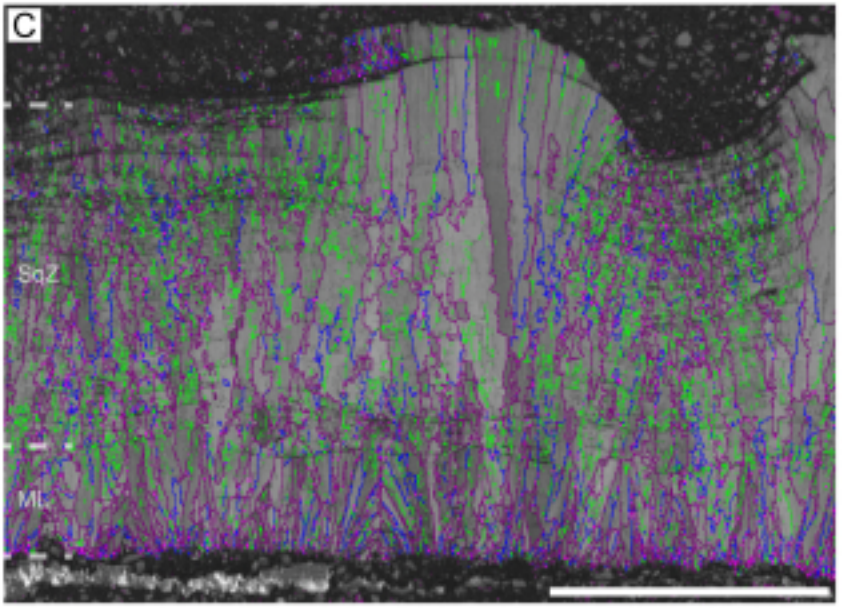

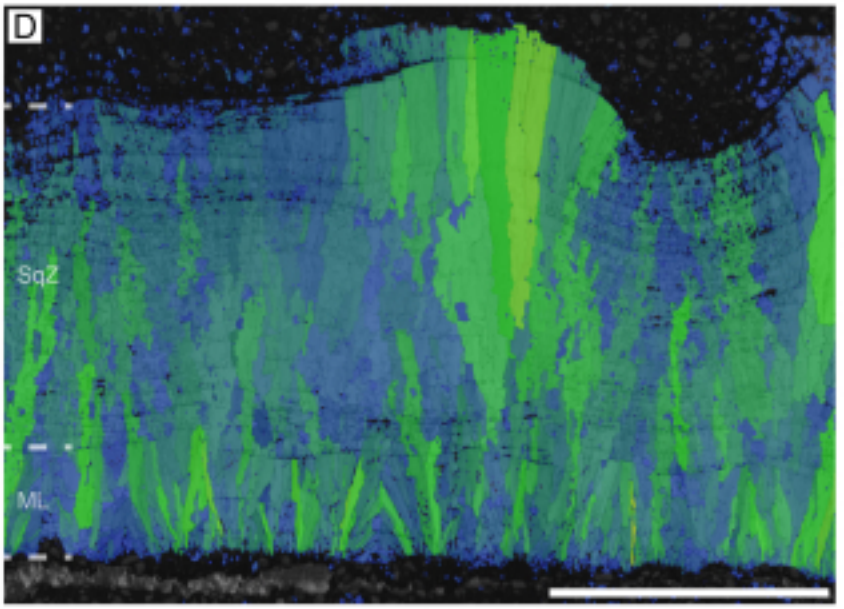

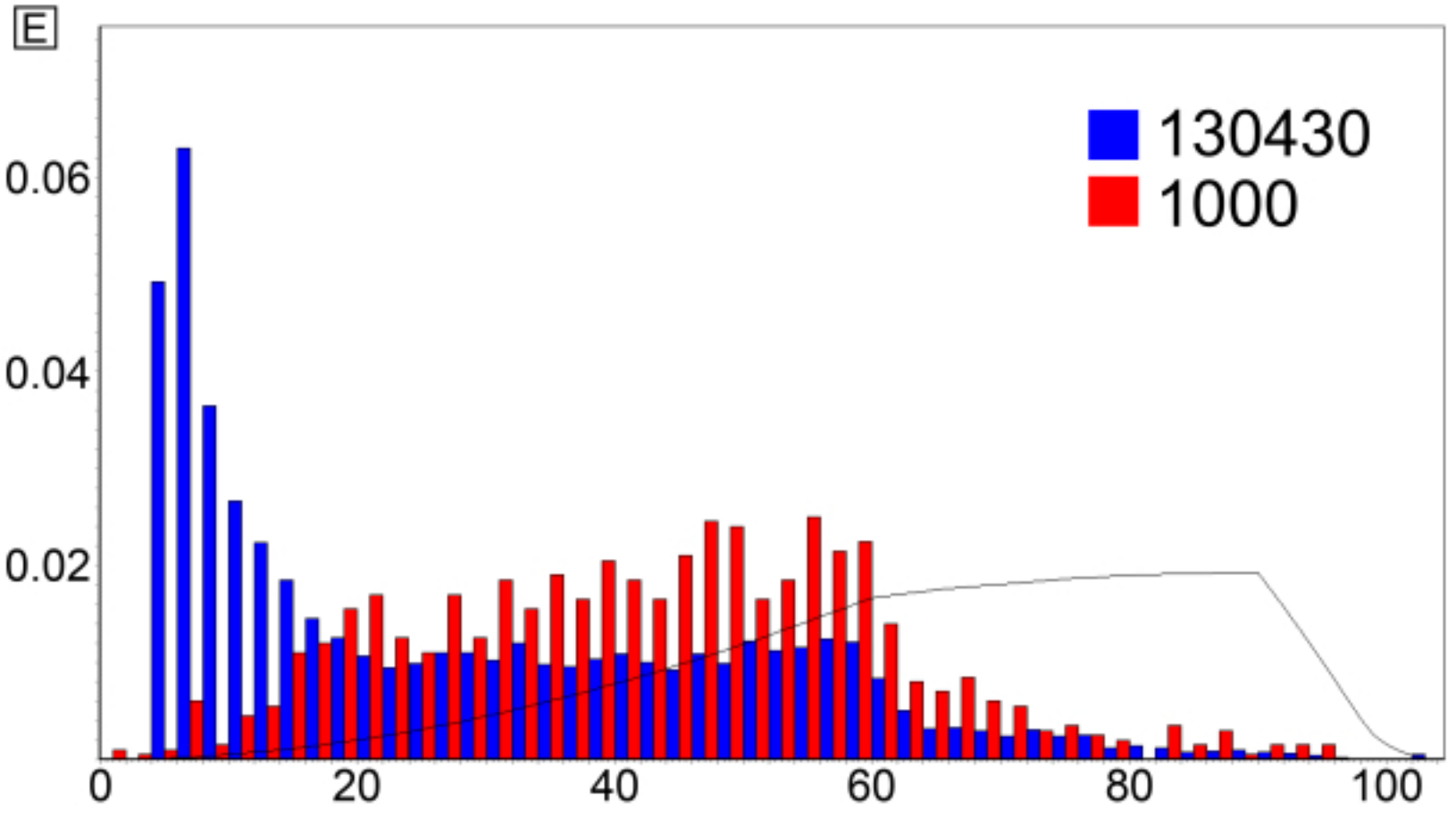

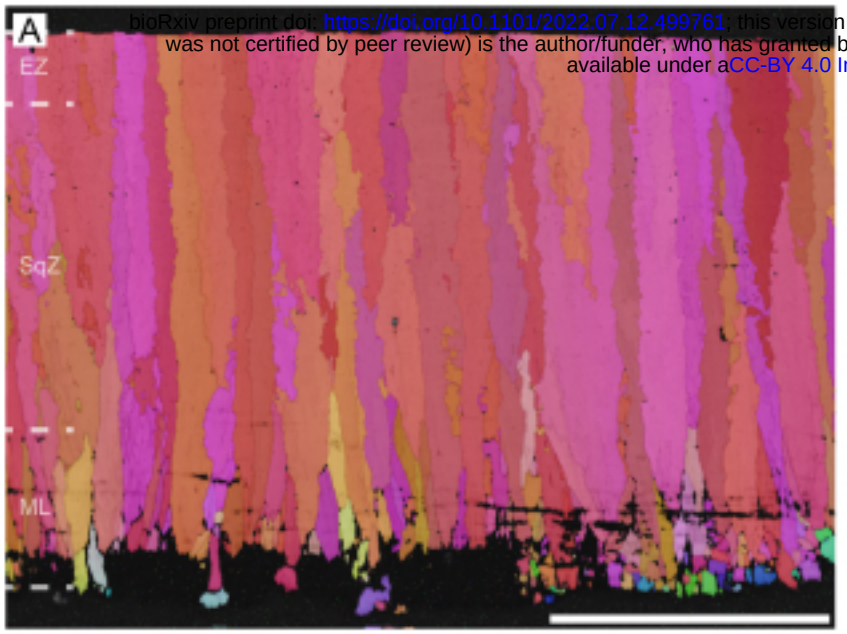

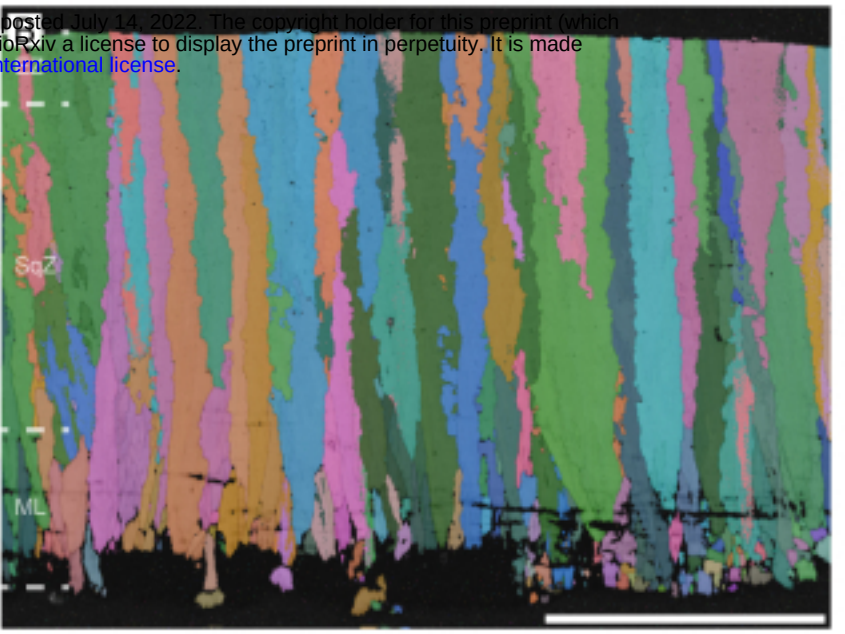

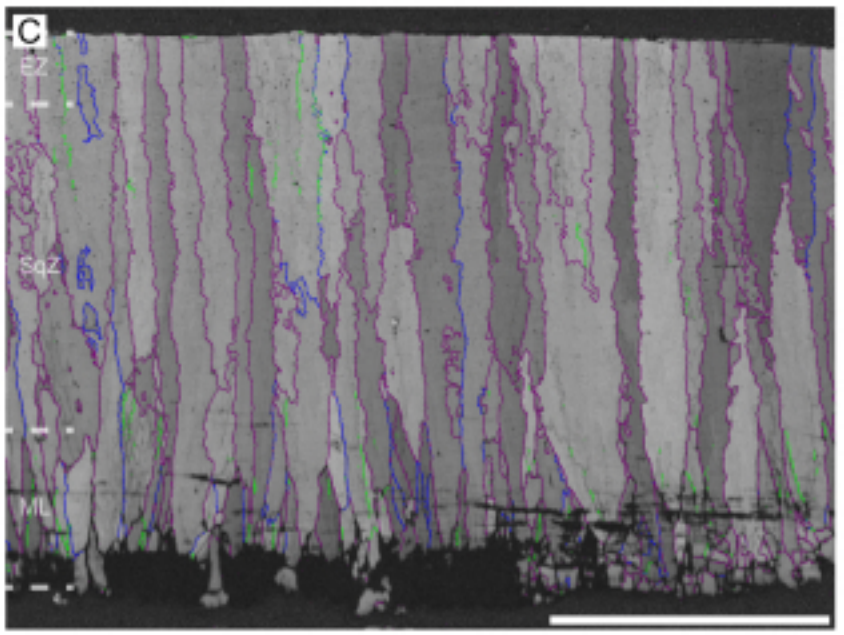

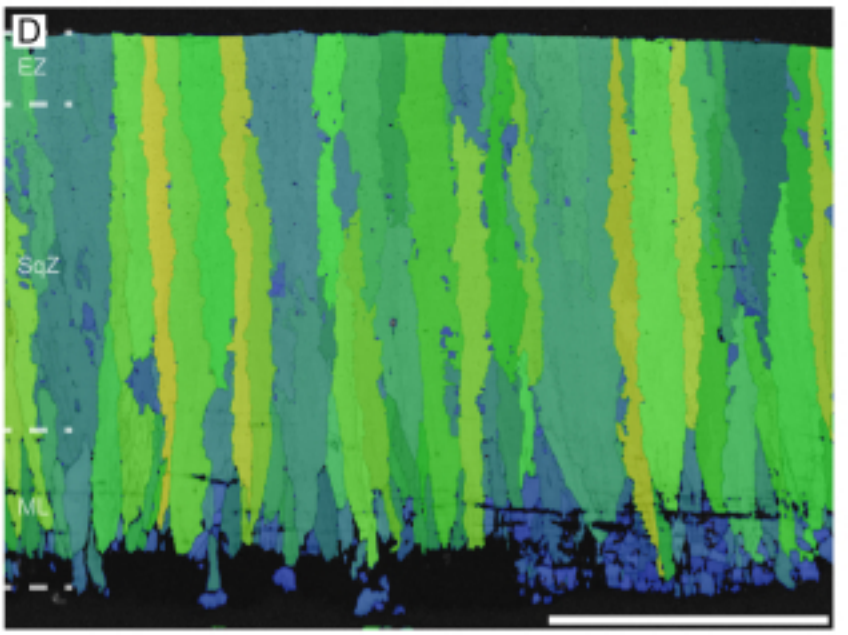

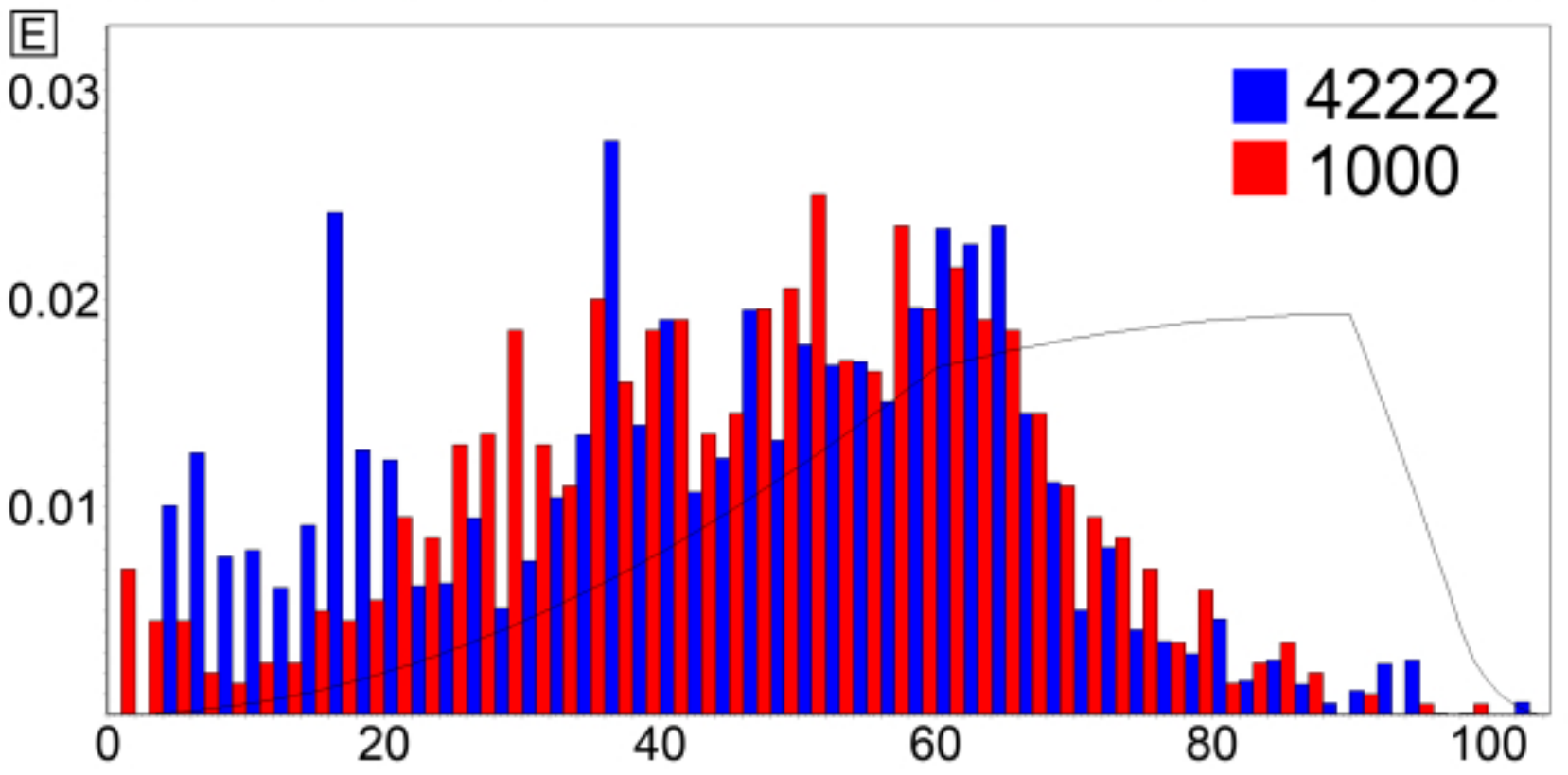

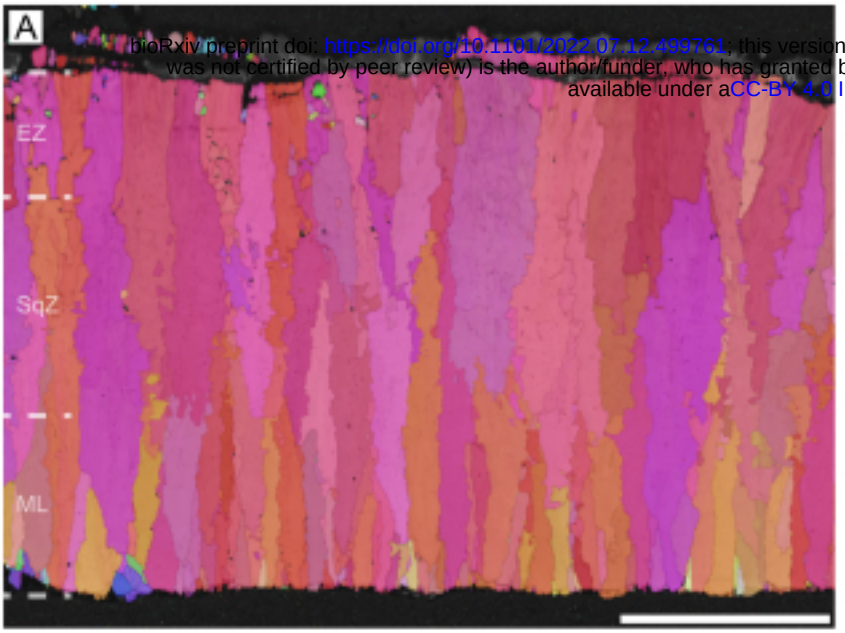

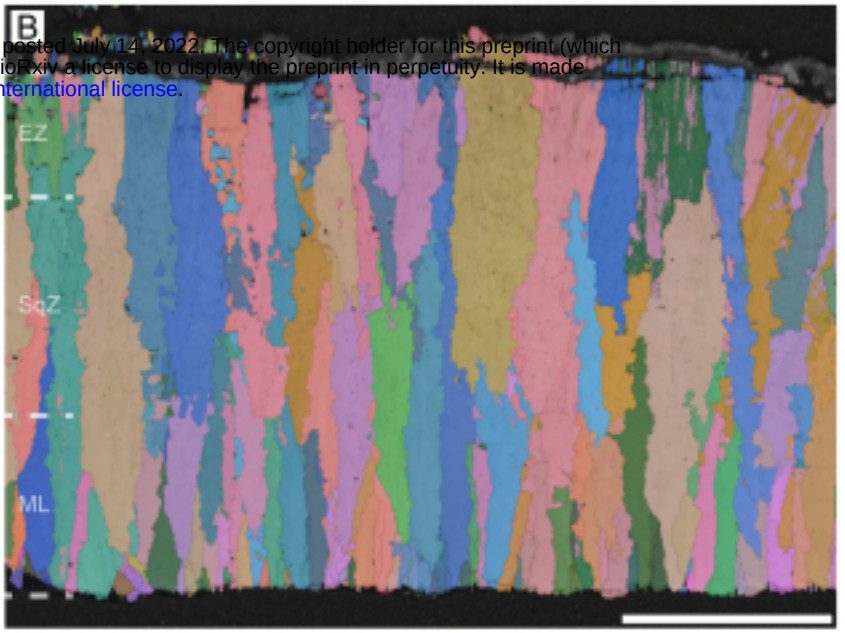

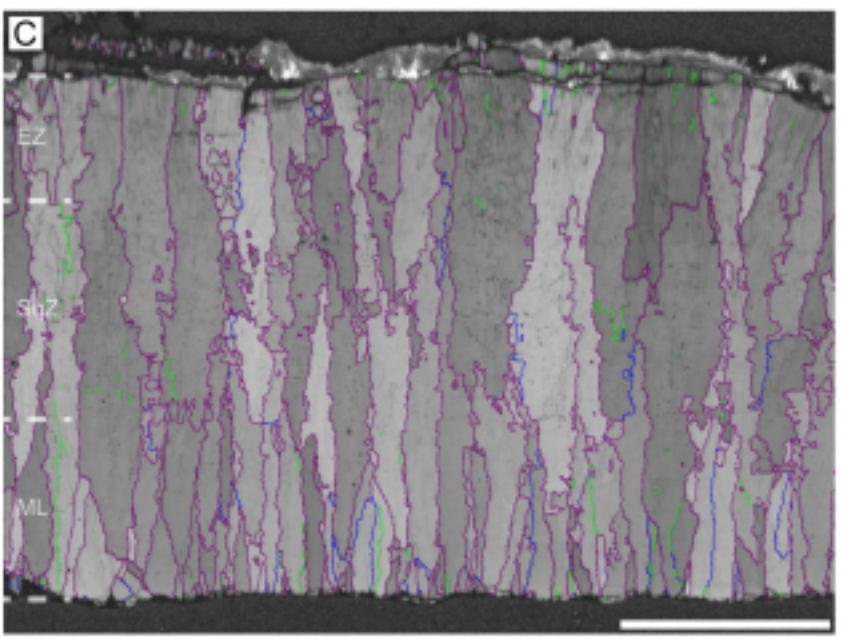

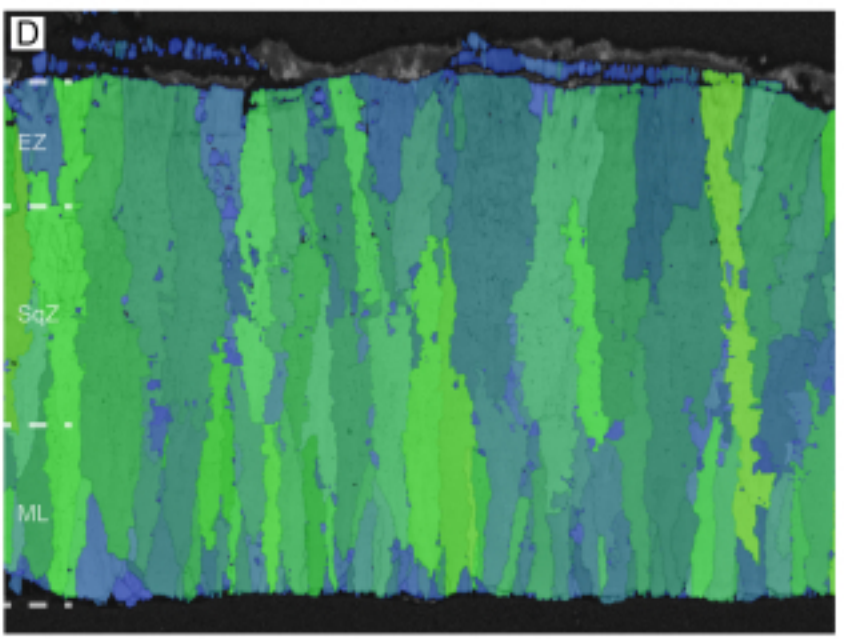

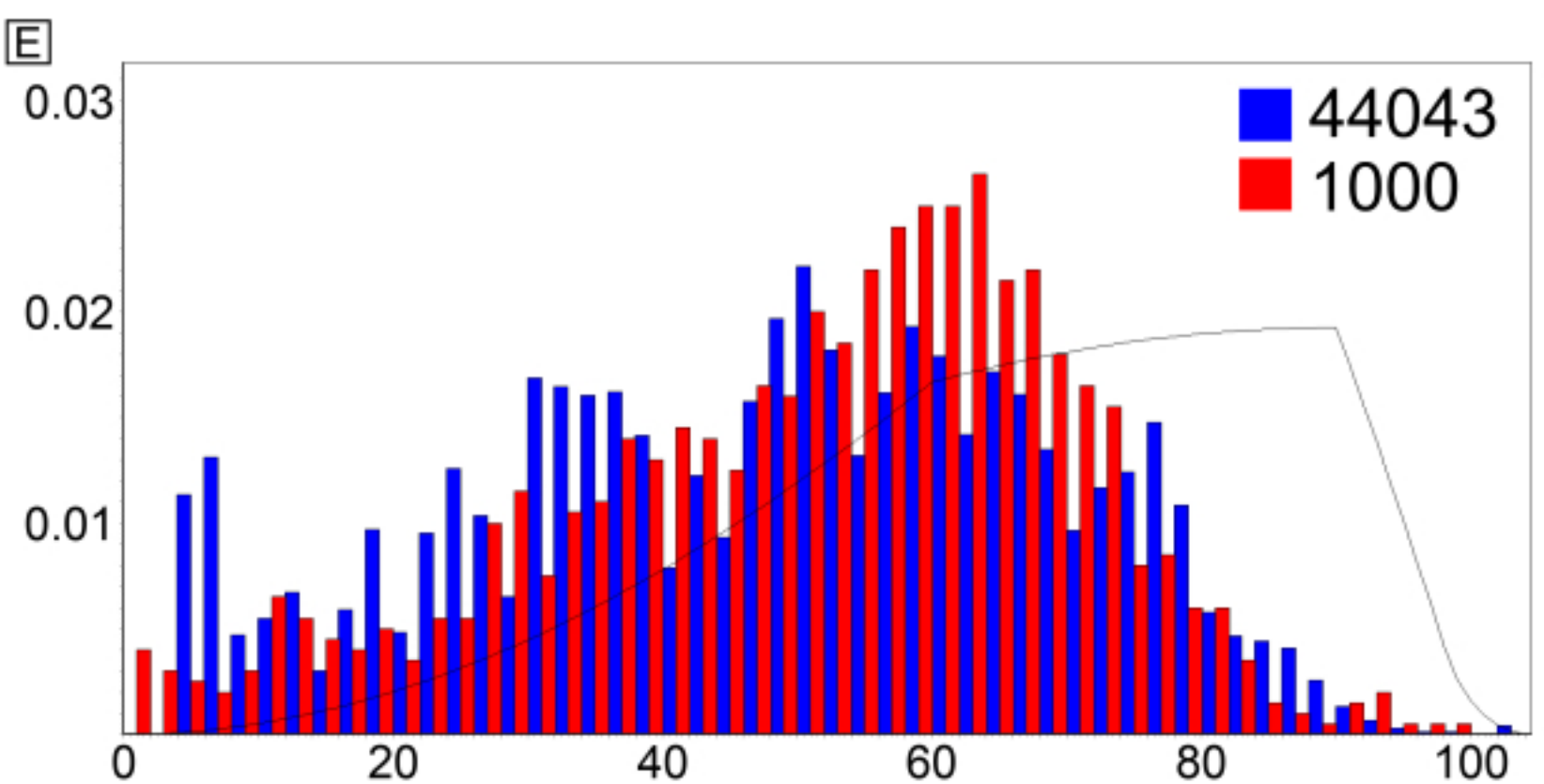

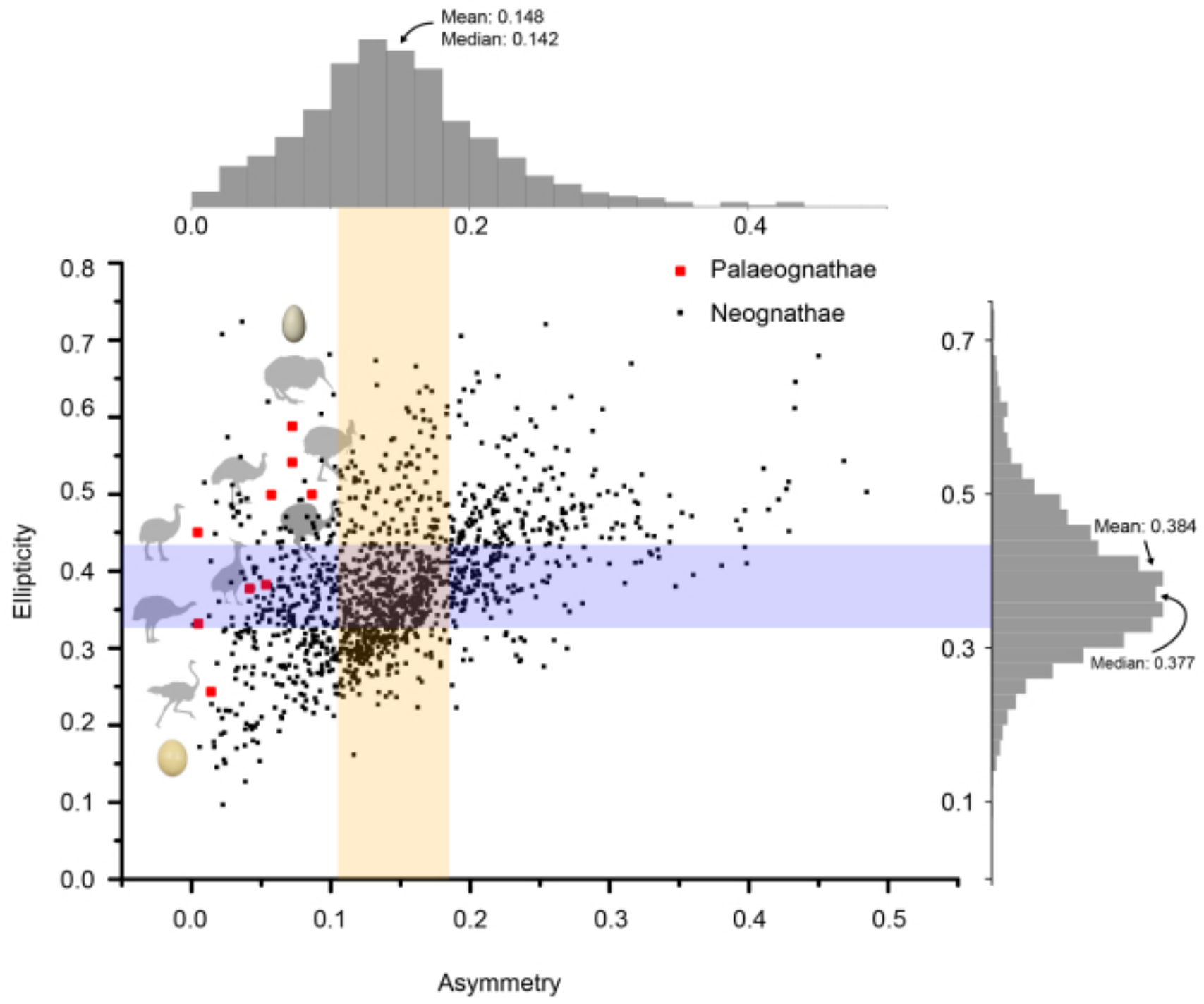
Mean: 0.148
Median: 0.142
0.0
0.2
0.4
Palaeognathae
Neognathae
0.8
0.7
0.6
0.5
0.4
0.3
0.2
0.1
0.0
Ellipticity
0.0
0.1
0.2
0.3
0.4
0.5
Asymmetry
0.7
0.5
0.3
0.1
Mean: 0.384
Median: 0.377

Elephant bird Gigantic

Kiwi Small

Cassowary Medium

Emu Medium

Rhea Medium

Large

Moa

Medium

200 µm

Palaeognathae

Tinamou Small

Ostrich Large

110.02

Aves

Lithornithidae Small

0 50 100

150.0

Pheasant

Neognathae

Northern goshawk

European green woodpecker

Non-avian Maniraptora

Prismatoolithus levis
(Egg of *Troodon formosus*)

Elongatoolithus oosp.
(Egg of medium-sized oviraptorosaur)

Macroelongatoolithus
(Egg of giant oviraptorosaur)

0 50 100

250 µm

Rhea-style

Tinamou-style

Ostrich-style

5°–10°

10°–20°

> 20°

?

circa 15th cen.

†

†

circa 11th cen.

Palaeognathae

Elephant bird

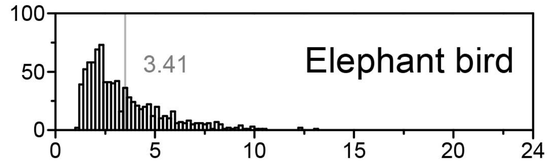

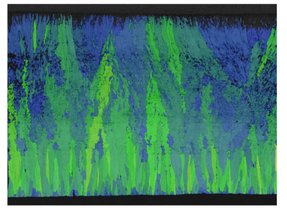

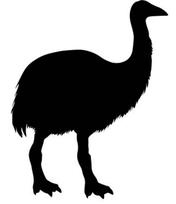

Kiwi

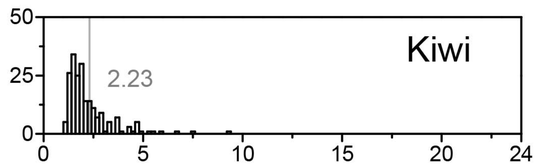

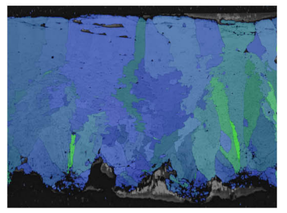

Cassowary

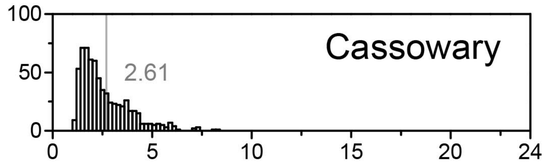

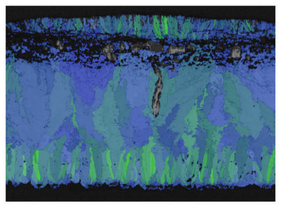

Emu

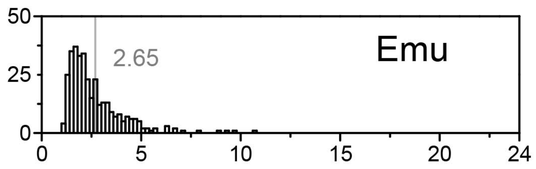

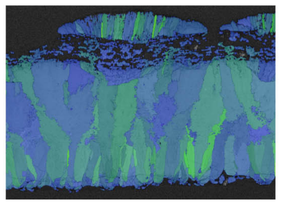

Rhea

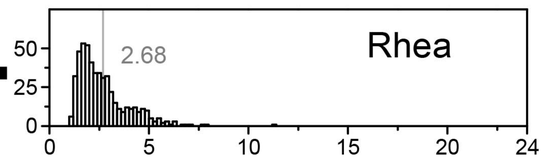

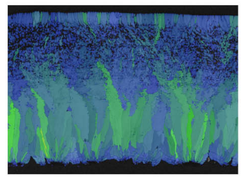

Thin moa egg

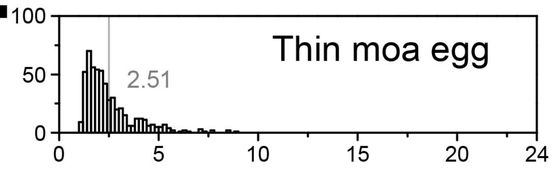

Thick moa egg

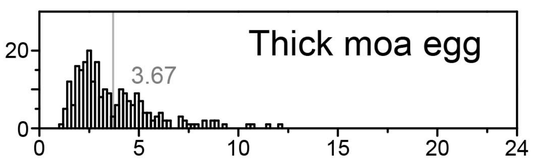

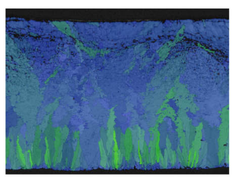

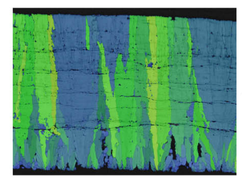

Chilean tinamou

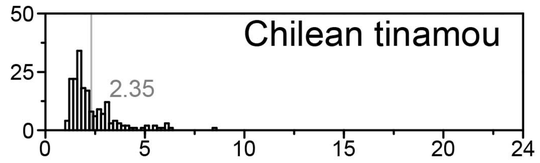

Elegant crested tinamou

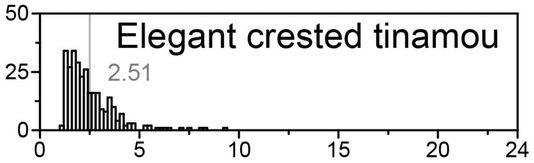

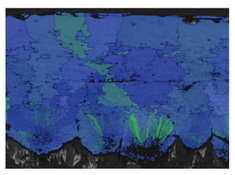

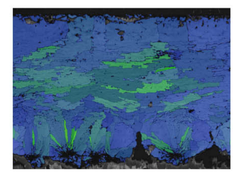

Ostrich

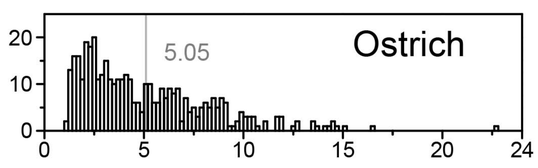

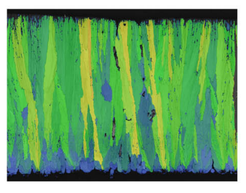

Lithornis

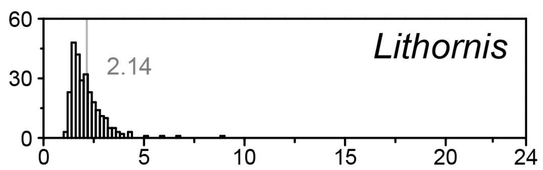

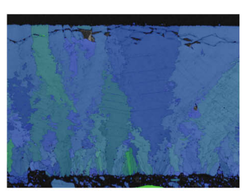

Prismatoolithus levis

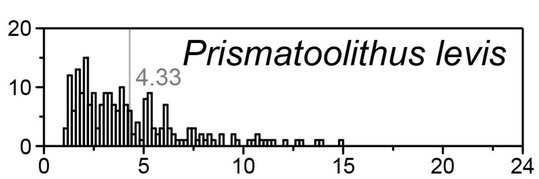

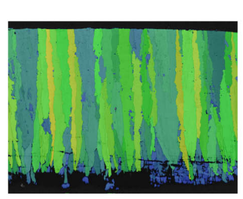

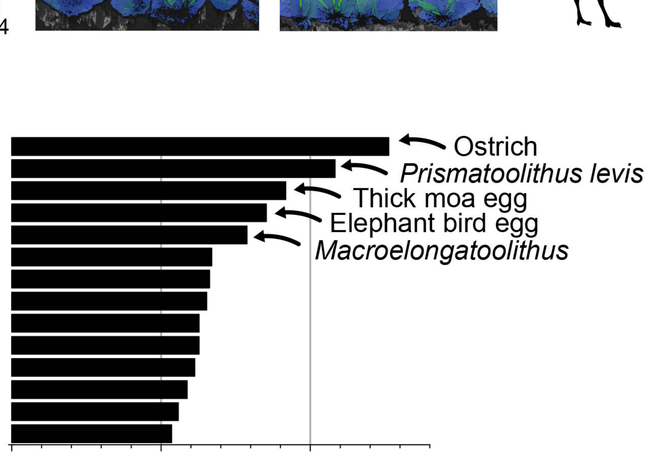

Macroelongatoolithus

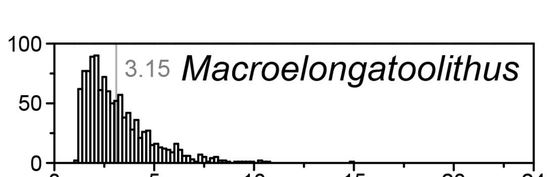

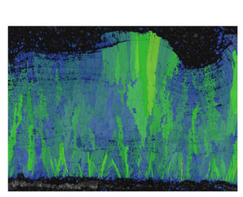

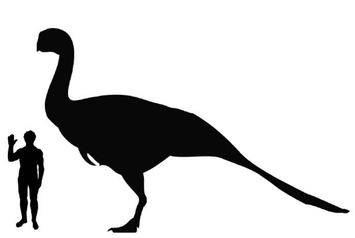

Elongatoolithus

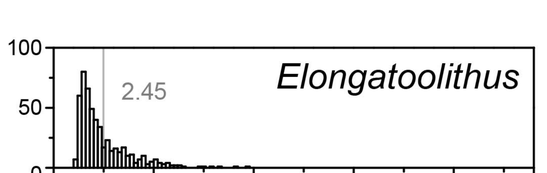

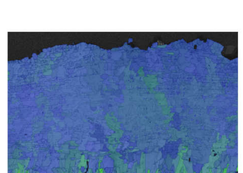

250 µm

5°–10°

10°–20°

> 20°

Rhea-style

Tinamou-style

Ostrich-style

circa 11th cen.

circa 15th cen.

?